LASER INDUCED BREAKDOWN SPECTROSCOPY AS A TOOL FOR DISCRIMINATION AND QUANTITATIVE CHARACTERIZATION OF GLASS FOR FORENSIC APPLICATIONS

By

ESPERANZA MARIELA RODRIGUEZ CELIS

A DISSERTATION PRESENTED TO THE GRADUATE SCHOOL
OF THE UNIVERSITY OF FLORIDA IN PARTIAL FULFILLMENT
OF THE REQUIREMENTS FOR THE DEGREE OF
DOCTOR OF PHILOSOPHY

UNIVERSITY OF FLORIDA

2009

To my family, for their love, support, and encouragement; to my best friend and love of my life, Oscar, for everything that you are and everything you have brought to my life

ACKNOWLEDGMENTS

I would like to express my sincere gratitude to my research advisor Prof. Nicolo Omenetto for his continued guidance and encouragement. His knowledge, patience and constant support have positively contributed to my formation as a scientist. I will not forget the many hours of discussion and how he enthusiastically explained to me hard to understand concepts. I would never be able to show my full gratitude to him for his friendship and advice.

I would like to acknowledge Dr. James Winefordner for his valuable research guidance and encouragement during my studies. His always positive attitude, during my presentations in group meetings and seminars, strongly contributed to shape my speaker skills and conquer my fears of presenting scientific data. I am also grateful to Dr. Benjamin Smith for all the invaluable help he has provided. Starting in late 2003, when I applied to graduate school, Ben has always been there offering continuous support and guidance. I appreciate all the insightful comments during group meetings and in the lab. I have much appreciation for Dr. Igor Gornushkin for teaching me to perform correlation analysis and LIBS in general. He always welcomed my ideas and patiently explained his. His support has been continuous, not only while in Gainesville but also from his new job in Germany. I would also like to thank Dr. Uwe Heitmann and Dr. Patricia Lucena, visitor scientists to the Winefordner-Omenetto-Smith group, for sharing their knowledge and for their friendship.

I thank all the previous and current members of the Winefordner-Omenetto-Smith research group, who have become like a second family to me over these years. Everyone brings some unique quality that makes the laboratory a great place to work. Some former group members that I cannot leave out my friends Lydia Breckenridge, Pamela Monterola, and Akua Oppong-Anane. I miss our time together and all the fun moments we shared in and out the lab. I also want to directly thank Galan Moore for his support in this research by providing the glass standards and

for patiently corresponding with me through e-mail to answer my questions about glass. My most sincere gratitude to the present group members, Jonathan Merten, Dan Shelby, Farzad Pakdel, Heh-Young Moon, and Andy Warren for understanding the frustrations involved in LIBS analysis and for sharing moments of joy every time I got a linear calibration plot. No list of acknowledgments would be complete without thanking Jeanne Karably, Lori Clark and Antoinette Knight for keeping the paperwork and degree requirements in line.

I made many sweet friends in Gainesville. I regret that space and time will not permit me to acknowledge them all by name. Nevertheless, I am thankful for the role every one of them played in my life and studies. I especially thank Elaine Muther and Cathy Silas who have been like mothers to me in the absence of my family. They have been great companions when I needed them, listening and advising whenever they could. I would never forget our Sunday nights dinner and domino tournaments. I also want to thank my Spanish-speaking friends: Frank, Aybi, Giovanni, Yeneire, Henry, Paula, Elizabeth, Oscar, Soledad, Karen, Jorge, Sarah, Fedra and Daniel. The time spent with you was remarkably fruitful and memorable.

Needless to say, I am grateful, as always, to my family for their patience, prayers and encouragement. To my parents, Eduardo and Lidia, your support and example have made me who I am. I hope you will always be proud of me. To my sister, Betsabe, brother, Wilson and, brother-in-law Abraham, who have also shown me great support, I want to say I am proud of you and of being your sister. I love you all so much. To my husband, Oscar, for all the support and encouragement and most importantly for his genuine friendship and love. I hope and pray we live a long and happy life together.

Finally, I would like to acknowledge my God who has always been the rock that makes up my foundation, and the calm in the storm.

TABLE OF CONTENTS

LIST OF TABLES

LIST OF FIGURES

Abstract of Dissertation Presented to the Graduate School
of the University of Florida in Partial Fulfillment of the
Requirements for the Degree of Doctor of Philosophy

LASER INDUCED BREAKDOWN SPECTROSCOPY AS A TOOL FOR DISCRIMINATION AND QUANTITATIVE CHARACTERIZATION OF GLASS FOR FORENSIC APPLICATIONS

By

Esperanza Mariela Rodriguez Celis

May 2009

Chair: Nicolo Omenetto
Major: Chemistry

Material analysis and characterization can provide important information as evidence in legal proceedings. Taking advantage of the multi-element detection capability and minimal to no sample preparation of LIBS, this technique is proposed as a viable alternative for glass analysis. Discrimination studies by linear and rank correlation methods were performed to glasses from automobile windows. Linear correlation combined with the use of a spectral mask, which eliminates some high-intensity emission lines from the major elements present in glass, provides effective identification and discrimination at a 95% confidence level. In the course of this study, several key instrumental parameters were identified and investigated, and a comparative study regarding the performance of up to four different commercial instruments for LIBS analysis of solids has been made. Results indicate that the spectral resolution and sensitivity of the systems were linked to the performance and suitability of the technique for material identification by correlation methods, especially when samples were of very similar composition.

While the qualitative characterization of materials without sample preparation is certainly one of the main advantages of LIBS, the possibility of performing accurate quantitative analysis relies on the use of calibration curves made with matrix-matched standards. Such quantitative

analysis would also improve the discrimination capability of the technique in the case of the glass samples analyzed. Quantitation is one of the analytical aspects of LIBS where improvements are needed. In addition to the conventional analytical procedures followed in LIBS analysis, a normalization procedure based upon the possible correlation existing between the background fluctuation and the analytical signal. This method has been applied to several types of solid samples. The results of all these investigations have allowed a fair assessment of the applicability of LIBS for discrimination and quantitative characterization of solid samples in general, and glasses in particular.

CHAPTER 1
INTRODUCTION TO LASER-INDUCED BREAKDOWN SPECTROSCOPY

Introduction

Laser-induced breakdown spectroscopy (LIBS), also called laser-induced plasma spectroscopy (LIPS), laser spark spectroscopy (LSS), and laser optical emission spectroscopy (LOES) is a fast-growing atomic emission analytical technique that involves focusing a high power, short pulse laser (usually in the nanosecond range) on a sample surface. A very energetic plasma that is rich in electrons, atoms and ions is formed. The plasma radiation, characteristic of the elements present in the sample, is collected and analyzed. LIBS provides a simple, fast and direct method of elemental analysis. Indeed, solid, liquid or gaseous materials can be analyzed with little-to-no sample preparation, and detection limits for solid samples in the part-per-million (ppm) range.

In this chapter, a brief summary of the historical development of LIBS is presented together with an overview of the characteristics of the LIBS process. Each important component of a LIBS apparatus and the many advantages of the method along with its limitations were also discussed.

History of LIBS

The evolution of LIBS has been summarized and discussed in great detail in books[1-4] and several review articles[5-22], therefore, only the most significant events in the history of LIBS are included here. The laser-induced plasma was observed in 1960 shortly after the discovery of the pulsed ruby laser[23-25]. Brench and Cross[26] first reported a laser plasma at the Xth Colloquium Spectroscopicum Internationale in 1962. They used the ruby laser to produce vapors from metallic and non-metallic materials.

Early on, the laser was used primarily, but not exclusively, as an ablation source with cross-excitation to provide the spectrum[10]. In 1963, the first analytical application of laser-induced plasma for spectrochemical analysis of surfaces was presented by Debras-Guedon and Liodec [27]. A year later, Maker, Terhune and Savage [28] reported the first observation of optically-induced breakdown in a gas. In the same year, Runge, Minck and Bryan described the use of a pulsed ruby laser for direct spark excitation on metals.[29] Later, collection of the plasma emission at time intervals was achieved using a streak camera and rotating mirrors in the detection system [1, 12].

In the period from 1964 to 1967 the first instruments based on this technique were developed by VEB Carl Zeiss (Germany) and Jarrell-Ash (USA) [11]. These instruments employed cross excitation, where the light for spectral analysis was generated by an auxiliary spark discharge and the laser was only used for ablation. The instruments were later discontinued because they could not contend in accuracy and precision with competing technologies at the time such as conventional spark spectroscopy, electrothermal atomization atomic absorption spectrometry (ATA-AAS) and inductively coupled plasma-atomic emission spectrometry (ICP-AES) [1].

Other research directions continued to develop. In 1966, Young, Hercher and Yu [30] described the optical properties of laser-induced air sparks. In the 1970s, spectrochemists were mostly interested in using LIBS for direct ablation, excitation, and observation of the spark, while physicists studied the breakdown in gases[10]. Scott and Strashiem [12] studied time-resolved spectra obtained using Q-switched and non-Q-switched lasers. In 1972, Felske, Hagenah and Laqua [31] described the analysis of steel by means of a Q-switched laser. Through this years, much of the LIBS research appeared in the Russian literature [32-36]. Other

significant milestone in the development of LIBS constitutes the generation of plasma in water [37-39] and the spectrochemical analysis of aerosols [40-43]. During this period, the sample matrix was recognized as an affecting parameter of the LIBS signal [44-46]. The initial findings showed that physical and chemical characteristics of the samples play a significant role in signal strength, and repeatability. Since the 1980s, there has been a renewed interest in spectrochemical application of LIBS driven by its unique advantages, significant technological developments in the components (lasers, spectrographs, detectors) and emerging needs to perform measurements under conditions not feasible with conventional analytical techniques [2].

As LIBS advanced further into the last decade of the 20th century, both analytical and industrial research employing LIBS developed rapidly. The technique began to move out from the basic science laboratory into the real world of applications. LIBS configurations concentrated on developing rugged, robust and field-portable systems. Optical fibers were built into LIBS systems with the purpose of carrying the spark light to the spectrometer [10].

Today, LIBS remains a very active field. The world-wide LIBS community has established international meetings that include LIBS 2000 (Tirrenia, Italy), Euro-Mediterranean LIBS Symposium (EMSLIBS) 2001 (Cairo, Egypt), LIBS 2002 (Orlando, USA), EMSLIBS 2003 (Crete, Greece), LIBS 2004 (Malaga, Spain), EMSLIBS 2005 (Aachen, Germany), LIBS 2006 (Montreal, Canada), EMSLIBS 2007 (Paris, France), North American Symposium on Laser Induced Breakdown Spectroscopy (NASLIBS) 2007 (New Orleans, USA), and LIBS 2008 (Berlin, Germany). In addition there have been a multitude of LIBS sessions at Pittcon and FACSS meetings. The interest in LIBS is also evident in the exponential increase in the number of publications and patents related to fundamentals and applications of this technique.

Significant progress has been made on the diverse and versatile applications of LIBS including process monitoring (for example, in the metallurgical and mining industries), environmental monitoring, biomedical and pharmaceutical applications, forensic analysis, military and homeland security, space exploration, and diagnostics of archaeological objects. As continuous improvements in instrumentation and data analysis are developed, the future for LIBS now appears brighter than at any time during its recent history.

Characteristics of the LIBS Process

The principle of LIBS is similar to that of conventional plasma-atomic emission spectroscopy (AES), such as inductively coupled plasma ICP-AES, microwave-induced plasma (MIP-AES), direct-current plasma (DCP-AES), arc- and spark-AES. What distinguishes LIBS from these other techniques is that the sample does not need to be transported into the plasma source; indeed the plasma is generated at the sample surface making it a simpler method because the ablation and excitation processes are carried out by the laser pulse in a single step [14].

In LIBS, the vaporizing and exciting plasma is produced by a high-power, short pulse laser (usually in the ns range) on a sample (solid, liquid or gas). Each firing of the laser, or single-shot, produces a single LIBS measurement. In practice, however, the signals from various laser plasmas are added or averaged to increase accuracy and precision [2].

LIBS of solids can be considered as a set of complex processes: laser-interaction with the solid, ablation or removal of sample particles, and breakdown or plasma formation. Briefly, there are two main steps leading to breakdown. First, there is a generation of a few free electrons which play a role of initial receptors of energy through three body collisions with photons and neutrals. Second, there is avalanche ionization in the focal region caused by collisions, ionization, more electrons, and energy absorption [2]. A schematic representation of the main processes for a laser-induced plasma on a solid surface is shown in Figure 1-1 [21].

The process is initiated by reflection or absorption (Fig. 1-1a) of energy by the sample from the pulsed laser. At moderate irradiances (~10^6 W cm^{-2}), the absorbed energy is rapidly converted into heat, resulting in melting and vaporization of small portion of material into ionized gas, when the local temperature approaches the boiling point of the material. In Fig. 1-1b, the removal of particulate matter from the surface leads to the formation of a vapor in front of the sample. When this vapor condenses as droplets of submicrometer size, it leads to scattering and absorption of the laser radiation inducing heating, ionization and plasma formation (Fig. 1-1c).

Other mechanisms that follow these include fast expansion of photoablated-material (Fig. 1-1d), formation of polyatomic aggregates and clusters and deposition of the ablated and molten material around the crater (Fig. 1-1e-f). During the expansion phase, the plasma emits useful signals. As it cools and decays, the ions and electrons recombine to form neutrals, and even molecules. Energy is released through radiation and conduction [2].

Because the laser plasma is a pulsed source, the resulting spectrum evolves rapidly in time. A schematic representation of the temporal history of the laser-induced plasma concerning the different predominant emitting species is illustrated in Fig. 1-2 [2]. At the beginning, a white light, or continuum, dominates the plasma light. This light is caused by *bremsstrahlung*, from German *bremsen* "to brake" and s*trahlung* "radiation", and the recombination radiation from the plasma as free electrons and ions recombine in the cooling plasma. If the light is integrated over the entire duration of the plasma, the continuum light could interfere with the detection of weaker emissions from minor and trace elements in the plasma. Therefore, another important parameter in LIBS is time resolution; time-resolved spectroscopy is essential to improve the sensitivity and selectivity in LIBS experiments because it allows rejection of the strong spectral

continuum emitted at the beginning of the ablation [47]. The parameters used for time-resolved detection are t_d also known as time delay, the time between plasma formation and the start of the observation of the plasma light, and t_b, or gate width, the time period over which the light is recorded. These parameters are highly dependent on the element and the matrix, and must be optimized for each type of sample. In the literature, delay times in the range of 1-3 μs, and integration times of 1-10 μs are mostly reported [21].

Instrumentation

The instrumentation for LIBS generally consists of a pulsed laser beam for sample ablation or breakdown, the optics for focusing the laser beam and plasma emission, a spectral resolution device for wavelength selection and a detector. A typical LIBS set-up is shown in Figure 1-3. The basic components of any LIBS system are similar but they are tailored to the particular application.

Laser Systems

Intensity, directionality, monochromaticity, and coherence are the main properties that distinguish laser light from conventional light sources. Laser radiation can be emitted continuously or in short pulses, and even be tunable over a wide range of wavelengths [4]. Pulsed lasers are mostly used in LIBS and must generate pulses of sufficient power to produce the plasma. Besides the laser power, it is also of importance the laser ability to deliver the energy to a specific location. The power per unit area that can be delivered to the target is known as "irradiance" and is also called "flux" or "flux density".

Since the discovery of the ruby laser [26], LIBS developments have been marked by the progress in laser technology. Each laser has its own properties such as wavelength, mode quality, and characteristics of operation. The most widely used lasers for LIBS include the Nd: YAG, ruby, gas and excimer lasers.

The Nd:YAG laser, with output wavelengths (λ) of 1064 nm, 532 nm (frequency-doubled), 355 nm (frequency tripled) and 266 nm (frequency quadrupoled) pulse length of 3-10 ns.[14] Nd: YAG lasers (flashlamp pumped) are preferred for most LIBS applications because they provide a reliable, compact, and easy to use source of laser pulses together with high irradiances [1].

The ruby laser with a wavelength (λ) = 694 nm and a pulse length of 10 ps (ruby picosecond pulse) – 10 ms (ruby normal pulse) [4].

Gas lasers, including CO_2 (λ = 10.6 μm and pulse length = 0.2 – 100 μs) and N_2 (λ = 337 nm and pulse length = 3 – 10 ns) [4, 48]. These lasers require periodic change of gases, and do not couple well into many metals.

Excimer lasers with pulse lengths of 10-35 ns, including ArF (λ = 193 nm), KrF (λ = 248 nm) and XeCl (λ = 308 nm). They also require periodic change of gases or gas flow and provide UV wavelengths only [1].

These lasers produce tipically-tens-to hundreds of mJ per pulse, and peak power outputs in the mW order. Once the laser pulses are focused by an appropriate lens to submicron-sized spots, the resulting irradiance is on the order of $10^{10} – 10^{12}$ W cm^{-2} which is enough to produce a plasma on solid samples.

Spectral Resolution Devices

The groundwork of a LIBS measurement is the collection and analysis of an emission spectrum. Resolution and width of the spectrum that can be observed are important properties of a spectrometer. These specifications depend on the particular application in mind; however a larger spectral window is needed for multi-element analysis. The following are examples of the most common spectral components of a LIBS system:

- Acousto-optic tunable filter (AOTF)

- Grating monochromator
- Grating spectrograph
- Echelle spectrograph

An AOTF is a diffraction based optical-band-pass filter that can be rapidly tuned to pass various wavelengths of light by varying the radio-frequency of an acoustic wave propagating through an anisotropic crystal medium (e.g. TeO_2). The transmitted light is then detected using a photon detector device [49]. In addition to a fast wavelength shifting, AOTF provide high energy throughput, robustness (no-moving parts) and usefulness for imaging [50].

A grating monochromator is a spectrometer that is tuned to monitor a selected wavelength which is presented at the exit slit of the device for detection. The most popular design of grating monochromator is the Czerny-Turner monochromator. It provides high resolution with an f # ~ 4. A spectrograph is similar in basic configuration to a monochromator except it has an exit plane at which a continuous range of wavelengths is presented for detection using some type of array detector or a series of single-wavelength detectors positioned behind individual slits. The spectral range recorded is limited by the width of the focal plane and the size of the array detector. However, it provides a wide spectral coverage with high resolution and f # ~ 4 [1].

For LIBS, echelle spectrographs are typically used. For analysis of a wide range of samples, a system based on an echelle spectrograph offers a combination of high resolving power ($\lambda / \Delta\lambda = 2500 – 10\ 000$) and wide wavelength coverage (190-800 nm). The strong emission lines of most elements lie in this region. An echelle grating with a prism order sorter disperses the spectrum into two dimensions (wavelength vs. order). Therefore, multiple exit slits and photomultipliers can be placed in the two-dimensional focal plane with f # typically >9.

Detectors

The choice of detector for LIBS experiments is dependant on the method of spectral selection and the number of elements to be monitored. The simplest detectors available are photodiodes (PD) and photomultiplier tubes (PMT). These are highly sensitive devices that measure instantaneous light intensity and are used together with line filters or monochromators providing only single wavelength detection. By placing many small photosensitive elements (pixels) in an array at the exit slit of the spectrometer a wider spectral range can be cover. Examples include photodiode arrays (PDA), charge-injection devices (CID) and charge-coupled devices (CCD). These are light-integrating devices since they collect the light for a period of time, and then the signals stored on each pixel are read out sequentially, one pixel at a time further increasing the response time. For time-resolved LIBS studies with array detectors, a micro-channel plate (MCP) is coupled to the detection system. The MCP acts as a regulator when the incident radiation is allowed to reach the detection device, amplifying the light by converting it to electrons which are then reconverted back to light before detection by the array detector. The coupling of a MCP with array devices are known as intensified detectors (e.g. ICCD) [2]

Advantages of LIBS

LIBS, like other methods of AES, is able to detect all elements and has the ability to provide simultaneous multi-element detection capability with *low* absolute detection limits. In addition, because the laser spark uses focused optical radiation to form the plasma, LIBS exhibits numerous appealing features that distinguish it from more conventional AES-based analytical techniques [2]. These are: simple and rapid or real time analysis, the ablation and excitation processes are carried out in a single step; little-to-no sample preparation, which results in increased throughput and reduction of tedious and time-consuming sample digestion and

preparation procedures (this, however, can lead to a loss of accuracy through contamination).[13] LIBS allows in situ analysis requiring only optical access to the sample. It can also be performed over a great distance, a technique referred to as *remote* sensing. Unlike remote analysis, in which some part of the LIBS system is close to the sample, is the method of *stand-off* analysis. Here, the laser pulse is focused onto the sample at a distance using a long focal length optical system [2].

Virtually any kind of sample can be analyzed: solids, liquids, aerosols, or gases. LIBS has the ability to analyze extremely hard materials which are difficult to digest such as ceramics, glasses and superconductors [14]. It is a non-destructive method, very small amount of sample (~0.1 μg – 0.1 mg) is vaporized. It provides good sensitivity for some elements (e.g. Cl, F) difficult to monitor with conventional AES methods. In addition, LIBS has adaptability to a variety of different measurement scenarios, e.g. underwater analysis, direct and remote analysis, compact probe with the use of miniature solid state lasers, stand-off analysis.

Considerations in the Use of LIBS

Among a few disadvantages of LIBS are the poor precision (5-15%), poor *relative* detection limits (in the ppm range), and matrix and spectral interferences. Sample homogeneity, physical and chemical matrix effects, sampling geometry, and safety in the analysis are some important considerations in the use of LIBS.

Sample Homogeneity

This is a direct consequence of no sample preparation and mostly affects the analysis of solids. Preparation typically produces a homogeneous sample; the lack of preparation complicates the analysis of non-homogeneous samples with a point detection method such as LIBS. The area interrogated is small, typically 0.1 – 1 mm diameter [2], involving a very small mass of material. Non-uniformities may be averaged out using a number of laser plasmas to

repetitively interrogate different areas of a sample and the results are combined to produce an average measurement.

Matrix Effects

Physical properties and sample composition affect the element signal such that changes in concentration of one or more of the elements forming the matrix alter an element signal even though the element concentration remains constant. These effects complicate the construction of calibration plots and hence the ability to obtain quantitative results. Matrix effects can be divided into two kinds, physical and chemical. Differences between specific heat, heat of vaporization, thermal conductivity, absorption at the laser wavelength, and particle size contribute to the presence of physical matrix effects. Chemical matrix effects occur when the presence of one element have an effect on the emission of another element. For example, easily ionizable species increase the electron density, thereby reducing the intensity of less ionizable components [1, 2].

Sampling Geometry

When the power density is high enough, a plasma is formed on the surface of a solid even though the distance between the sample and the lens may be different from the lens focal length. The lens-to-sample distance affects the mass ablated that, in turn, affects the element emission intensity. Maintaining the sample geometry constant is critical to obtain the best analytical results.

Safety

There are certain operational parameters that must be consider for the safe use of LIBS [2]. These are:

- Ocular hazard by the laser
- High voltage circuits used on the laser operation
- Explosive potential of the laser spark for certain materials
- Possibility of generating toxic airborne particles.

Industry safety standards and preparation of Standard Operating Procedures (SOP) or Hazard Control Plans (HCP) that identifies the hazards associated with the experiments and indicates steps to be taken to mitigate the hazards are recommended for LIBS users.

Conclusions

The development of LIBS has progressed rapidly during the last decade. Numerous research groups have worked on improving LIBS measurements of different samples by using advanced lasers, detection systems and data processing methods. These improvements are opening new application areas for LIBS. However, there are still major difficulties in this technique. To overcome the known problems and advance LIBS for future applications, the knowledge of this technique needs to be expanded through basic research in the fundamentals, quantification, pulse to pulse fluctuations, and study of the laser-material interactions[4].

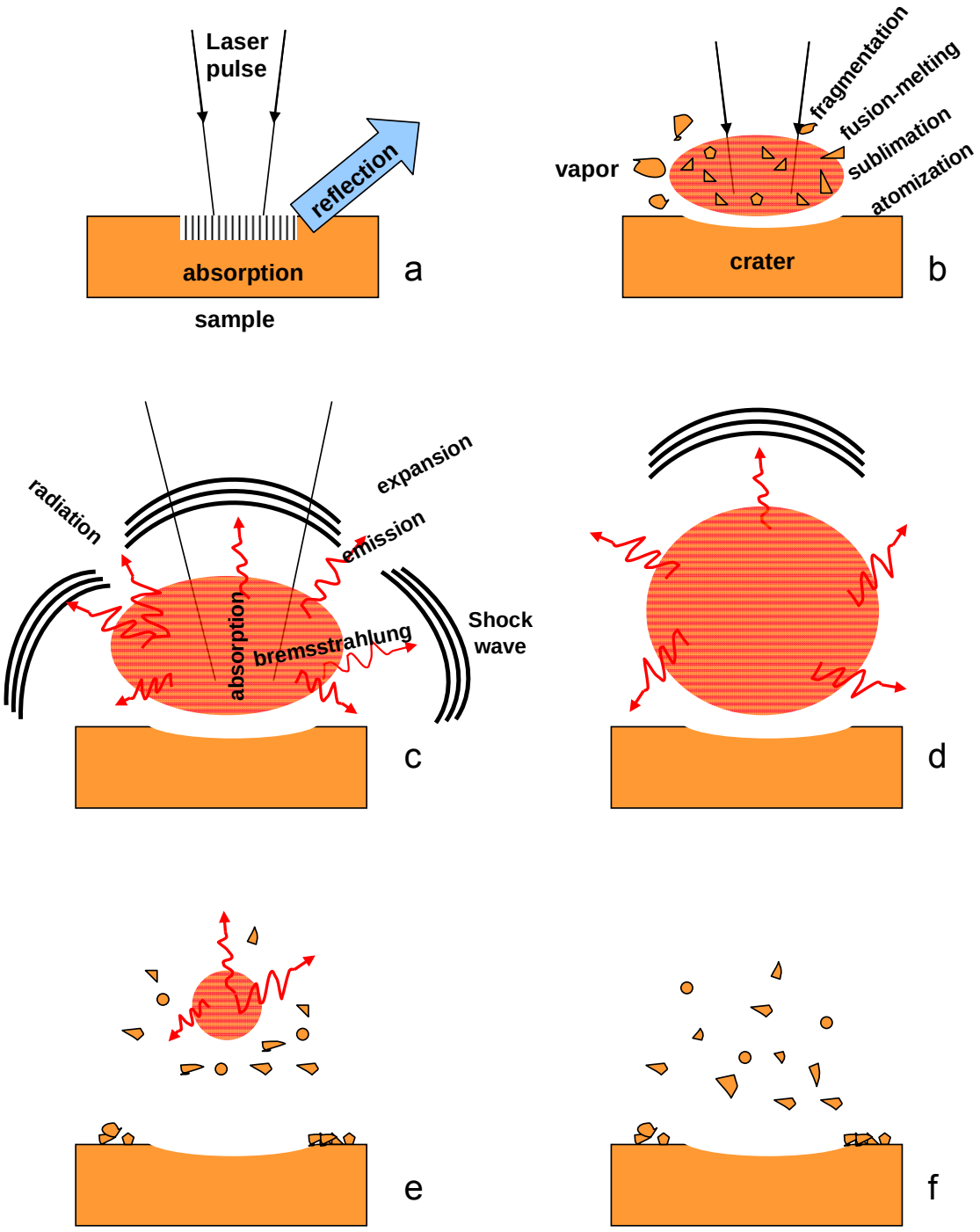

Figure 1-1. Diagram showing main events in the LIBS process: (a) laser-material interaction, (b) heating and breakdown, (c) expansion and shockwave formation, (d) emission, (e) cooling and (f) crater formation. Adapted from Ref [21]

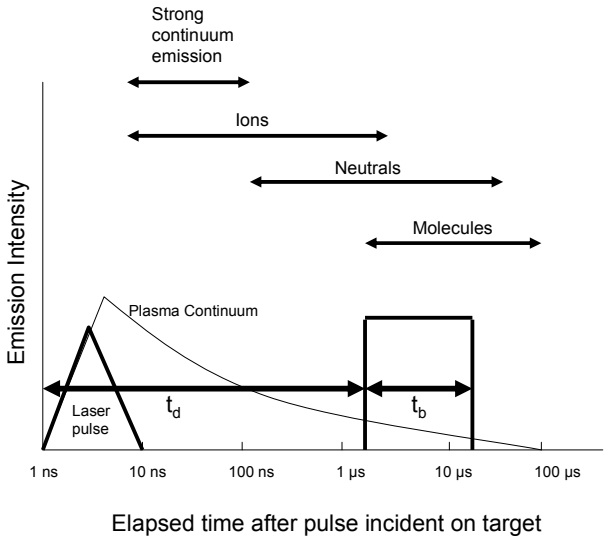

Figure 1-2. A schematic overview of the temporal history of a LIBS plasma during which emissions from different species predominate. The box represents the time which the plasma light is monitored using a gatable detector; t_d is the delay time and t_b the gate pulse width. Adapted from Ref [1, 2]

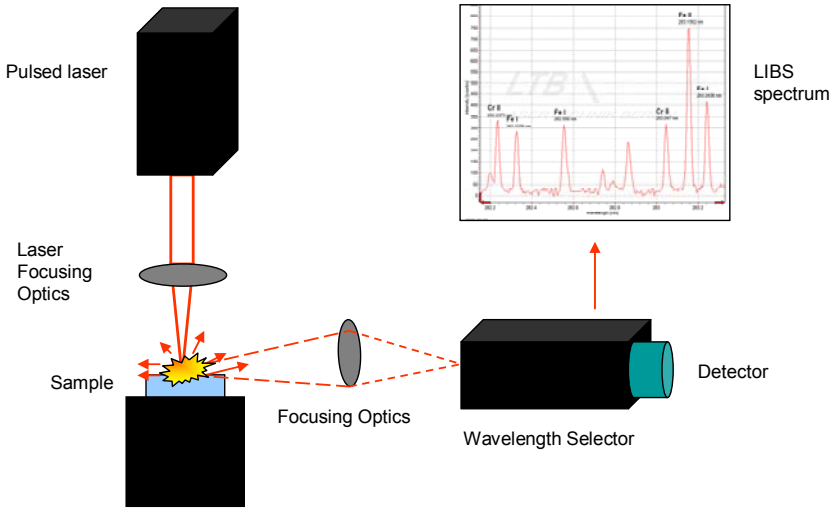

Figure 1-3. Diagram of a typical laboratory LIBS apparatus.

CHAPTER 2
BRIEF OVERVIEW OF GLASS AS FORENSIC EVIDENCE

At identifying glass as forensic evidence, there is a continued move away from dependence on physical properties measured such as index of refraction and density, towards methods of elemental analysis of its trace components. This chapter focuses on the potential of LIBS for the discrimination of glass fragments for forensic applications.

Glass as Forensic Evidence

Trace evidence is a generic term for small, often microscopic, materials transferred between people, places, and objects. There is an enormous range of materials cover by this terminology including fibers, paint, glass, hair, soil, feathers, metal, brick, dust, sand, pollen, sawdust, and vegetation [51]. Fragments of broken glass collected at crime scenes such as burglaries, car crashes, hit and runs, and vandalism constitute forensic trace evidence in criminal investigations[52].

These glass fragments, known as control samples, can be compared with those recovered from the victim's body and/or the suspect's belongings. If they are found to come from the same source, they might associate a suspect with the perpetration of a particular crime. Hence, it is essential that the method chosen for the analysis is capable of handling small sample fragments to provide adequate confidence in the results. There are two main goals for the analysis of glass for forensic purposes [53]. First, to classify the glass fragments into one of a number of possible categories, e.g. sheet, container, vehicle window, vehicle headlamp or tableware. This classification could help crime investigators focus their search for an appropriate type of glass sample. Second, to determine whether two groups of glass fragments, the control sample, and the recovered sample from the suspect, "could have" shared a common origin.

Glass as a Chemical Matrix

Glass is defined as an inorganic product of fusion which has been cooled to a rigid condition without crystallization. Transparency, durability, electrical and thermal resistance, and a range of thermal expansions are a unique combination of glass properties [52]. The main component of glass is silica sand (60-75%). Silica (SiO_2) is a glass former with a melting point higher than 1700°C, and while it can be made into a specialized glass where high temperatures resistance is required, other components or additives are added to simplify its processing. Soda ash (sodium carbonate, Na_2CO_3, 12-16%) and potassium oxide (K_2O) are included in the mixture to reduce the fusion temperature. Lime or limestone (calcium oxide, CaO, 7-14%) or dolomite (magnesium oxide, MgO, <1%) are added as stabilizers to provide for a better chemical durability. Depending on the end use of the product and on the manufacturing process, additional ingredients are intentionally used. The following examples serve to illustrate the range of commercial glass compositions:

- Fused silica glass
- Soda lime silicate glass
- Borate silicate glass
- Lead glass
- Aluminosilicate glass
- Alkali barium silicate glass
- Borate glass
- Phosphate glass
- Chalcogenide glass

Most glass manufacturers rely on a steady supply of recycled crushed glass, known as "cullet," to supplement raw materials and to prolong furnace life since cullet melts at a lower

temperature. Cullet also adds some measure of heterogeneity as trace contamination which is an ideal effect for the forensic scientist because it introduces additional contrast between batches originating from the same plant. Heterogeneity is also imparted by iron or chromium in the sand deposits, contaminants of concern for the manufacture process since they can lead to undesirable coloring. For decolorization, manufacturers rely on CeO_2, As_2O_3, SbO, $NaNO_3$, $BaNO_3$, K_2SO_4, or $BaSO_4$.Other contaminants such as potassium oxides in soda ash, magnesium and aluminum oxides in lime, or even strontium in dolomite are useful for the forensic discrimination of glass [54].

Glass manufacture in all sectors broadly follows the stages illustrated in Figure 2-1. Most manufactured glass has a specific soda-lime composition, producing windows (flat glass) for buildings and automobiles and containers of all types. Table 2-1 shows the typical composition of a soda-lime glass. The properties of these glasses make them suitable for a wide range of applications in container, sheet (or "float", the name of the process for the manufacture of most sheet glass), vehicle window (also made by the float process), vehicle headlamp (a borosilicate glass) and tableware glass (including leaded glass).

Microscopic Techniques for Glass Examination

A range of techniques is available for the forensic examination of glass. The possibility of a physical match between the fragments is explored. This requires the two broken edges to match perfectly, an outcome that is hard to find in real cases [55]. However, if the surface shape of a fragment is different from that of the control item, the fragments could not have come from the same source. If the fragment shows fluorescent properties typical of a flat float glass and the control glass has no fluorescent properties, the glasses are not from the same source either. Other physical properties such as color, thickness, refractive index (RI), and density are also examined.

The method of RI relies on the temperature variation effect first described by Winchell and Emmonds back in 1926 [56]. The RI of a liquid changes when heated and cooled while there is less RI variation for a solid. Therefore, if a transparent glass fragment is immersed in proper oil and then heated, the RI of the oil and the glass will be identical and the glass will not be seen. The temperature at which the glass disappears is recorded and by using standards a calibration plot can be drawn. The RI of an unknown glass fragment is determined by knowing the disappearance temperature [52]. The determination of RI is not a straightforward procedure; fragments from the same object might give a range of RI readings, making necessary the use of statistical tests such as t-test, cluster analysis to provide more incisive analysis of the data.

The determination of the RI has been the technique of choice for many years [57-68]. Nevertheless, technological improvements in the glass manufacturing process have led to less variability in physical and optical properties between manufacturers and different plants of the same manufacturer [59]. The reduction of the spread among RI values reduces the informing power of this technique and highlights the need for additional techniques to facilitate reliable identification.

Elemental Analysis of Glass Fragments

Ever since there is a better quality control of the batch components, the analysis of trace elements impurities within the raw materials constitute a useful path for discrimination. The following is a list of the most important factors (not listed in specific order) forensic scientists consider when choosing an analytical technique for analysis [69].

- Detection limits
- Accuracy
- Precision
- Sample destruction

- Sample size requirements
- Total analysis time and ease of sample preparation
- Feasibility to control matrix effects and interferences
- Sources of error understood and controlled
- Linear concentration range
- Cost of equipment, operator expertise, and maintenance
- Level of reliable identification

Several elemental analysis techniques are available for the characterization and discrimination of glass fragments. These available methods include atomic absorption and atomic emission spectroscopy, X-ray methods, and inorganic mass spectrometry.

Atomic Spectroscopy

Atomic absorption [70] and atomic emission (AE) are two types of atomic spectroscopy which have been applied to the analysis of forensic glass samples. Flame Atomic Absorption Spectroscopy (FAAS), is simple to use, relatively inexpensive, and provides outstanding sample throughput for the analysis of a small number of elements. Sensitivity in the part-per-billion (ppb) results in a minimal sample size required for analysis, generally 100 μg or less. FAAS equipment is available in many forensic science laboratories which perform gunshot residue analysis. Despite these features, the need for a different lamp per element, limited number of elements that can be analyzed, sample destruction and tiresome preparation makes the technique inflexible for forensic work. Analytical procedures for the measurement of Mg, Mn, Fe, Cr, Na, and As in glass have been reported using AA [52, 69, 71].

In forensic glass analysis, three types of sources for AE have been reported: spark, inductively coupled plasma (ICP) and lasers. Using the spark source and AE, levels of Al, Ba, Ca, Fe, Mg, and Mn have been determined in glass samples weighing approximately 1 mg [72].

The development of ICP-AE represented a significant advance in the use of emission spectroscopy and in the analysis of glass for forensic purposes [61, 73-80]. Glass samples can be introduced in the plasma either by dissolving them and nebulizing the resulting solution or by direct solid sampling. The initial ICP-AES methods for glass analysis were primarily designed for purposes of classification. In 1981, an analytical method using this technique was developed to determine the concentration of Mn, Fe, Mg, Al, and Ba, and together with refractive index measurements, 91% of correct identification was achieved [75]. Over the next several years, the concentrations of additional elements were determined. The most widely used protocol for casework was developed for determining the concentrations of 10 elements (Al, Ba, Ca, Fe, Mg, Mn, Na, Ti, Sr, and Zr) with good precision in milligram-sized glass fragments [61, 76]. ICP-AES has also been used by the Food and Drug Administration laboratories (FDA) to associate baby food containers to the manufacturing plants in which they were made and to identify sources of contaminated glass in cases involving product tampering [80].

In ICP-AES, sample dissolution is a limitation because it destroys the sample, and it is time consuming compared to other methods. In addition, ICP-AES instrumentation is costly and requires more extensive operator training, reason why only a limited number of forensic applications for this technique have been found. An alternative to sample dissolution is direct solid sampling. Laser ablation (LA) ICP-AES has the clear advantage of providing localized analysis with little-to-no sample preparation. The effects of the laser parameters on the amount of glass ablated, and the analytical figures of merit of LA-ICP-AES for the study of glass have been reported in the literature [73, 74]. Another AE technique with direct solid sampling is LIBS. More on LIBS and forensic glass analysis will be discussed further in this chapter.

X-Ray Methods

Numerous studies of discrimination and categorization of glass fragments based on X-ray methods and direct comparisons with other elemental analysis techniques have been reported in the literature. X-ray analysis techniques such as Wavelength-Dispersive X-ray Fluorescence (WD-XRF)[81-83], Wavelength-Dispersive Electron Probe Microanalysis (WD-EPMA)[82, 84], Scanning Electron Microscopy with Energy-Dispersive X-ray microanalysis, (SEM-EDX)[82, 85, 86], Energy-Dispersive X-ray fluorescence spectrometry (ED-XRF)[61, 81, 87-89], synchrotron radiation X-ray fluorescence spectrometry [67, 90-93] and Total reflection X-ray fluorescence (TXRF) [94] have been successfully applied for the analysis of forensic glass fragments. For example, SEM-EDX has been reported for discrimination of glass samples. In this study, 81 samples, indistinguishable by RI and density measurements, were efficiently discriminated (~97.5% correct identification) by SEM-EDX using calcium concentrations and the elemental ratios to calcium for Ti, Mn, Fe, Cu, Zn, As, Rb, Sr, and Zr [89]. Another SEM-EDX method, with similar results, was later reported using instead Na/Mg, Na/Al, Mg/Al, Ca/Na, and Ca/K concentration ratios [86]. The ability to standardize the peak area ratios from different X-ray fluorescence instruments for the collected glass data to be related and compared has also been studied [88]. Effective glass identification of 23 glass fragments was achieved by comparison of five elemental ratios of Ti/Sr, Mn/Sr, Zn/Sr, Rb/Sr, and Pb/Sr calculated from TXRF spectra [94]. Synchrotron radiation XRF has also been successfully applied to the discrimination of glass using quantitative data of six elements: Ca, Fe, Sr, Zr, Ba, and Ce [93].

The most significative advantage of X-ray methods is that they are non-destructive. In addition, spectra are relatively simple, there is little spectral line interference, relatively small samples can be analyzed and the multi-element analysis capability makes it a speedy and convenient technique for forensic samples. The main limitations are that matrix-matched multi-

element standards are needed to obtain accurate quantitative results. Actually, quantitative analysis of forensic glass has been best achieved by an evaluation of the ratios rather than by the absolute concentration of the elements. Very small and irregularly shaped samples are not amenable to this type of analysis. Commonly, sample preparation requires embedding the glass fragments in a plastic resin and then polishing the surface until flat by grinding methods. The surface is usually coated with a carbon layer and the fragment is sampled at different locations [52].

Inorganic Mass Spectrometry

Inductively coupled plasma mass spectrometry (ICP-MS) combines the multi-element capability and the broad dynamic range of ICP emission with the enhanced sensitivity and ability to perform quantitative analysis of the elemental isotopic concentration and ratios. Typically, samples are introduced into an ICP-MS by aspirating a solution of the sample. Often, liquid samples require little preparation, but solid samples need to be dissolved. This preparation process requires time and use of acid-dissolution reagents.

ICP-MS has been successfully applied for the discrimination of glass [68, 70, 92, 95-103]. The first reported application of ICP-MS to forensic glass analysis was made in 1990 [70] Seven glasses, statistically indistinguishable by RI, were 85-90% successfully discriminated. The samples were as small as 500 μg with detection limits below 0.1 ng mL^{-1}. Later, a more extensive investigation of ICP-MS analysis was presented [101]. Sample digestion methods were compared and up to 62 elements were determined in a range of glass samples. Successful differentiation of glasses of similar RI was accomplished by comparing element concentrations and ratios (e.g., Sr/Ba). The precision of ICP-MS, percentage relative standard deviation (RSD) < 3.9%, in trace element concentration determination was sufficient to provide adequate discrimination.

The incorporation of laser ablation (LA) in ICP-MS has greatly simplified the analysis of glass samples [100, 103-120]. There is already a validated method for glass discrimination using LA-ICP-MS [107]. The elemental menu comprises 10 elements: K, Ti, Mn, Rb, Sr, Zr, Ba, La, Ce, and Pb. It was shown than the method could be used for glass fragments sizes down to $1mm^2$ with limits of detection (LOD) in the order of $\mu g\ g^{-1}$, and precision and accuracy <10% for most of the measured elements. Current work suggests LA-ICP-MS offers great promise for the fast and accurate multi-element comparison of small samples in a non-destructive manner.

Advantages of this technique include minimal sample preparation, multi-elemental capability, greater sensitivity and better detection limits than conventional absorption and emission techniques, speed of analysis, and minimal sample destruction and contamination. However, in spite of its relatively high sensitivity, this technique is very expensive, which precludes its use in many forensic laboratories. Another limitation, which also affects LIBS, is its matrix dependence: laser parameters change depending on the matrix. Moreover, the quantification is less straightforward than with solution analysis due to the lack of solid calibration standards, particularly matrix-matched standards. Laser ablation is also susceptible to elemental fractionation. Fractionation is a dynamic process that includes the effects of the ablation, sampling, transport, and ionization and is defined as producing ablation products that are not stoichiometrically representative of the sample composition [52, 115].

LIBS and Glass Analysis

In this study, LIBS is proposed as a viable alternative for glass analysis. LIBS has the potential to become an attractive technique for forensic applications. A few forensic applications have been reported for the analysis of gun pulse residues[121], minerals in hair[122], Rb traces in blood [123], detection of latent fingerprints [124], wood in a murder case [125], analysis of human cremation remains and elemental composition analysis of prosthetic implants [126].

Our group has evaluated the potential of LIBS for discrimination of glass samples of similar RI values by comparing the LIBS spectra over a short period of time (same day) [127]. Research by Bridge et al.[108] have recently focused on the characterization of automobile glass fragments by LIBS and LA-ICP-MS. For the LIBS analysis, 18 ionic and atomic emission lines, from the elements Al, Ba, Ca, Cr, Fe, Mg, Na, Sn, Si, and Ti, were evaluated and used to form ten different ratios of emission intensities. With use of these ratios, 93 and 82% correct discrimination of 23 glass samples was achieved at confidence intervals of 90 and 99%, respectively. With the addition of RI data, the discrimination was improved to 100 and 99% for the confidence intervals of 90 and 99%. Later, this study was extended to the examination of four sets of glasses (automobile windows, headlamp, and side mirror, and drink container glasses). The use of LIBS in combination with RI determination provided 87% discrimination at a 95% confidence level[128].

Characterization of the influence of irradiation wavelength has been carried out on the analytical results form glass matrices with varying optical and elemental composition by Barnett et al.[129] Two harmonics of the Nd: YAG laser (266 and 532 nm) were used to create the plasma of several glass standards and soda-lime glass samples. Good correlation for the quantitative analysis results for Sr, Ba, and Al were reported along with the calibration curves. The Nd: YAG 532 nm laser produced greater emission intensities with less mass removal than the 266 nm laser. Later, the authors present a comparison study of LA-ICP-MS, micro-XRF, and LIBS for the discrimination of 41 automotive glass fragments [130]. Excellent discrimination (>99%) results were obtained for each of the methods. Different combinations of 10 element ratios for the elements Al, Na, K, Ca, Fe and Sr were employed for the analysis and discrimination by LIBS.

Consequently, good performance of LIBS is encouraging for its use in forensic laboratories. There have been previous studies of glass analysis by LIBS, although they did not focus on discrimination analysis for forensic purposes [131-154].

Conclusions

Currently, there are a number of satisfactory techniques available for the elemental analysis of glass fragments for forensic purposes. Each of the various instrumental techniques has particular strengths and limitations. Table 2-2 summarizes the characteristics of some of the instrumental techniques described in this chapter. Every one has its advantages and disadvantages and all of them have found applications in forensic science laboratories.

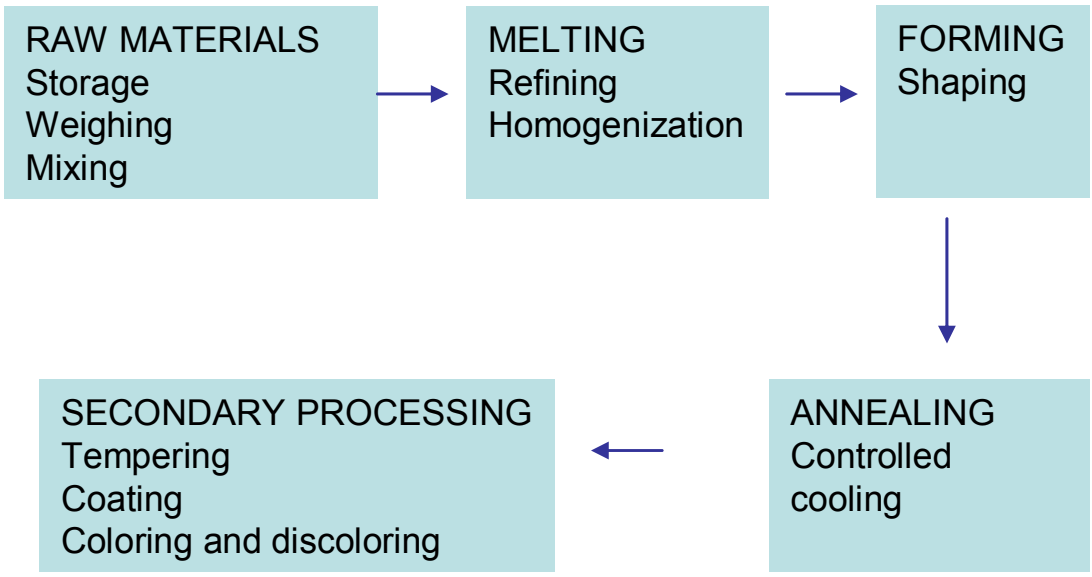

Figure 2-1. The glass-manufacturing process. Adapted from Ref. [52]

Table 2-1. Composition of soda-lima container glass. Standard Reference Material (SRM) 621 from the National Institute of Standards and Technology (NIST).

Constituent	Percent by weight
SiO_2	71.13
Na_2O	12.74
CaO	10.71
Al_2O_3	2.76
K_2O	2.01
MgO	0.27
SO_3	0.13
BaO	0.12
Fe_2O_3	0.040
As_2O_3	0.030
TiO_2	0.014
ZrO_2	0.007

Table 2-2. Characteristics of the instrumental methods for the elemental analysis of glass. Adapted from Refs.[127, 130]

Characteristics	AA	XRF	ICP-AES	ICP-MS	LA-ICP-MS	LIBS
Detection limit (ppm)	1	100	0.1 – 1	< 1	< 1	10-50
Sample penetration (microns)	-	100	-	-	80	50-100
Multi-element	No	Yes	Yes	Yes	Yes	Yes
Destructive	Yes	No	Yes	Yes	No	No
Sample preparation	Yes	Yes (low)	Yes	Yes	No	No
Cost	Low	Moderate	Moderate	High	Very high	Low
Ease of use	Easy	Intermediate	Intermediate	Difficult	Difficult	Easy
Glass discrimination	Fair	Good	Good	Very good	Excellent	Good

CHAPTER 3
CORRELATION ANALYSIS AND THE DISCRIMINATION OF GLASS FOR FORENSIC APPLICATIONS

Introduction

As discussed in chapter 2, material analysis and characterization can provide important information as evidence in legal proceedings. The potential of LIBS for the discrimination of glass fragments based on correlation analysis is presented in this chapter. In this study, we examine the LIBS spectra of glass from a slightly different perspective than the ones available in the literature [108, 128, 130]. That is, we do not seek a detailed chemical composition or to calculate intensities or intensity ratios of some particular elements. Instead, we identify glass fragments from their unique LIBS spectral "fingerprints" by using statistical correlation methods.

The procedure used in this research is the following. First, an unknown glass fragment is identified by correlating its spectra against an available spectral database. Second, the spectra of the fragments are compared against each other to statistically determine if they originated from the same glass source. Third, the long-term reproducibility of the analysis is presented. Optimal sampling conditions for acquisition of accurate LIBS spectra are also reported. A summary of the results and their statistical significance is presented.

Experimental

Samples

A total of ten fragments from seven automobile glasses (side and rear windows) were used in this study. These ten fragments provide 45 possible pair comparisons. They were collected from automobiles at a local auto glass shop corresponding to 5 years of manufacturing and five vehicle manufacturers. Their height, length, and width were approximately 0.3, 1.0, and 0.9 cm, respectively. All of them were transparent and uncoated. A more detailed sample description is shown in Table 3-1.

All samples were mounted on a microscope glass slide using double-sided mounting tape and then placed on an XYZ translation stage that allows movement of the sample to a fresh spot. A laser positioning system consisting of a diode laser and a photodiode detector ensured a reproducible position of the sample.

Instrumentation and Data Acquisition

The LIBS instrumentation used in this study consisted of an Ocean Optics (Dunedin, FL, USA) LIBS2000^{+}spectrometer coupled to a Big Sky (Bozeman, MT, USA) Ultra *Q*-switched Nd:YAG laser operating at 1,064 nm. This laser delivered a maximum of 50 mJ in 10 ns, providing an irradiance of approximately 5.2 GW/cm^2 on the sample surface. The laser beam was focused onto the glass surface using a 5-cm focal length lens. The radiation emitted by atoms ablated from the glass samples was collected by a quartz lens and guided into a seven-channel spectrometer. It is worth pointing out that the optical collection system used in this work was not achromatic: this may affect the line intensities obtained in widely different spectral regions and as a consequence also the discrimination power. Chromatic effects should then be taken into consideration when transferring different spectra from laboratory to laboratory. Each channel covered a spectral range of about 100 nm; the full range of the spectrometer was from 200 to 980 nm. The detector was a linear CCD with 2,048 pixels. The instrument spectral resolution (full width at half maximum) was 0.1 nm.

The instrumental parameters used were as follows: laser power 50 mJ per pulse, detector delay time and gate width 1 μs and 2 ms, respectively. For data acquisition, each sample was ablated at 15 positions; each position consisted of 130 ablation pulses at 1 Hz and the data were obtained at atmospheric pressure. The first 30 spectra were discarded and the next 100 were averaged, providing an individual spectrum per position on the sample. For the correlation analysis, 15 individual spectra per sample were averaged to create a sample library.

Software

A homemade program for correlation analysis written in Visual Basic 6.0 was used [155]. This program has already been successfully applied to the identification of different classes of materials using their LIBS spectra [155-158]. The program allows creation of libraries by averaging individual spectra. Linear and rank correlation coefficients are calculated for each individual spectrum versus the library. Finally, a correlation plot is displayed, corresponding to the maximum correlation coefficient and the name of the sample associated with the highest correlation coefficient.

Results and Discussion

Sampling Considerations

Experimental conditions capable of providing high precision and repeatability between experiments are needed to obtain an accurate spectral fingerprint of each sample.

First, the effect of the laser power was studied. The Nd:YAG laser used has a specified maximum pulse energy of 50 mJ which can be changed in increments of 5 mJ. In our experiments, it was found that the highest laser power (50 mJ) resulted in better signal-to-noise ratios.

In LIBS, small unpredictable experimental fluctuations can cause a significant change in the appearance of the spectra. To check the stability of our measurement setup the following procedure is envisaged: the intensity of a Si atomic line at 288.16 nm is chosen and monitored at regular time intervals in a standard glass sample (NIST 612) used as a reference for the optimization of the experimental setup. The analysis is not continued and correlation is not performed if the difference in the intensities observed for this line exceeded the expected statistical variation of our method, $\sigma = \pm 15\%$. In this case, the entire experimental setup is inspected and optimized again until the results are satisfactory. In particular, three experimental

parameters are checked, namely, the alignment of the collection optics with respect to the plasma volume observed, the focusing distance of the laser beam on the target, which affects the ablation efficiency, and the short-term pulse-to-pulse energy fluctuation of the laser.

A detector delay of 1μs and a fixed spectrometer integration time of 2.1 ms were used. These values resulted from an optimization study carried out for the detection of carbon in soils[159]. Although the choice seems to be arbitrary, in view of the different matrices examined, the optimization study was repeated with different samples such as glass and cast iron standards, confirming the choice of the values obtained previously. The repetition rate did not play a significant role during data acquisition and was set at 1 Hz.

No sample preparation is required for elemental analysis by LIBS. However, relatively low spectral intensities were recorded after the first laser pulse which slowly increased, reaching a constant value after approximately 25 pulses on the same sample spot; this behavior is only observed when working with glass fragment samples. Fig. 3-1 presents a typical plot of the variation of net intensities for the glass fragments (number of counts above the background level) for six emission lines versus the number of laser pulses (up to 250) at one spot on the sample. This behavior is caused by the laser–glass interaction [73, 106]. For the first few laser pulses, the samples were almost transparent and there was minimal ablation. However, as the glass interrogation progresses, defects in the glass were formed, making ablation stronger. Thus, about 25 preparation pulses were needed, in our case, to achieve reproducible ablation.

The percentage relative standard deviation (%RSD) of the net intensity versus the number of laser pulses at one sample spot (in groups) is shown in Fig. 3-2. It is observed that the RSD values decrease from 100 to 300% RSD for first 30 pulses to 15–20% RSD for the next 200 pulses. Consequently, the first 30 ablation pulses were discarded and considered as preparation

pulses. The influence of the roughness of the glass surface was not examined but it has been reported not to cause significant changes in the emission spectra of glass [120, 137].

To determine the number of individual spectra to be averaged for the analysis, 180 pulse measurements were made at each position; ten positions per sample were examined. The first 30 spectra of each measurement were discarded and the remaining spectra were averaged in groups. The percentage RSD was calculated by using the averaged signals from each of ten sequential measurements. The plot of the percentage RSD against the number of averaged individual spectra is presented in Fig. 3-3 for some emission lines. It was found the percentage RSD reached a constant level of 10–20% after approximately 30 pulses; therefore, 100 individual spectra were averaged per position in our measurements.

Next, the effect of day-to-day changes in humidity, which might affect the laser air spark [160], was studied. The intensity of the hydrogen Balmer α emission line at 656.3 nm was monitored for this purpose since its variation is an indication of the changes in humidity of the ambient air. No significant changes in humidity were observed in 1-week period, and to simplify the sampling our experiments were performed in ambient air. In general, the overall reproducibility of the spectra taken on different days was within a variation of $\sigma = \pm 15\%$.

The effect of the offset distance or focal depth on pulse-to-pulse reproducibility was also considered. The offset distance is the difference between the lens-to-surface distance and the focal length of the lens[161]. It is an important parameter that must be held constant to obtain reproducible spectra[162]. No significant change in precision was found when moving the sample up or down 5mm relative to the focal point of the lens and we simply focused the laser on the sample's surface.

The minute amount of material removed per sample spot was approximately 3 μg. The mass ablated per spot was determined after examining the crater made with a calibrated optical microscope and using the known value of the density. The overall precision of these measurements was estimated to be approximately 10%. This mass of material has been proven to be representative of the whole piece of glass in studies using synchrotron micro XRF spectrometry[163] and LA-ICP-MS[114].

Sample Identification by Linear and Rank Correlation

Linear correlation measures the strength of the linear relation between two variables, in our case two glass LIBS spectra. The Pearson correlation coefficient, also known as linear correlation coefficient, is given by

$$r = \frac{\sum_i (x_i - \bar{x})(y_i - \bar{y})}{\sqrt{\sum_i (x_i - \bar{x})^2}\sqrt{\sum_i (y_i - \bar{y})^2}} \tag{3-1}$$

where $\bar{x}$ represents the mean of x's and $\bar{y}$ is the mean of the y's from two data sets; x_i and y_i are intensities of the two spectra measured at the same pixel i.

We also used the rank (Spearman) correlation coefficient. The equation for rank correlation is similar to Eq. 3-1 but the values of the x and y distributions are replaced by their corresponding ranks R and S:

$$r = \frac{\sum_i (R_i - \bar{R})(S_i - \bar{S})}{\sqrt{\sum_i (R_i - \bar{R})^2}\sqrt{\sum_i (S_i - \bar{S})^2}} \tag{3-2}$$

where the ranks have numbers 1, 2, 3, …, N. The highest rank, N, is the total number of data points, or the highest pixel number. These ranks replace the true values of the x values and the y values in accordance with their magnitudes.

The value of *r* lies between -1 and +1. Values close to zero indicated uncorrelated data sets. The absolute value of *r* can be used as an indicator of the association between the data sets since the strongest correlation is represented by the absolute value of 1.

This study focused on the identification of ten glass fragments using linear and rank correlation coefficients. Fifteen individual spectra were collected from each sample. Each spectrum was the average of 100 ablation pulses. We refer to a library as the collection of averaged spectra; a library was created containing ten averaged spectra (library 1). Each of the 150 individual spectra were correlated against the library spectra. The highest correlation coefficient indicated a similarity of a tested spectrum to one from the library. The difference between this and other correlation coefficients indicates spectral and, hence, compositional differences.

The results obtained on the "yes–no" basis for the identification of the 150 individual spectra (set 1) using correlation coefficients are presented in the top half of Table 3-2. These results include the name of the library the individual spectrum was "identified as" and the number of times (out of 15) correct identification was achieved. All the data points present in the spectra (13,701 pixels) were used for the correlation. From this table, linear correlation suggests that there is similarity between samples A2 and A3 and between samples A5 and A6, which is in fact correct since those glass fragments came from the same window. However, linear correlation did not identify similarities between samples A8 and A9, which also came from the same source. The rank correlation also indicates similarities for pairs A2 and A3 and A5 and A6, as does the linear correlation, but in addition suggests similarities for pair A1 and A9, which are not expected since these two samples came from different sources. Rank correlation also failed to identify similarities between samples A8 and A9. It is important to mention that all these ten

samples have very similar LIBS spectra, and the correlation coefficients between these samples are all in the range of 0.9 or higher. This is understandable since all the samples have very similar elemental composition.

It is important that identification is reproducible within an arbitrary long time period, e.g., spectra from unknown samples taken on different days could be compared with the existing spectral library. For this purpose, a new experiment was performed in a period of 1week. This time, however, only five individual spectra were collected from each sample, under the same experimental conditions reported earlier, and a new library was created containing ten averaged spectra (library 2). The identification of individual spectra for this second set of data compared with library 2 showed similar results to the results obtained previously and presented in the top part of Table 3-2. In addition, this set of individual spectra was correlated versus the library created the previous week (library 1). The bottom half of Table 3-2 shows that the correlation coefficients obtained by linear correlation indicate similarities for pairs A2 and A3, A5 and A6, and A8 andA9, which came from the same window; there were also no misidentifications. On the other hand, rank correlation also suggests similarities for the three previous pairs but in addition shows similarities for pairs A1 andA9 and A4 and A5, which were not expected since the samples were from different sources. So far, it is felt that linear correlation provides good identification for samples that are the same and distinction for the ones that are different even when the data are obtained on different days. Therefore, linear correlation is robust with respect to changes in spectral intensities on different days.

Besides the apparent differences and similarities between samples determined by the use of correlation coefficients, strict statistical criteria must be applied in order to quantify the level of significance. To do so, a simple analysis by Student's *t* test was applied. This hypothesis test

determines whether two normally distributed populations are significantly different[164]. The normality of the distribution of the correlation coefficients was confirmed using normality plots (*Q–Q* plots). If the test's *p* value is less than the significance level chosen ($\alpha = 0.05$ to give a 95% confidence level) the null hypothesis is rejected and it is concluded that the samples are different. Otherwise, the results suggest there is no significant difference between the two populations; in other words, there is no significant difference between the two samples.

Based on these *p* values, the top half of Table 3-3 presents the discrimination between glass fragments when the second set of individual spectra was correlated against the library created a week earlier (library 1). The *p* values for linear correlation coefficients indicate no significant difference for the means of pairs A2 and A3 and A5 and A6, which was expected. However, linear correlation also indicates that a significant difference exists between samples A8 and A9, which is not true. Therefore, linear correlation provides 98% correct identification at a 95% confidence level. On the other hand, the *p* values for rank correlation coefficients indicate no significant difference for the means of pairs A2 and A3, A5 and A6, and A8 and A9, which is correct and expected. However, this analysis also indicates similarities for pairs A1 and A8, A1 and A9, A1 and A10, and A4 and A5, which is incorrect, providing an overall 91% correct identification at a 95% confidence level.

We conclude, therefore, that linear correlation provides better results than rank correlation but does not find similarities for samples A8 and A9. Rank correlation finds these pair to be similar but suggests that four other pairs are also similar.

To improve correlation analysis of spectra, "masking" the spectra prior to evaluation was chosen. Masking is a simple multiplicative process that retains only the selected peaks of the components to be analyzed, thus eliminating analytically useless parts of the spectra (e.g., peaks

or bands from the matrix) [165, 166]. The criteria for choosing a valid mask is to strengthen spectral similarities between samples that are the same and improve differences for the ones that are different. One of the consequences of better quality control in the manufacture of glass is less variability between concentrations of major elements, e.g., Si, Mg, Na, Ca, Fe, and Al. As a result, analysis of trace element impurities within major materials emerges as a useful path for discrimination [70]. Some high-intensity lines from major elements present in glass were blocked since the concentrations of those elements are expected to be very similar among the glass fragments. By doing so, we focused our analysis on elements of lower concentration. Fig. 4-4 shows the spectral lines that were masked for the analysis.

It is advantageous to eliminate regions of the spectrum where no lines are present since the noise affects negatively the correlation coefficients. Another possibility of masking is to correlate lines from the trace elements present in the samples instead of just blocking the high-intensity lines; however, this might require a higher-resolution spectrometer capable of resolving and detecting K, Ti, Mn, Rb, Sr, Zr, Ba, La, Ce, and Pb, which have been proven to provide effective discrimination by LA-ICP-MS [107].

The results obtained when using the spectral mask are presented in the bottom half of Table 3-3. Linear correlation revealed that three pairs are indistinguishable (A2 and A3, A5 and A6, and A8 and A9); therefore, linear correlation together with masking provides 100% correct identification at the 95% significance level. By rank correlation, these pairs are also similar, but three pairs (A1 and A9, A1 and A8, and A4 and A5) out of 45 possible pair combinations are also judged to be similar, yielding 93% correct identification at a 95% significance level.

It is clear that masking improves the result by linear correlation. However, there is no significant improvement with rank correlation, probably owing to the nature of the mask itself,

which only blocks high-intensity lines. Current research in our group suggests that rank correlation is very sensitive to noise and less sensitive to small systematic changes in line intensities [167]. Therefore, only linear correlation is the method of choice.

Conclusion

In this work, linear and rank correlation techniques were applied for discrimination of LIBS spectra from glass samples with similar chemical composition, some of them from the same source. The robustness of this technique was demonstrated by the 100% correct identification (95% confidence level for a type 1 error) obtained by linear correlation when used in combination with a spectral mask. The identification was reliable even when experiments were performed on different days when ambient conditions might be different and affect the line intensities in the LIBS spectra.

The rationale of using spectral masking is to eliminate regions of the spectra containing several intense lines common to all samples and to take advantage of the trace element impurities present in these glasses. We are aware of the fact that there are more sophisticated ways to generate a mask than the one used in this study. However, it was felt useful to focus at first on a simple masking procedure to see whether any further elaboration of this concept was worth pursuing. More refined procedures are planned for the future.

The main advantages of this LIBS method relative to other elemental analysis studies of glass for forensic applications are:

- Lack of sample preparation
- Short analysis time, since spectral acquisition and correlation analysis could be done in minutes.
- No need for quantification or calculation of intensity ratios
- No need for supplemental measurements such as measuring RI values

Future work for this study might include the use of masks for spectral regions instead of lines, the use of background correction, and a study of different normalization procedures to assess the quantitative analytical performance of the technique.

In conclusion, elemental analysis of glass by LIBS has the potential of becoming a useful technique for the discrimination of forensic glasses. Its usefulness as an analytical method for legal purposes will be determined by its general acceptance in the relevant scientific community. Evidence of "general acceptance" normally includes known error rates and publication of the methods in peer-reviewed journals[168]. These legal aspects and corresponding implications, which would require more in-depth statistical analysis, have not been considered in this work.

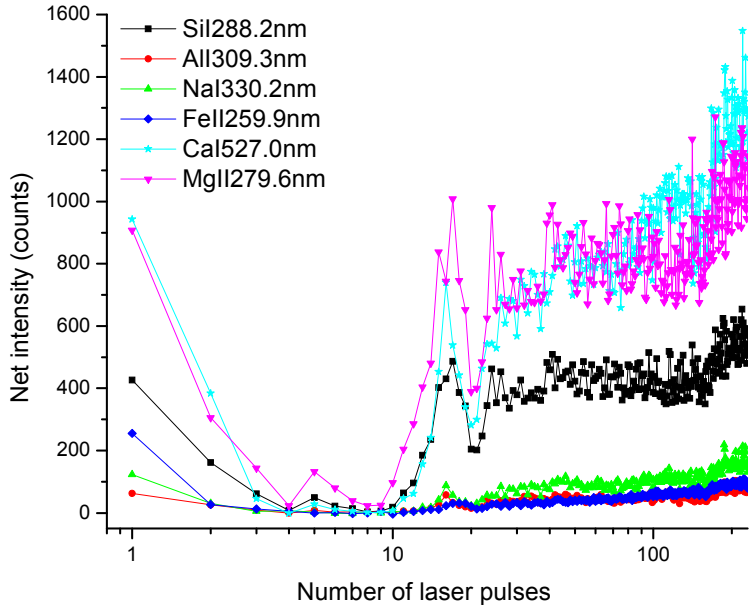

Figure 3-1. Intensity dependence with the number of laser pulses

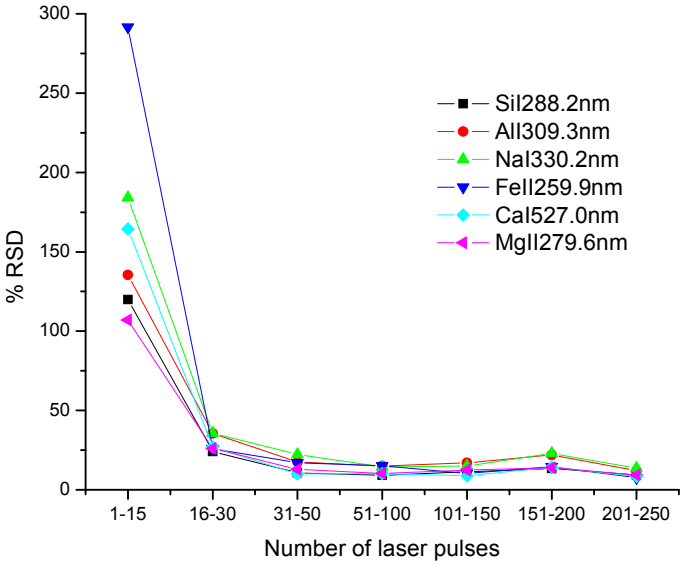

Figure 3-2. Percentage relative standard deviation (%RSD) variability with the number of laser pulses on the same spot

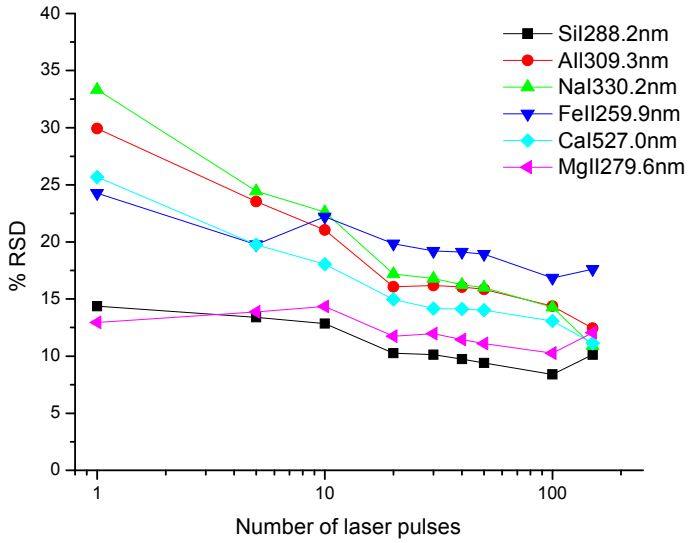

Figure 3-3. Percentage relative standard deviation (%RSD) variability with the number of laser pulses on separate spots

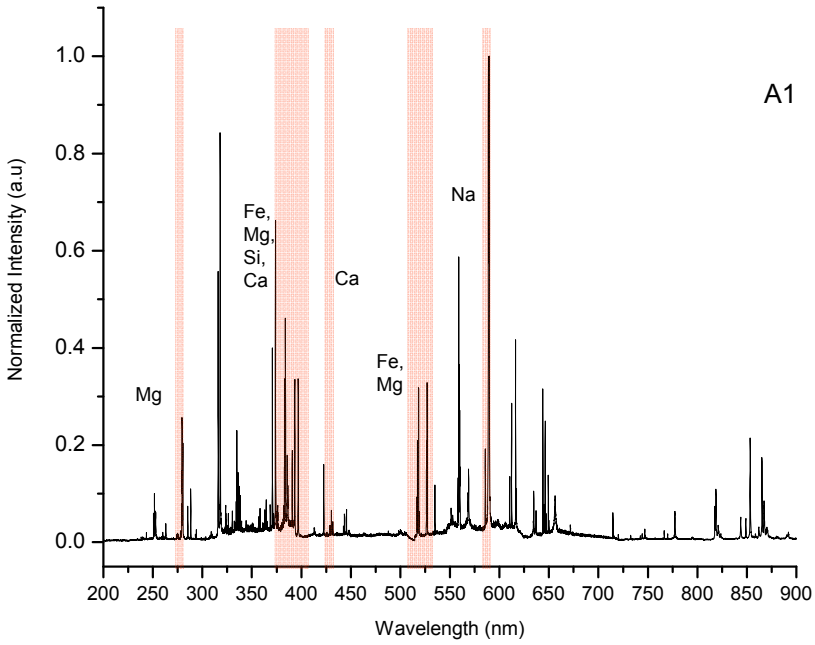

Figure 3-4. Spectral lines that were masked for the analysis

Table 3-1. Information of the glass samples

Sample name	Vehicle information
A1	2007 Buick Lucerne, side window
A2	2002 Ford Focus, rear window
A3	2002 Ford Focus, rear window
A4	2003 Honda Accord, side window
A5	2003 Toyota Tundra rear window
A6	2003 Toyota Tundra rear window
A7	2002 Toyota Camry side window
A8	2004 Chevy Blazer side window
A9	2004 Chevy Blazer side window
A10	2003 Chevy Trailblazer side window

Table 3-2. Identification using linear and rank correlation. First and second set of individual spectra are correlated against spectral library 1.

	A1	A2	A3	A4	A5	A6	A7	A8	A9	A10
	First set of individual spectra correlated against spectral library 1									
Linear	A1 (15/15)	A2 (10/15) A3 (5/15)	A3 (13/15) A2 (2/15)	A4 (15/15)	A5 (8/15) A6 (7/15)	A6 (11/15) A5 (4/5)	A7 (15/15)	A8 (15/15)	A9 (15/15)	A10 (15/15)
Rank	A1 (12/15) A9 (3/15)	A2 (12/15) A3 (3/15)	A3 (14/15) A2 (1/15)	A4 (15/15)	A5 (11/15) A6 (4/15)	A6 (8/15) A5 (7/15)	A7 (15/15)	A8 (15/15)	A9 (13/15) A1 (2/15)	A10 (15/15)
	Second set of individual spectra correlated against spectral library 1									
Linear	A1 (5/5)	A2 (5/5)	A3 (1/5) A2 (4/5)	A4 (5/5)	A5 (5/5)	A6 (1/5) A5 (4/5)	A7 (5/5)	A9 (5/5)	A9 (1/5) A8 (4/5)	A10 (5/5)
Rank	A9 (5/5)	A2 (5/5)	A2 (5/5)	A4 (5/5)	A5 (1/5) A4 (2/5) A6 (2/5)	A6 (3/5) A5 (2/5)	A7 (5/5)	A8 (5/5)	A9 (1/5) A1 (1/5) A8 (3/5)	A10 (5/5)

A*z* (*x*/*y*) : *x* out *y* individual spectra are identified as sample *z*.

Table 3-3. Detected similarities between samples using p-values obtained by Student's T-test (p-value >0.05)

	A1	A2	A3	A4	A5	A6	A7	A8	A9	A10
	All lines in the spectrum are used, no spectral mask									
Linear		A3	A2		A6	A5				
Rank	A8	A3	A2		A4	A5		A9	A1	
	A9				A6				A8	
	A10									
	Selected lines in the spectrum are used, spectral mask is applied									
Linear		A3	A2		A6	A5		A9	A8	
Rank	A8	A3	A2		A4	A5		A9	A1	
	A9				A6				A8	

CHAPTER 4
COMPARATIVE STUDY OF FOUR LIBS SYSTEMS FOR THE ANALYSIS AND IDENTIFICATION OF SOLIDS

Introduction

Identification and discrimination of individual specimens out of a set of similar samples, can be considered as an important task for forensic applications and for the industrial sorting of materials. Consequently, as much spectral information as available should be used for an accurate sample identification analysis. This means that a spectrometer should be capable of first, resolving individual emission lines while avoiding spectral interferences and second, recording a large spectral interval for obtaining a detailed spectral fingerprint of the material of interest. Material identification using LIBS spectra has been demonstrated to successfully discriminate between compositionally close materials [155, 156, 158, 169-176]. Our group has contributed to the development of a LIBS-based method for identification of different types of materials [155-158, 167, 177] .

The growing interest on LIBS, together with the broad availability of less expensive and more robust lasers, high-resolution spectrometers, and the ease of data collection and processing make this technique very popular in many analytical labs. Moreover, there are already several LIBS systems with the above configuration available on the commercial market. The final choice of a system is merely determined by the desirable mode of instrument operation (laser, spectrometer and detector), the type of application and monetary constraints.

The purpose of this study is to evaluate the performance of four spectrometers for the specific task of quantitative compositional analysis and identification of alloys. Three echelle grating spectrometers: Aryelle (LTB Lasertechnik Berlin, Germany), SE200 (Catalina Scientific Instruments, USA) and Mechelle 5000 (Andor Technology, USA), and a conventional broadband grating spectrometer LIBS 2000^{+} (Ocean Optics, USA) were used sequentially to collect spectra

from the same samples under the same laboratory conditions. Instrumental characteristics such as resolution, LOD, and reproducibility were measured and compared. For material identification, correlation analysis was performed using spectra and spectral libraries collected with the same or other spectrometer from the group. The effect of spectrometer characteristics on the robustness of identification was investigated. The results of this study may assist one in choosing an adequate spectroscopic system based on a reasonable compromise between the system performance and its cost.

Experimental

To fairly compare the performance of the four spectrometers for LIBS analysis, the experiment was carried out using the same laser source and light collection geometry. Due to manufacturer's configurations each spectrometer was coupled to a different detector.

LIBS Setup

The laser used for these studies was a 1064 nm Q-switched Nd:YAG, model Ultra manufactured by Big Sky Laser Technologies, USA. This laser delivered maximum pulse energy of 50 mJ with a length of 10 ns. The laser beam was focused onto the sample surface using a 5 cm focal length lens, which resulted in an irradiance of ~5.2 GW/cm^2 on the sample surface. The radiation emitted by atomic and ionic species ablated from the sample was collected by a quartz lens and guided into the spectrometers. Figure 4-1 shows the general experimental setup used with the four systems.

A sample was placed on an XYZ translation stage for sample height adjustment and fresh spot ablation. A laser positioning system consisting of a diode laser and a photodiode detector ensured a reproducible height positioning of the sample.

For data acquisition, each sample was ablated at 10 positions; each position consisted of 35 ablation shots taken at 50 mJ, 10 Hz and atmospheric pressure. The first 10 spectra were

discarded and the next 25 were averaged providing an individual spectrum per position on the sample. For the correlation studies, 10 individual spectra per sample were averaged to create a sample library.

The principal technical characteristics of the spectrometers and detectors used in this study together with the delay/gate combinations are presented in Table 4-1.

Samples

Seven cast iron standards (SRM 232-239, Cast Irons C18.8, Czechoslovakian Research Institute) were used. These standards are compositionally close to each other with small (~ <1%) variation in concentrations of trace components (Cr, Ni, Mn, Co, Si, etc). The composition of these standards is presented in Table 4-2.

Methods

Calibration curves for some selected spectral lines representing different elements present in the samples were recorded using matrix-matched standards.

For material identification by linear correlation methods, a home-made program, described in Chapter 3 was used.

Results and Discussion

Spectral Resolution

High spectral resolution is helpful because it reduces spectral interferences caused by other elements and provides more spectral information for correlation analysis.

The spectra of solid cast iron samples recorded with the four spectrometers yield a huge wealth of information for atomic and ionic lines of elements present in the samples. First we compared the spectral resolutions of the spectrometers. Figure 4-2 shows spectral fragments obtained with the four spectrometers for the sample cast iron 236 (91.8% Fe and 1.08% Mn). The experiments show that the spectral resolution of the Aryelle system is approximately three

times higher. Thus, the Aryelle spectrometer can eliminate spectral interferences such as the Fe-Mn line pair at ~294.8 nm shown in Figure 4-2. This figure also shows the Aryelle detection of the atomic Fe line at 294.1nm. Although less than the Aryelle, the Mechelle 5000 spectrometer still shows better spectral resolution than the SE200 and LIBS2000$^+$ systems. The latter has an approximately 30% lower number of pixels per line compared to the other three systems that, in addition, affects the obtainable spectral information.

Limits of Detection and Precision

Quantitative measurements in LIBS rely on a linear relation between the elemental concentration and the corresponding emission signal. Calibration curves were constructed relating the specific line integrated intensity to the corresponding element concentration present in the cast iron standards.

Both, atomic and ionic emission lines were measured for Mn (900 - 18600 ppm). Atomic lines were studied for Cr (180-19200 ppm), and Cu (380-9200 ppm). Each point of the calibration curve corresponds to the average integral intensity of a spectral line based on 10 subsequent measurements. The integral intensity and background subtraction were systematically calculated using self-written software in MATLAB. The calibration plots (Figure 4-3) show good linearity within the concentration range and high correlation coefficients ($R > 0.95$).

The LOD in LIBS are typically poorer than those obtained by other elemental analysis techniques.[178] In the present study the LOD (Table 4-3) were calculated based on the three time standard deviation of the corresponding blank measurement. It should be kept in mind, however, that these results are not general but specific to the experimental equipment and conditions adopted during our experiments. Optimization of LOD was not an objective in this study; LODs better than those in Table 4-3 have been previously reported using lasers with higher energies [178-181].

Under these conditions, the LOD obtained with the Aryelle for manganese and chromium lines were significantly better than those obtained with the other three systems. For the copper line studied, the Mechelle 5000 provided the lowest LOD. In general lower LOD were obtained when working with Aryelle, followed by Mechelle 5000, LIBS 2000^{+} and SE200 in the corresponding order. The missing LOD values in Table 4-3 correspond to lines that were not detected by the specified instruments.

Table 4-3 also presents the precision (in parentheses) as the percent relative standard deviation (% RSD) for 10 consecutive measurements in sample cast iron 236. There were no mayor differences in precision between the spectrometers. However, lowest % RSD values were obtained by the Aryelle for manganese and chromium. For the copper line, Mechelle 5000 provides the best precision in the experiments. The LOD obtained were in close agreement to the precision, e.g., lines with larger LOD have larger % RSD values.

Material Identification by Linear Correlation

This section focuses on the performance of the four spectrometers used for the identification of seven cast iron standards by linear correlation. Ten individual spectra were collected for each sample. Each individual spectrum is the average spectrum from 25 ablation shots. For the correlation analysis, we compare a set of individual spectra vs. a spectral library. We refer to library as the collection of the samples averaged spectra; hence, a library was created containing 7 averaged spectra. Each of the 70 individual spectra was correlated against the entire spectral library and linear correlation coefficients were calculated. The highest correlation coefficient indicated a similarity of a tested spectrum to one from the library. The difference between this and other correlation coefficients indicates spectral and, hence, compositional differences.

Spectra were correlated using only the wavelength range 225-463 nm which was common for all four spectrometers. Excellent identification was achieved for all spectrometers (~100%) when individual spectra were correlated vs. spectral libraries obtained with the same spectrometer (Table 4-4). The somewhat lower performance of LIBS 2000^{+} (~98%) might be caused by its lower spectral resolution and smaller number of pixels per line.

Correlation using spectra and spectral libraries collected with other spectrometers from the group was also studied, e.g. spectra obtained with one spectrometer were compared to the libraries obtained with the other spectrometers. For this purpose, each spectrum, individuals and from the libraries were brought to the same wavelength scale using linear interpolation. Therefore, the converted spectra have the same number of pixels for the group of spectrometers. The use of this type of "inter-correlation" didn't provide good identification probably due to the differences in resolution and sensitivity between the four spectrometers (Table 4-5).

Conclusions

In summary, we have carried out preliminary studies of the performance comparison between four spectrometers in terms of spectrochemical figures of merit and their capability for material identification by statistical correlation methods. We note that this is not an absolute comparison of systems since each spectrometer was coupled to a different detector which affects the overall system performance.

All four spectrometers have essentially the same performance with respect precision. The higher spectral resolution and better LOD of the Aryelle system make it more useful for quantitative analysis and material identification especially when samples are of very similar composition. However, the price of this system is higher than the ones of the other spectrometers. Therefore, the final choice of LIBS system must also be based on the individual application and budgetary constrains.

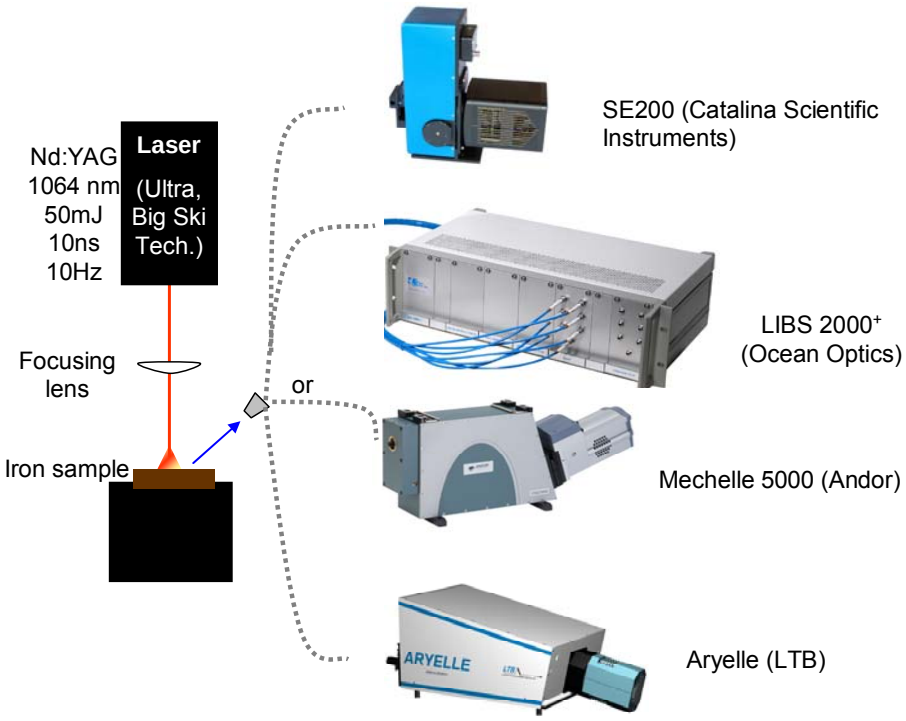

Figure 4-1. Experimental setup used to compare the four systems.

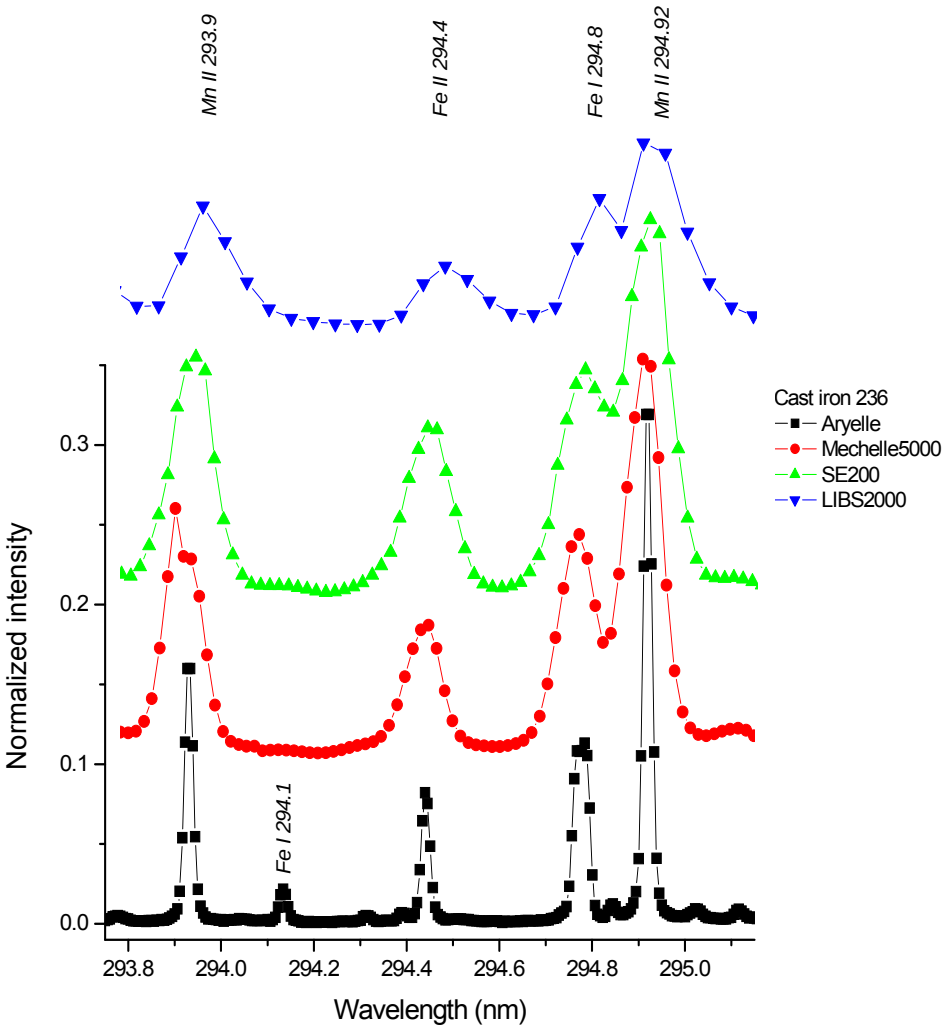

Figure 4-2. Comparison of spectral resolution for the four spectrometers.

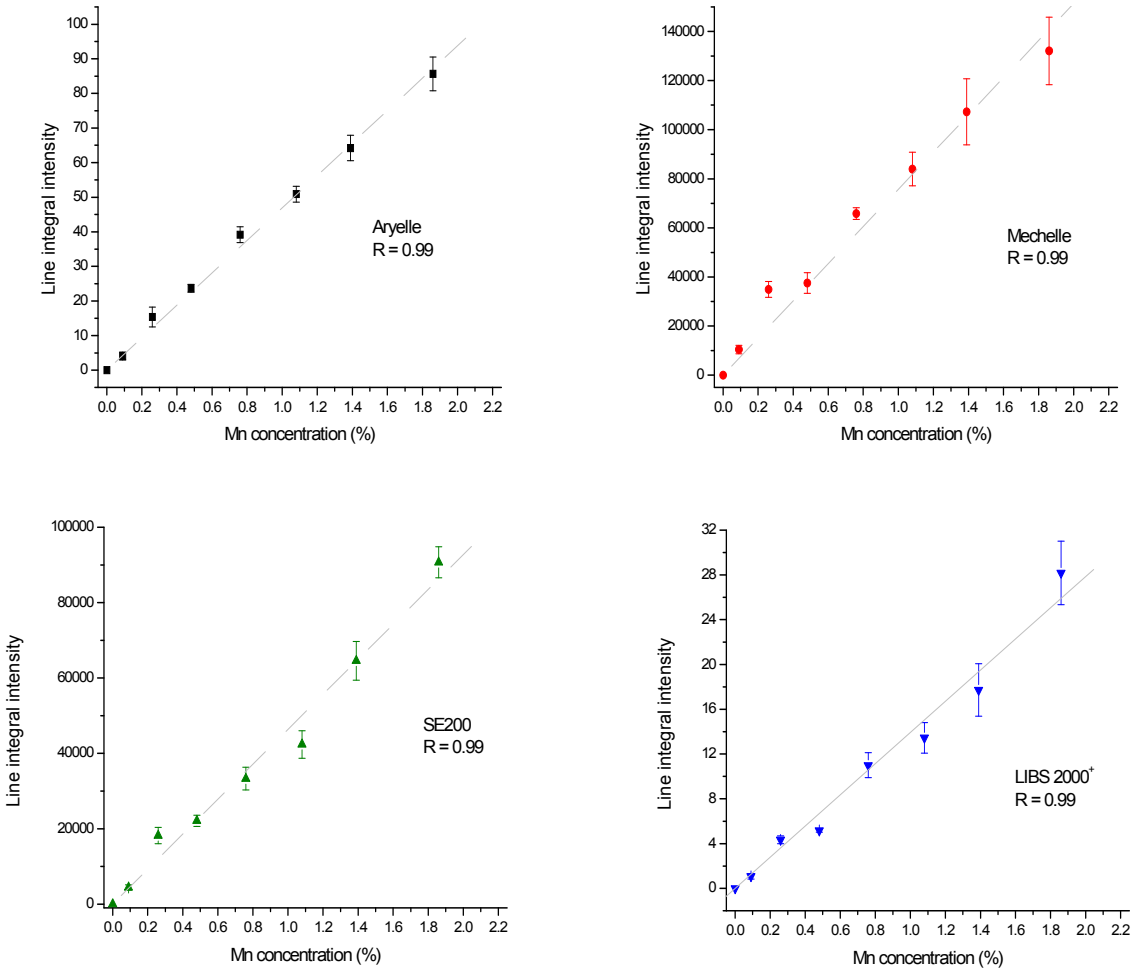

Figure 4-3. Calibration plots for the Mn II ion line at 293.9 nm.

Table 4-1. Technical characteristics of the LIBS spectrometers used in this study.

Characteristic	ARYELLE LTB	MECHELLE5000 Andor	SE200 Catalina Sci. Ins	LIBS 2000^{+} Ocean Optics
Grating	Echelle	Echelle	Echelle	Conventional
Focal Length (mm)	400	195	200	101
Aperture	f/10	f/7	f/10	f/4
Entrance (slit width, um)	50	50	25	10
Resolving power ($\lambda/\Delta\lambda$)	12000	4000	3000	4000*
Dimensions (mm)	438 x 200 x 232	571 x 165 x 160	127 x 152 x 318	130 x 483 x 350
Weight (kg)	12	12	13	8
Detector	CCD (Andor)	ICCD (Andor)	ICCD (Princeton)	CCDs (Ocean Optics)
	2048 x 512 pixels	1024 x 1024 pixels	576 x 384 pixels	7 channels x 2048 pixels
Delay time (μs)	10**	1	1	1
Gate	Non-gated	2μs	2μs	Non-gated, 2ms***
Wavelength range	227 – 465****	200 - 975	190-1100	200-980
Price (US $)	70K	50K	50K	30K
Wavelength calibration	Built-in Hg and Pt spectral lamps	Deuterium/Halogen calibration, Hg-Ar light source	Deuterium/ Halogen calibration, Hg-Ar light source	Deuterium/ Halogen calibration, Hg-Ar light source

* Calculated @ 400 nm, spectral resolution = 0.1 nm
** Delay time set by a mechanical chopper non-gated CCD detector.
*** Integration time
**** This range refers to the instrument available in our laboratory; other ranges can be covered upon request.

Table 4-2. Elemental composition in percentages (%) for Cast Iron Standards C18.8, Czechoslovakian Research Institute.

Standard	C	Cr	Cu	Fe	Mg	Ni	P	Si	Mn
232	1.93	1.19	0.038	91.859	0.007	0.026	0.009	3.5	0.09
233	2.12	1.92	0.11	92.184	0.005	0.062	0.033	2.59	0.26
234	2.46	0.46	0.275	91.969	0.009	0.305	0.38	2.02	1.39
235	2.73	0.41	0.157	91.772	0.005	0.195	0.78	0.92	1.86
236	2.85	0.05	0.215	91.814	0.075	1.77	0.084	1.65	1.08
237	3.03	0.15	0.545	92.135	0.017	0.7	0.175	1.2	0.13
238	3.36	0.018	0.92	91.897	0.046	1.11	0.052	1.55	0.48
239	4.15	0.052	0.085	91.877	0.038	2.42	0.024	0.27	0.76

Table 4-3. Limits of detection (ppm) and precision (% RSD, shown in parentheses) obtained with cast iron standards.

Line	ARYELLE	MECHELLE	SE200	LIBS 2000^{+}
Mn II 257.6	76 (3.8)	630 (6.2)	*	340 (5.6)
Mn II 293.9	190 (4.5)	310 (8.1)	360 (8.6)	270 (10)
Mn II 294.9	130 (4.3)	250 (8.5)	400 (20)	180 (7.0)
Mn I 403.3	260 (6.4)	1600 (12)	*	*
Cr I 425.4	360 (7.4)	1040 (9.8)	6900 (10)	4200 (7.1)
Cr I 427.5	580 (8.9)	2300 (16)	2300 (13)	5700 (7.3)
Cu I 324.8	68 (6.9)	39 (5.3)	370 (11)	250 (10)

* Calibration plots were not constructed for this peak since they were not detected in the spectra.

Table 4-4. Correct Material Identification (%) using linear correlation. Individual spectra were correlated against libraries obtained with the same spectrometer.

SPECTROMETER	CORRECT IDENTIFICATION (%)
ARYELLE	100
MECHELLE	100
SE200	100
LIBS 2000^{+}	99

Table 4-5. Correct Material Identification (%) using linear correlation. Converted individual spectra were correlated against converted libraries.

SET OF INDIVIDUALS	LIBRARIES			
	ARYELLE	MECHELLE	SE200	LIBS 2000^{+}
ARYELLE	100	79	40	39
MECHELLE	43	100	80	66
SE200	31	51	100	29
LIBS 2000^{+}	29	64	31	100

CHAPTER 5
CALIBRATION CURVES FOR THE QUANTITATIVE ANALYSIS OF GLASS

Introduction

Several methods have been proposed to obtain quantitative information from LIBS measurements. Most LIBS applications focus on the determination of various trace elements in a relatively constant matrix. At present, no generally accepted approach exists for the use of LIBS to determine main and trace components in varying matrices. The variation in composition of such samples (e.g., soil, sewage sludge, steel, cement and glass) influences the laser-sample interaction process because of variable absorption, reflection and thermal conductivities properties of the sample surface[182]. Thus, the characteristics of the plasma and the determination of the composition of the sample will be affected [2].

One of the aims of this project is to identify matrix effects occurring in the analysis of glass by LIBS and to investigate several different approaches which could lead to the development of an analytical procedure which enables the correction of these matrix effects to achieve accurate quantitative analysis. Such quantitative analysis would also improve the discrimination capability of the technique in the case of the glass samples analyzed. As mentioned earlier, quantitation is one of the analytical aspects of LIBS where improvements are needed.

In a LIBS experiment, the wavelength resolved detection of the emission lines provides quantitative information of the elemental composition of the sample. The sensitivity for each element is influenced by plasma parameters, which are in turn strongly influenced by the sample matrix[138]. Under the assumption of local thermodynamic equilibrium [170], atomic and ionic states will be populated and depopulated predominantly by collisions with electrons rather than by radiation [183]. In this case, the excitation (Boltzmann) and ionization (Saha) temperatures

coincide with the electronic temperature, which is the temperature of the Maxwellian distribution of electron velocities[184]. Thus, the plasma electronic excitation temperature, T, and the plasma electron number density, n_e, derived from the plasma emission, can be used for a meaningful description of the plasma characteristics.

Many methods have been described for determining *T[1, 2, 4]*. The most widely used method, based on the measurement of relative line intensities normalized to their spectroscopic parameters, relies on the so-called Boltzmann plot. In its simplest form, T can be calculated from the intensity ratio of two emission lines[2], originating in different upper levels of the same element and ionization stage

$$T = \frac{E_i - E_m}{k \ln\left(\frac{I_{mn} g_i A_{ij}}{I_{ij} g_m A_{mn}}\right)} \tag{5.1}$$

where E_i and E_m are the excitation energies (eV) for the upper levels i and m, k is the Boltzmann constant ($J.K^{-1}$), I_{mn} and I_{ij} are the integrated line intensities (e.g.,$W.m^{-3}$) corresponding to the transitions between the upper levels i or m and the lower levels j, or m respectively; g is the statistical weight, and A (s^{-1}) is the transition probability. By extending the above to several transitions and by linearization of the expression, the Boltzmann plot equation is obtained,

$$\ln \frac{I_{ij}}{g_i A_{ij}} = \ln\left(\frac{n_s}{U^s(T)}\right) - \frac{E_i}{kT} \tag{5.2}$$

where n^s is the total number density (m^{-3}) of the species s in the plasma and $U_s(T)$ is the internal partition function of the species at temperature T. This equation allows the evaluation of T from the measured intensities of a series of lines, provided that the transition probabilities and statistical weights are known. By plotting ln (I_{ij}/g_iA_{ij}) vs. E_i, T can be obtained from the slope

-1/kT. In this case, a good correlation of the experimental data to a linear fitting is an indication of the validity of the Boltzmann equation[2].

Calibration plots are useful for determining the concentration of species in an unknown sample by comparing the sample to a set of standard samples of known concentration. They are constructed by measuring the LIBS intensities in relation to known calibration standards. This approach is the most practical for extracting quantitative information on sample composition, despite the fact that the laser material interaction is highly matrix dependent and therefore variations in the matrix between the unknown sample and the standard must be minimal. Besides matrix dependence, calibration plots are also susceptible to fluctuations in laser fluence and sample inhomogeneity. As a result, unusual behaviors such as negative slopes and widely scattered experimental points can be observed. [165]

The measured integral line intensity (counts), $\bar{I}_{ij}$, can be expressed by [2]

$$\bar{I}_{ij} = FC^s A_{ij} \frac{g_i e^{-\frac{E_i}{KT}}}{U^S(T)} \tag{5.3}$$

where C^s is the concentration of the emitting species in the sample and F is an experimental parameter which takes into account the optical efficiency of the collection system as well as the plasma density and volume. $\bar{I}_{ij}$ is proportional to the population of the corresponding energy levels via the transition probability A_{ij} between the upper "j" and lower "i" levels of the transition, and the other terms have already been defined (see Eq. 5.2).

Eq. (5.3) illustrates that the concentration values for each element can be obtained by comparing a selected line intensity from an unknown sample to the corresponding one from a certified sample since all factors in the equation are common, except for the concentration and the line intensity.

Since several reference glass samples were available, covering a wide range of concentrations, a calibration curve can be constructed which relates the specific line intensity and its corresponding elemental concentration. Using this calibration curve, the line intensity measured for an unknown sample can be related to the corresponding unknown elemental concentration. This equation, however, applies to the plasma species concentration. As a result, one must assume that there is a constant relationship between elemental concentrations in the sample and species concentrations in the plasma among all the standards and unknown materials for this approximation to be satisfactory. If the matrix of the certified glass samples differs from the unknown samples, the calibration curve approach might fail. Subsequently, other analytical methods are necessary to obtain more accurate results.

As mentioned in Chapter 2, the forensic discrimination of glass relies mostly in elemental analysis techniques. Since there is a better control of the batch components in the glass manufacturing process, the minor and trace elements present in glass are considered good sources of discrimination between glasses. Validated methods for discrimination of glass based on quantitative data exist for ICP-MS and LA-ICP-MS. XRF studies of glass are also available in the literature as described in Chapter 2. These methods characterize the unknown glass fragments by providing quantitative information for a menu of elements. The discrimination of glasses is based on the quantitative results. For example, a validated method for LA-ICP-MS made use of an elemental menu of 10 elements: K, Ti, Mn, Rb, Sr, Zr, Ba, La, Ce, and Pb [107]. A recent study by Micro-X-ray fluorescence (μXRF) and LA-ICP-MS for the discrimination of automotive glass focuses on the concentrations of 5 elements: Sr, Zr, Ti, Rb, and Ba [130].

The application of LIBS to the forensic analysis of glass is relatively new. Some selected published work on the use of LIBS and the discrimination of glass based their analysis in the following:

First, identification by using 10 line intensity ratios from 18 ionic and atomic emission lines from the elements Al, Ba, Ca, Cr, Fe, Mg, Na, Sn, Si and, Ti in automobile float glass. It was possible to discriminate 83% of the glass samples with 99% confidence based on LIBS spectra alone and 96-99% if the samples were discriminated based on LIBS spectra taken in conjunction with RI data at the same confidence level [108]. Later, this study was extended for the discrimination of four common glass types (float, headlamp, brown, and side-mirror glass) [128].

Second, identification by correlation analysis (Chapter 4) [177]. The glass fragments were identified from their unique LIBS spectral "fingerprints" by using statistical correlation methods combined with the use of a spectral mask. A 100% correct identification was achieved at a 95% confidence level.

Third, identification by using different combinations of 10 line intensity ratios from the elements Al, Na, K, Ca, Fe, and Sr. Excellent discrimination results were obtained (>99%) [130].

The studies mentioned above focused the discrimination into using the spectra as a whole or in the calculation of intensity ratios for some particular elements (Al, K, Sr, Ba, Ca, Cr, Fe, Mg, Na, Sn, Si and, Ti). These approaches provide qualitative information of the glasses. In this chapter, we examine the LIBS spectra of glass from a different perspective. That is, we are looking at the detailed composition in glass for some of the elements mentioned above by using glass standards. This chapter focuses on the construction of conventional calibration graphs made by plotting intensities versus concentration for glass samples from different matrices.

Outliers or different slopes in the calibration graphs will indicate the potential presence of a matrix effect.

Experimental

Glass Standards

A total of twelve glass standards were used in this study. They all have a unique aspect and represent different chemical matrices. Magnified pictures of these standards are presented in Figures 5-1 to 5-3. The composition of the nine standard reference materials (SRM) from National Institute of Standard and Technology (NIST) used in this study are listed in Tables 5.1 and 5.2.

In Table 5-1, the concentrations of the main and minor elements present in different types of glasses: soda-lime, soft-borosilicate and multi-element are given in percent by weight (%) in the solid form. Pictures of these standards are presented in Figure 5-1; soda-lime glasses are transparent while the others (SRM1411 and SRM 1412) are opaque.

Glass made from silica sand will normally have a green tone depending on the amount of iron oxide. To decolorize the glass, manufacturers add small amounts of other colorants which produce a complimentary color to green so that the finished product appear colorless.[52] Ancient glass makers used antimony to produce a white opacity in glass [185]. Nowadays, opacity is achieved when SnO, TiO_2 or ZrO_2 are added to the glass mixture as opacity agents [186]. Other less common opacifiers are Al_2O_3 [187] and ZnO [188]. A reported combination for opacity is based on the system SiO_2-Al_2O_3-B_2O_3-CaO-K_2O-TiO_2 [189]. Both SRM1411 and SRM1412 have no reported values of the known opacity agents, SnO and ZrO_2, while SRM 1411 has only a relatively low (120 ppm) concentration of Ti. However, they have a higher concentration (Table 5-1) of Al_2O_3, ZnO, BaO, K_2O and B_2O_3. The presence of Al_2O_3 (6 – 7 %) and ZnO (~ 4%) might explain their opacity.

The composition of trace elements present in glass (soda-lime type) is presented in Table 5-2 in μg/g (ppm). The nominal glass composition of these glasses (SRMs 610 through 617) is 72% SiO_2, 12% CaO, 14% Na_2O, and 2% Al_2O_3. In addition to the elements presented in Table 5-2, these glasses contain the following 25 elements: As, Be, Bi, Cs, Cl, F, Ge, Hf, Hg, Li, Lu, Mg, Nb, P, Pr, Se, S, Te, Tb, Tm, Sn, W, V, Y, and Zr. The SRM names for this group, e.g. SRM 610-611 are only related to the wafer thickness (in mm) which are 3 and 1 mm respectively. Standards of at least 3 mm thickness were used in this study; therefore only the first part of the name is employed when referring to them. These glasses are all transparent and colorless but SRM 610 which has a dark blue appearance (Figure 5-2). This darkness can be explained by the relatively higher concentrations (~ 400 ppm) of Co and Fe present in SRM 610 [52].

In addition to the SRMs, three standards designed to be representative of ancient glass were used in this study. These standards were provided by Corning Inc. Their chemical composition (%) is presented in Table 5.3. These three standards are dark and non-transparent; their picture is presented in Figure 5-3.

Instrumentation

The schematic diagram of the experimental system used for LIBS experiments performed under atmospheric conditions is depicted in Fig. 5-4. It consisted of a laser, a spectrometer, and intensified charge-couple device (ICCD), detector gating and control electronics, and a computer for control and data acquisition.

A Q-switched Nd:YAG laser (Quantel Brilliant T27; Big Sky Laser Technologies, Inc) operating at 1064 nm was used in this study. This laser delivered a maximum of 200 mJ in approximately 5.3 ns at a maximum repetition frequency of 10 Hz. The laser beam is focused onto the sample surface using a 3.5 cm diameter, 10 cm focal length lens. The firing of the laser flash lamp was triggered by a boxcar (SR250; Stanford Research Systems). The Q-switch output

served as the trigger for the pulse generator opening the shutter and beginning the gated detection. For these experiments, a pulse energy of 90 mJ was used providing an irradiance of ~5 GW/cm^2 on the sample surface. The repetition rate was set to 1 Hz.

The radiation emitted by atoms ablated from the glass samples is collected by a 5 cm diameter quartz lens with a focal length of 7.5 cm. An adjustable iris was attached to the lens in order to match the F-number of the spectrometer (F/6.5). The plasma emission was then guided to a 0.5 m focal length Czerny-Turner spectrometer (SpectraPro-500i; Acton Research Corp) by using a 35 μm entrance slit. The optimization of the micrometer slit dial and slit width values resulted from a previous study carried out for the analysis of different types of samples: aluminum alloys, brass, soil, and powder alloys [190].

The spectrometer is equipped with a 2400 grooves nm^{-1} grating. The detector is a two-dimensional ICCD (576/RB-E; Princeton Instruments) with 576 x 384 pixels. The ICCD controller (ST-138; Princeton Instruments) was used to gate the detection. Data acquisition was controlled using Winspec 32 software (Version 2.5.18.2; Princeton Instruments) installed on an Intel Pentium 4, 1.80 GHz computer.

The instrumental parameters used are: laser power 90 mJ/pulse, the detector delay time and gate width values were selected according to the emission lines to be analyzed.

Results and Discussion

Optimization of Experimental Conditions

Experimental conditions capable of providing high precision and repeatability between experiments are needed to obtain accurate quantitative information.

First, the effect of the laser power is studied. The Nd: YAG laser used has specified maximum pulse energy of 200 mJ. In our experiments, it is found that the laser power (90 mJ) resulted in better signal-to-noise ratios without detector saturation.

In LIBS, small unpredictable experimental fluctuations can cause a significant change in appearance of the spectra. To check the stability of our measurement set-up the following protocol is envisaged: the plasma image at zero-order for SRM 612 is monitored at regular time intervals. If the difference between the plasma intensities is between the expected statistical variation of our method ($\sigma = \pm 15\%$), there is trust is the measured intensities and the experiments are continued. Fluctuations in the intensities of the plasma image were always below 10% and there was no need of optimization, unless the collection lens was accidentally moved requiring then the entire collection optics to be re-aligned until the results were satisfactory. The short term pulse-to-pulse energy fluctuation of the laser was not expected to affect the results.

The position in the sample, where the plasma is formed, relative to the collection optics and spectrometer entrance slit was shown to affect the signal in this configuration. Since the ablation is perpendicular to the collection optics, this particular configuration is prone to be affected by the geometry of the sample. When ablating in the extreme opposite side of the sample, the signal was of different magnitude than when ablating at the edge closer to the entrance slit. Figure 5-5 shows the zero-order plasma image for an iron sample (Cast-Iron 236) with 2 cm thickness and 3.5 cm diameter. In a similar way, Figure 5-6 shows the zero-order plasma image for glass (SRM 1831) with a 0.25 cm thickness and 4 cm length. These two images were taken when working in "image-mode" for the ICCD camera. Then, there is a distortion of the plasma image when working "far" from the spectrometer slit. This distortion affects the signal intensity, up to a 25% increase, when working far from the edge and using the entire CCD frame. For small samples (~ 1 cm or less in diameter or length) this distortion was

not observed. The sample thickness doesn't seem to contribute to the distortion in the image. Therefore, it is recommended to ablate close to the edge in relatively long samples (> 1cm).

Data collection was mainly performed in "spectroscopy mode" rather than in "image mode" for quantitative analysis. Image mode was mainly used to determine the stability of our measurement set-up and to reproduce the distance from the focusing lens for each sample; this was done by centering the zero-order plasma image to the center of the ICCD camera. All plasma images in this study were taken at a delay time of 2 μs and 0.25 μs integration time; to prevent ICCD spot damage from intense plasma light emission, a neutral density filter was placed in front of the spectrometer input slit. From this check, it was observed that each standard has a unique plasma image intensity when working in the zero-order grating. Figure 5-7 presents the plasma zero-order image for the twelve glass standards used in this study.

Another parameter of interest in this study was the number of CCD vertical pixels to be binned during spectra acquisition. "Binning is the process of combining charge from adjacent pixels in a CCD into one large pixel"[191]. A spectral line is typically an image of the slit formed on the CCD. The signal from a single spectral line can be binned to achieve the best SNR [190, 192]. The zero-order plasma image for Corning, Glass C, taken at a delay time of 2 μs and 0.25 μs integration time is presented in Figure 5-8. Five groups of pixels have been selected for spectral binning. The effect of binning was determined using a Mg I line at 518.4 nm shown in the first panel in Figure 5-9. The signal, background, %RSD, noise and signal-to-noise (S/N) were calculated as a function of the binning group and shown in Figure 5-9. Each point is the average of 5 successive experiments performed at different positions in Corning glass C. The Mg peak intensity and background around the peak decrease as less pixels are summed, behavior that is expected. The corresponding %RSD is higher when the total number of pixels is binned,

having a relative constant value (4-6%) for the other groups. The noise, calculated as the standard deviation of a background pixel located at the left of the Mg peak, decreases with the number of binned pixels. Since the noise is reduced by binning, the signal-to-noise ratio is improved when fewer pixels are used. From these results, it would make sense that the limit to the number of binned pixels for all succeeding measurements should be the height of the plasma (100 pixels in this case). However, as Figure 5-7 shows, the height and intensity of the plasma varies with the type of sample. To ensure the whole plasma is binned in all samples, 200 pixels were chosen as the limit for the subsequent experiments. This binning set also provides relative good precision, low noise, and adequate signal-to-noise values.

There is no sample preparation required for elemental analysis by LIBS. However, relatively low spectral intensities were recorded after the first laser pulses which slowly increased reaching later a constant value. This behavior was specially presented in transparent glass standards. Figure 5-10 presents plots of the variation of the net intensity of Sr for SRM 620 and Corning C. The intensity of a strontium atomic emission line at 460.73 nm was monitored vs. the number of laser pulses (up to 100) taken at one spot in the samples. The behavior in SRM 620 was also observed in Chapter 4. For the first few laser pulses, SRM 620 is almost transparent and there is minimal ablation. However, as the glass interrogation progresses, defects in the surface were formed making ablation stronger. The variation of peak intensities was calculated for each glass standard. The precision (%RSD) variability with the number of laser pulses at one sample spot (in groups) is presented in Table 5-4 for glasses SRM 620 and Corning C. %RDS values observed for SRM 620 were common to other transparent glasses; the %RSD improves with the number of laser pulses. After 20 laser pulses, %RSD has a relative constant value close to 6%. For non-transparent samples (e.g. Corning C) there is no major variation in precision

(~6%) with the number of laser pulses. Consequently, the first 20 ablation pulses were discarded in all samples and considered as preparation pulses.

Construction of Calibration Plots

As mentioned earlier in this chapter, the identification of glass by elemental analysis relies mostly in the study of elements present in minor or trace concentrations. In order to obtain an accurate characterization of glass, as many elements as possible should be taken into consideration. From previous LA-ICP-MS and LIBS studies, the elements most commonly used for discrimination analysis are the following: Al, K, Sr, Ba, Ca, Cr, Fe, Mg, Na, Sn, Si and, Ti. This analysis focuses on the study of Sr, Ti, and Mg.

The selection of spectral lines is critical for the success of a quantitative LIBS measurement. Spectral resolution, sensitivity, and absence of interferences are important factors to be considered when selecting lines. To extend the dynamic range of the calibration plots, one may select different analyte lines to be used alternatively within a certain concentration range. The stronger analyte lines, even when exhibiting self-absorption at higher concentrations, could be used in the lower concentration range, while the weaker lines may be used for higher concentrations[193]. In addition, time-resolved detection is important to discriminate the atomic emissions against the strong background radiation. The background radiation is mainly composed of bremsstrahlung from free electrons and recombination emission which start almost simultaneously with the plasma ignition[182]. The detector delay and gate width or integration time were selected depending on the line to be studied.

Determination of strontium

Two strontium peaks were selected, Sr atomic (I) present at 460.73 nm and Sr ionic (II) present at 407.77 nm. Glass spectra for two glasses SRM 1411 and Corning D (for comparison

purposes) were observed in Figure 5-11 (Sr 460.73 nm, 2 μs delay time and 10 μs gate width) and Figure 5-12 (Sr 407.77 nm, 2.5 μs delay time and 0.75 μs gate width).

The effect of gate delay after the laser pulse on the peak intensity was studied for both lines. The integration time or gate width for detection was set to 0.5 μs. Figure 5-13 presents the temporal evolution of Sr I at 460.73 nm. Higher intensities were obtained when working at delays between 2 to 5 μs. Relatively good sensitivity was observed at gate widths around 10 μs. Consequently, a detector delay of 2 μs and an integration time of 10 μs maximize the signal of this Sr peak. Figure 5-14 presents the temporal evolution of Sr II at 407.77 nm. Higher peak intensities were obtained when working at delays between 1.5 and 2.5 μs. For Sr II at 407.77 nm, a detector delay of 2.5 μs and an integration time of 0.75 μs maximize the signal for the studied concentrations.

For data acquisition, the first 20 spectra were discarded and the next 20 were accumulated per position in the sample. Each point in the calibration plot is the result of three measurements or positions per sample. Calibration plots for these lines are presented in Figure 5-15 (Sr I) and Figure 5-16 (Sr II).

It is observed in Figure 5-15 that the peak intensity for Sr I at 460.73 nm in SRM 1411 was higher than expected. To confirm this observation, the calibration plot for this peak was repeated at a later day with similar results (Figure 5-17). A 7% variation between both experiments was observed when averaging 20 laser pulses (from 21 to 40).

Besides concentration of the analyte, the intensity of peaks in LIBS is also affected by many experimental parameters such as interferences or spectral overlap, self-absorption, and matrix effects[194]. One obvious reason for the anomaly observed could be the presence of a spectral interference under the Sr line. Table 5-5 contains a list of spectral lines present in the

vicinity of Sr I 460.73 nm[195]. As mention earlier, the main difference between SRM 1411 and the other standards is a higher concentration of Al_2O_3, ZnO, BaO, K_2O, and B_2O_3. Within the spectral bandwidth of our apparatus, there are no lines for Al, O, Zn, Ba, and B near this Sr peak. Further experiments, for example, using a higher resolution spectrometer to check for an asymmetry in the line shape, are needed to confirm or refute if the higher Sr signal intensity is due to spectral interferences.

If the value for Sr I at 460.73 nm in SRM 1411 is withdrawn from the calibration plot, (Figure 5-15 A) a linear plot with a high correlation coefficient is obtained (Figure 5-15 B). Even for Corning C, with a Sr concentration (2500 ppm), the correspondence between peak intensity and concentration is linear. Therefore, it is not expected that the higher intensity in SRM 1411 might be due to self-absorption at ~ 800 ppm.

Another possibility for this unexpected higher Sr peak intensity in SRM 1411 is the potential presence of a matrix effect. SRM 1411 is a soft-borosilicate glass while most of the other glass standards used in the calibration plot are of soda-lime composition.

It was then decided to use another Sr analytical line. A new calibration plot was constructed for a Sr ionic line present at 407.77 nm (Figure 5-16). Surprisingly, this time the calibration plot does not show any obvious outlier and the intensity of Sr in SRM 1411 fits nicely in the linear regression plot.

The detection limit is defined as the concentration that produces a net line intensity equivalent to three times the standard deviation of the background[193]. It can be evaluated with the expression

$$LOD = \frac{3\sigma_B}{S} \tag{5.4}$$

Where σ_B is the standard deviation of the background, and S is the sensitivity defined as the slope of the calibration plot for the selected line.

For each peak, the standard deviation in the background of the Sr peak was calculated. The glass with the lowest Sr concentration SRM 616 (~ 40 ppm) was selected for this task.

The variation of the Sr intensity at 460.73 nm with the number of laser pulses (from 21 to 40) in SRM 616 is shown in Figure 5-18. Since there is no blank for LIBS measurements, the standard deviation around the Sr 460.73 peak was calculated for the 20 spectra shown in Figure 5-18. As reported in the recent literature[196], if the standard deviation for each pixel is plotted vs. wavelength a plot that resembles the studied spectra is obtained (Figure 5-19). The standard deviation for the background region around the Sr peak has an average value of ~ 3200 counts. By using the slope of the calibration plot for this peak (Figure 5-15 B), the calculated LOD is 21 ± 2.4 ppm.

In a similar way, the LOD for Sr at 407.77 nm was calculated. The plot of standard deviation for the region around 407.77 nm is presented in Figure 5-20. The standard deviation for the background region around the Sr peak has an average value of ~ 22 000 counts. By using the slope of the calibration plot for this peak (Figure 5-16), the calculated LOD is 1.7 ± 0.30 ppm.

LODs for Sr determination with LIBS, using the 460.73 nm atomic line, are 2 ppm in wastewater [197] and 80 ppm in soils [198]. The ionic line at 407.77 nm has been mostly used in the quantitative analysis of solid waste (13 ppm)[48], soils (30 and 42 ppm) [198, 199] the latest when using a portable LIBS instrument, and Sr in a UO_2 pellet (130 ppm) [200]. In a recent study of wavelength dependence on the elemental analysis of glass, the authors were able to provide quantitative information for vehicle glass samples with Sr concentrations higher than 30

ppm [129]. Sr II at 421.5 nm has also been reported in LIBS for the determination of Sr (LOD 0.3 ppm) in starch based flours [200].

Determination of magnesium

For the determination of Mg, the atomic line at 517.27 nm was selected (Figure 5-21). A combination of 2 μs for both delay and integration time was selected for this line. The calibration plot for peak intensity vs. concentration is presented in Figure 5-22.

Following the same methodology as with strontium for LOD determination, the standard deviation around the peak was calculated (Figure 5-23). The plot of the standard deviation of the measurements vs. wavelength is presented in Figure 5-24. The calculated LOD was 120 ±7.5 ppm. This LOD is much lower than those usually required for ordinary glass analysis, e.g. Mg concentration in vehicle window glasses is about 2-3% (3-5% MgO)[99]. Reported LIBS LODs for Mg in glass are 130 and 28 ppm in air at 1 and 5 torr respectively when using the peak intensity of Mg I at 383.83 nm[201]. Most quantitative studies for Mg focus on its determination in aluminum alloys and soils, LODs as low as 0.5 ppm have been reported[193].

Determination of titanium

For the determination of Ti, the ionic line at 336.12 nm was selected. Glass spectra for two glasses SRM 1411 and Corning D (for comparison purposes) are observed in Figure 5-25. Optimum delay and integration times were found at 1 and 4 μs respectively. The calibration plot for peak intensity vs. concentration is presented in Figure 5-26. For LOD calculation, the standard deviation in the background for standard SRM 612 was calculated over 20 laser pulses (Fig. 5-27). The plot of standard deviation for 20 laser pulses vs. wavelength (Fig. 5-28) also resembles the shape of the line. The calculated LOD was 19 ± 0.98 ppm. This LOD is much lower than those usually required for ordinary glass analysis, e.g. Ti concentration in vehicle

window glasses is ~ 70 ppm (120 ppm TiO_2)[99]. Reported LIBS LODs for Ti in glass are 410 and 350 ppm in air at 1 and 5 torr respectively when using the peak intensity of Ti I at 365.35 nm[201]. Similarly to Mg, most reported studies of titanium determination are focus on aluminum alloys and soil matrices with reported LODs as low as 4 ppm in aluminum alloys (Ti II 323.45 nm)[202].

In these experiments, it can be observed that the detection limits are a function of the studies elements and the selected emission lines. This observation can be explained by the following factors[193]:

- The intensity of the analytical line, which is related to the transition probability.
- The upper energy of the analytical line (it is more difficult to populate higher energy levels).
- The spectral surroundings of the analytical line which is related to the detector sensitivity.

The detection limits (Table 5-6) for Sr, Mg and Ti were comparable to those reported in LIBS studies in glass, aluminum alloys and soils.

Conclusions

The feasibility of constructing calibration plots for NIST and Corning glass samples was evaluated for Sr, Mg, and Ti. These three elements are common to most types of glasses and its determination can provide useful information for discrimination studies. When determining concentrations, linear calibration curves are desirable because they result in the best accuracy and precision. All four constructed calibration plots were linear ($R > 0.9$) over the studied range of concentrations. Linearity was achieved even when the glass standards were from different matrices: soda-lime, borosilicate, multi-component and lead-glass. The only exception was the relatively higher intensity of Sr 460.73 nm in SRM 1411. In most cases, relative errors of less than ±10% were obtained. The delay time and gate width chosen for the detector was also an

essential parameter to conclude on the efficiency of these measurements. The obtained LODs were significantly lower than those required for the analysis of glass; therefore, these calibration plots could be use as to determine the quantitative composition of unknown glass fragments

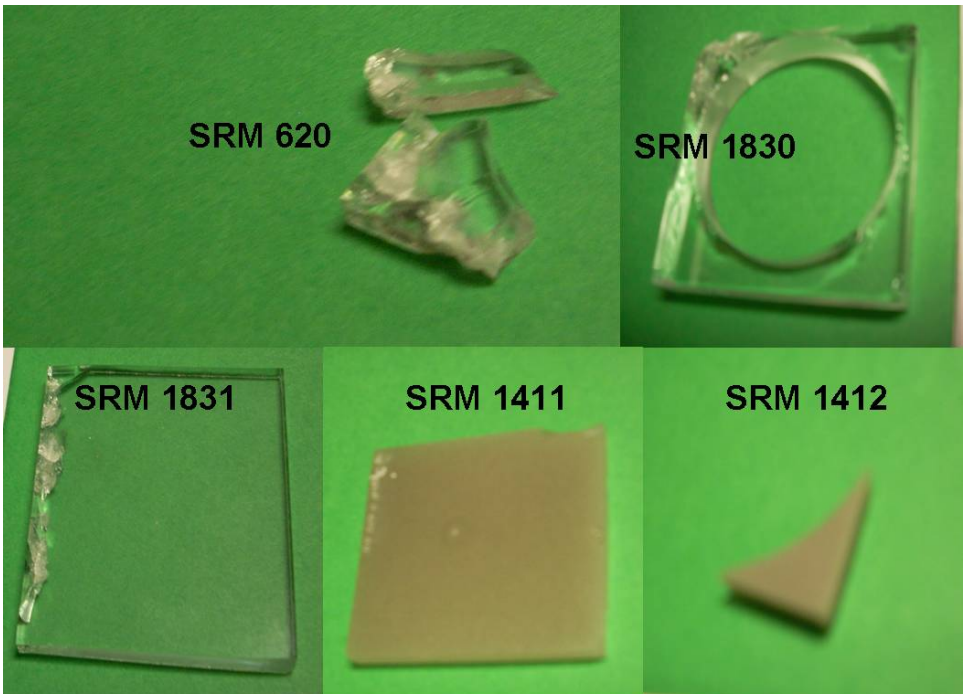

Figure 5-1. SRM-NIST Series 112.3 (glasses in powder and solid forms).

Figure 5-2. SRM-NIST Series 112.4 (trace elements, wafer form).

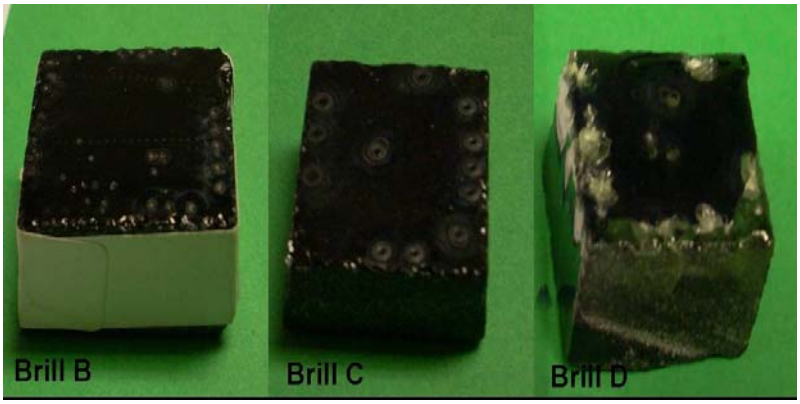

Figure 5-3. Corning glass standards.

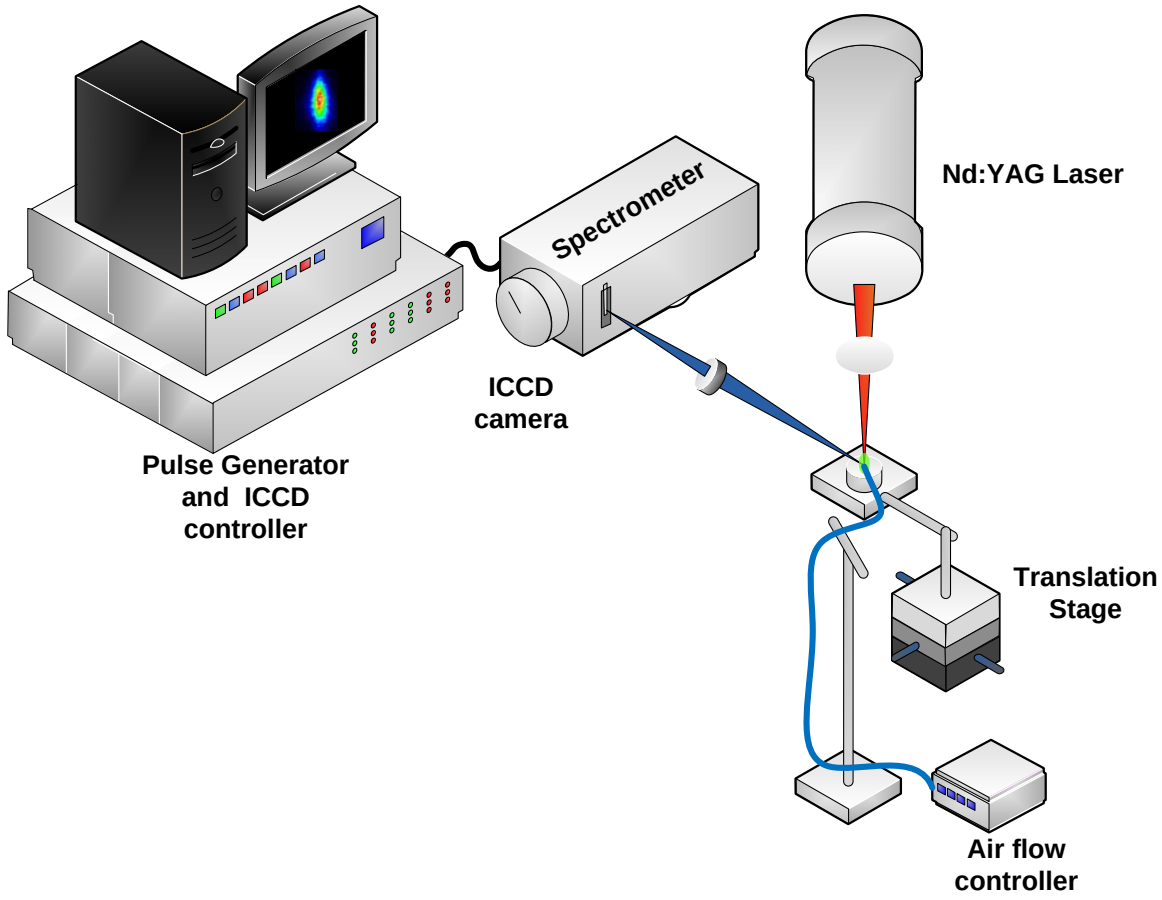

Figure 5-4. Diagram of the experimental LIBS system used in the experiments.

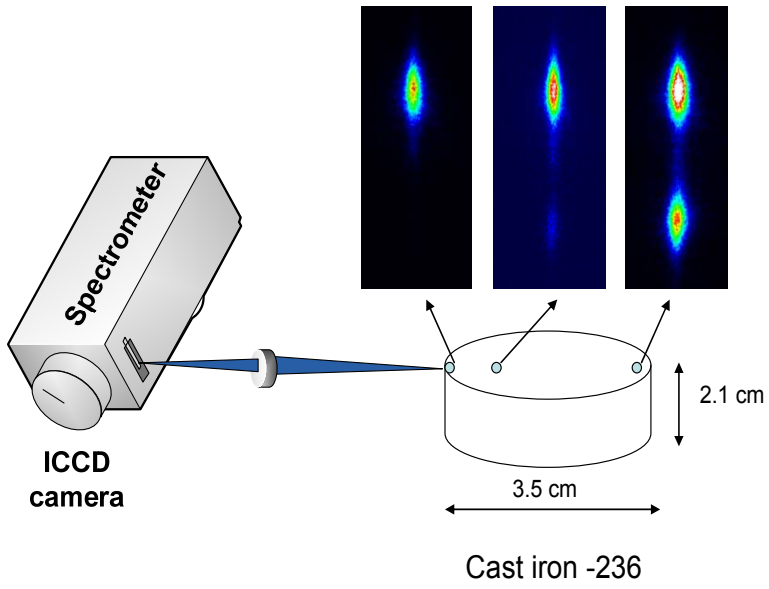

Figure 5-5. Zero-order plasma images obtained at different positions in standard cast iron – 236.

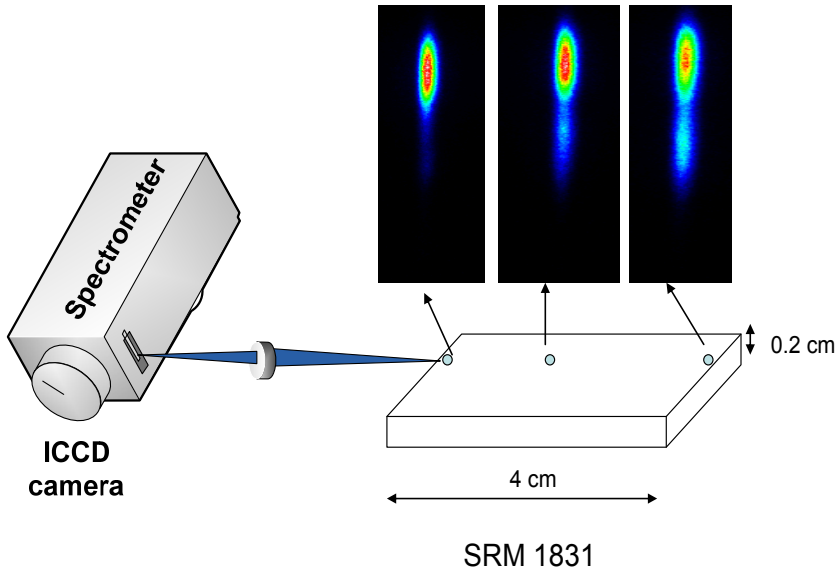

Figure 5-6. Zero-order plasma images obtained at different positions in SRM 1831.

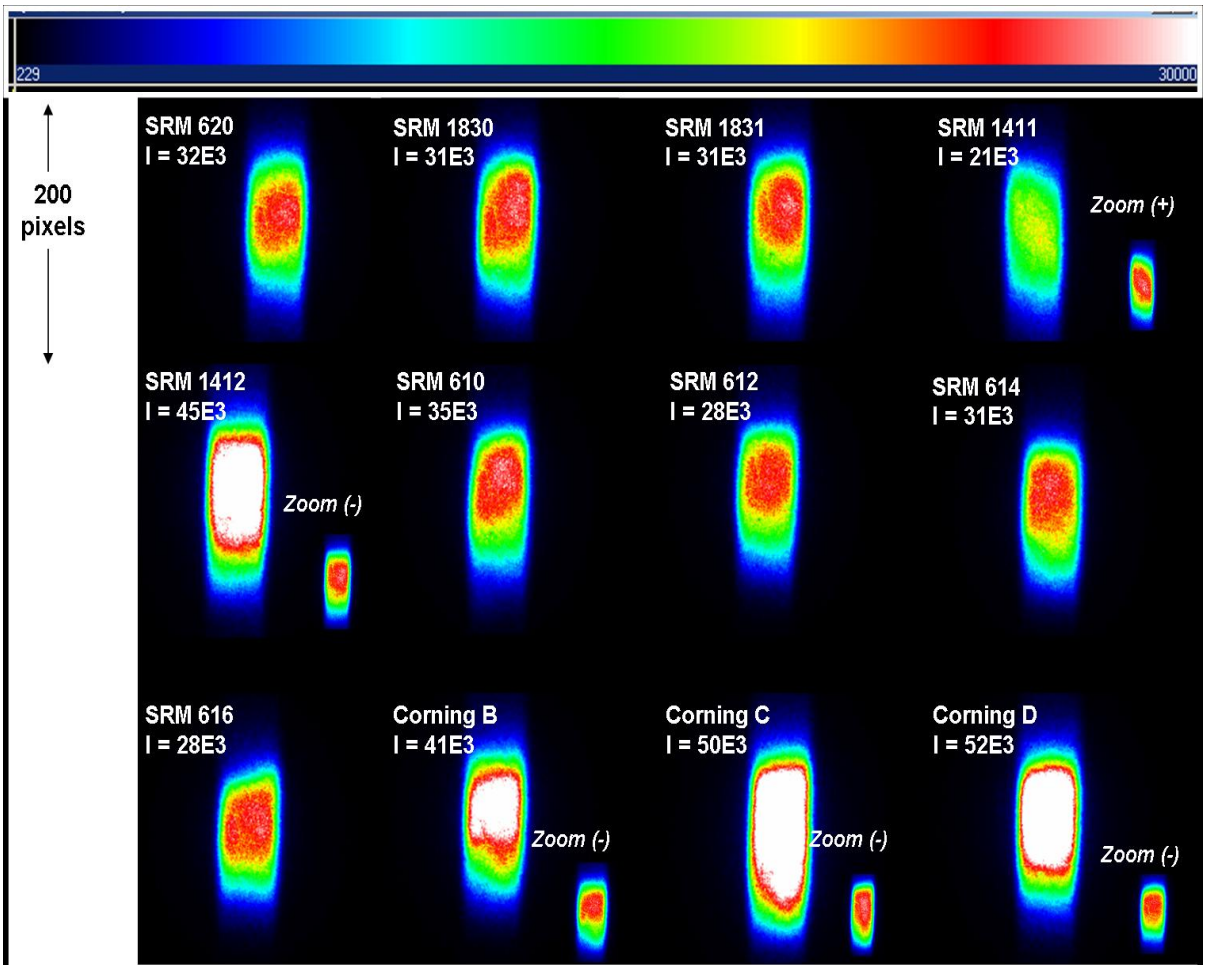

Figure 5-7. Zero-order plasma images and their intensities (a.u) for the glass standards used in this study.

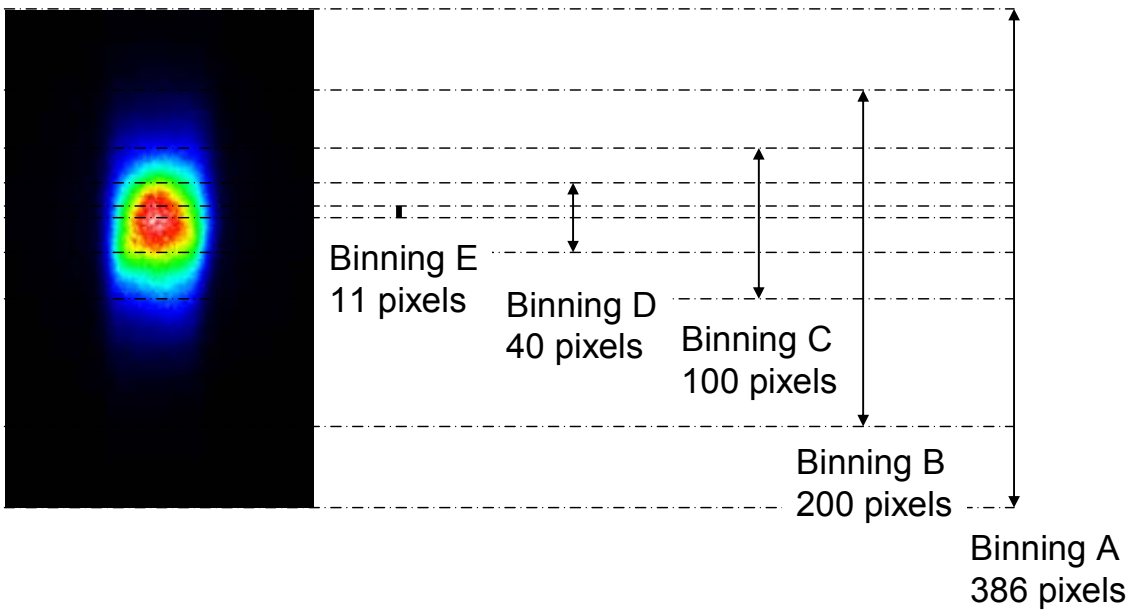

Figure 5-8. Zero-order plasma image for Corning glass C showing five regions for detector binning.

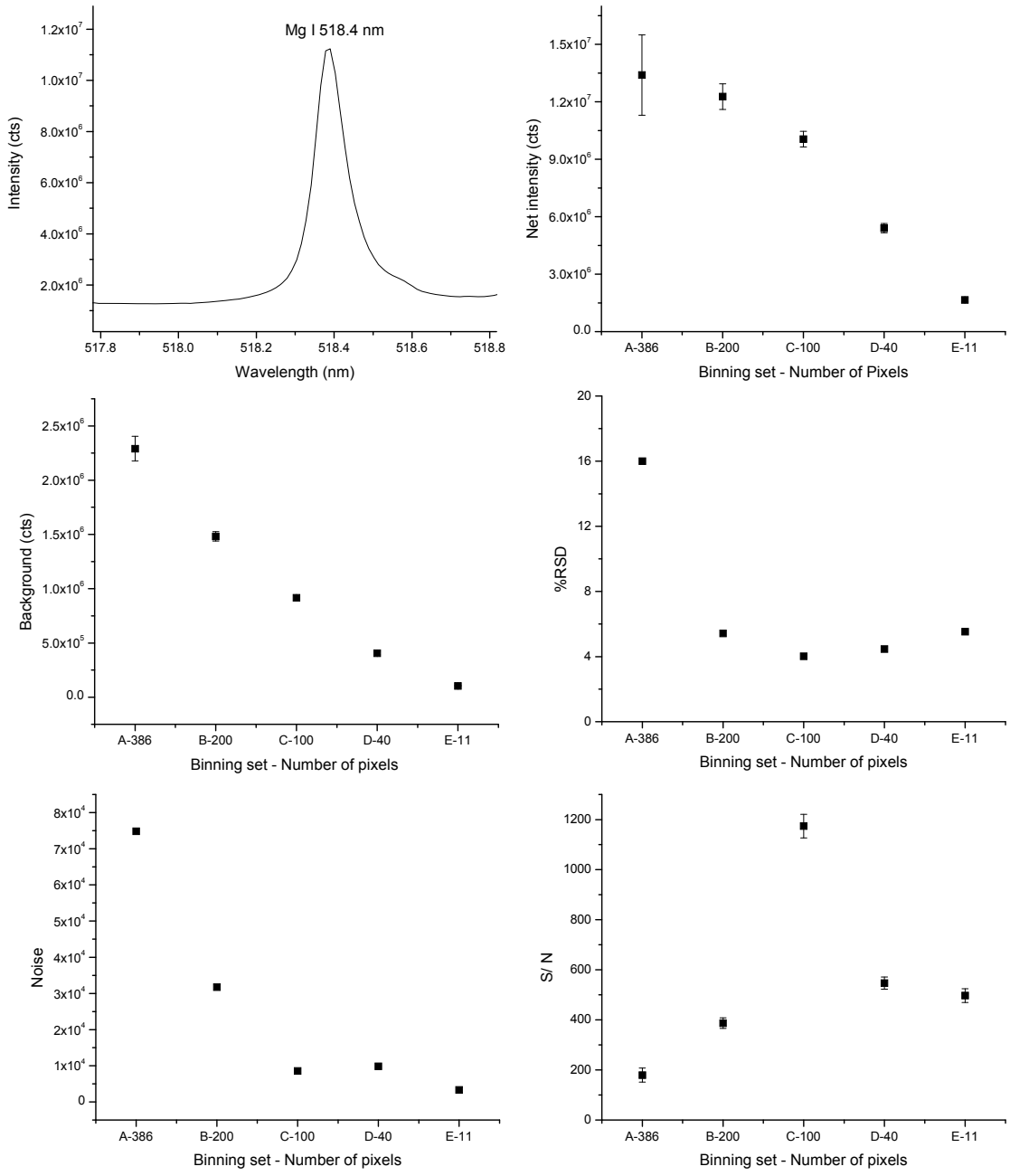

Figure 5-9. Binning effects on the intensity, background, %RSD, noise and signal-to-noise ratio for Mg I line at 518.36 nm.

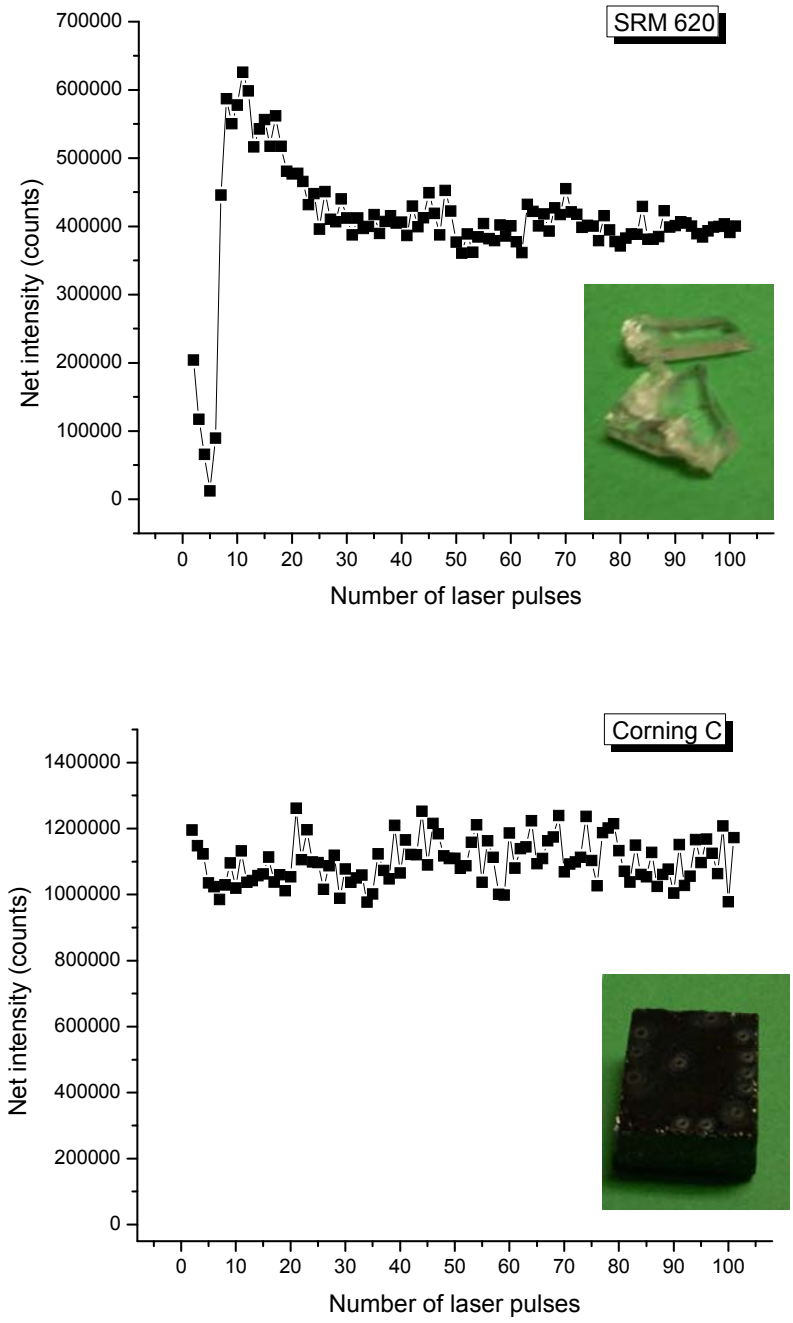

Figure 5-10. Strontium (460.73 nm) peak intensity dependence with the number of laser pulses for standards SRM 620 and Corning C.

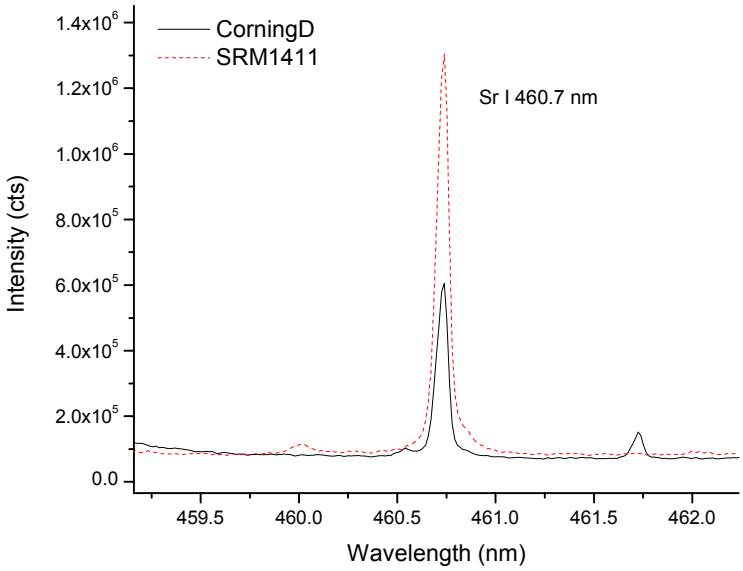

Figure 5-11. Strontium peak at 460.73 nm.

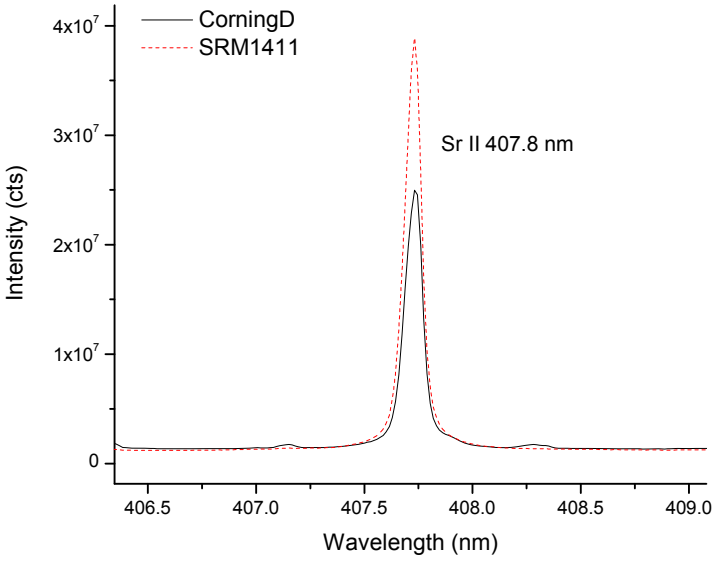

Figure 5-12. Strontium peak at 407.77 nm.

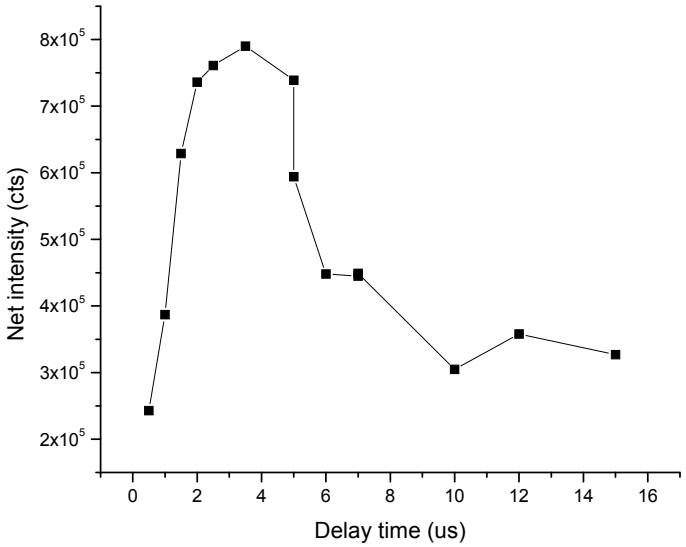

Figure 5-13. Optimization of the gate delay for Sr atomic line at 460.73 nm

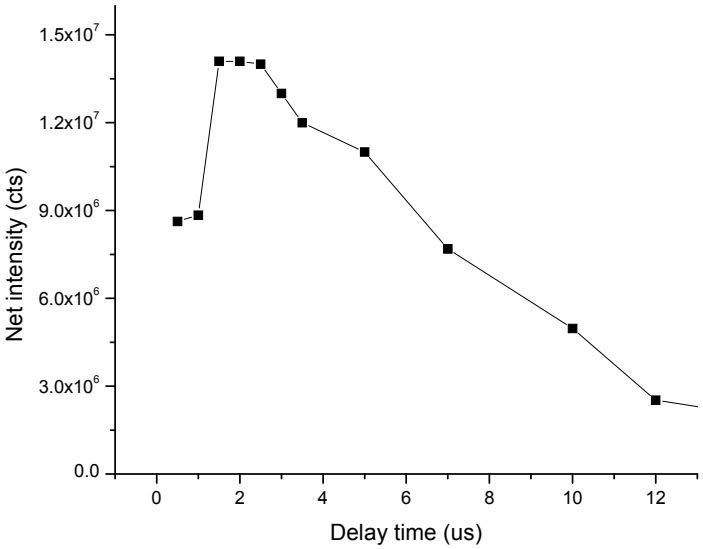

Figure 5-14. Optimization of the gate delay for Sr ionic line at 407.77 nm

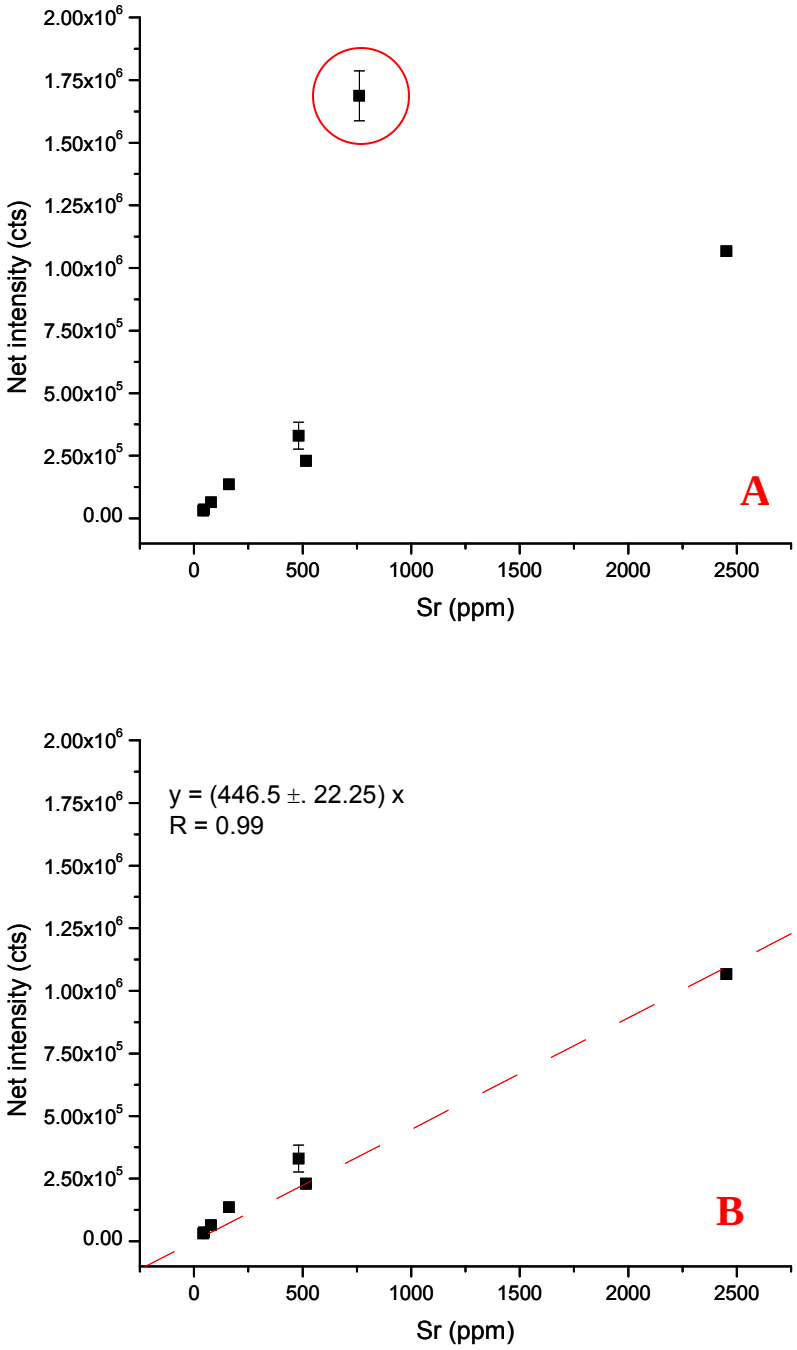

Figure 5-15. Calibration plot for Sr atomic line at 460.73 nm. Linearity is achieved (B) after removing the intensity of SRM 1411 present in A.

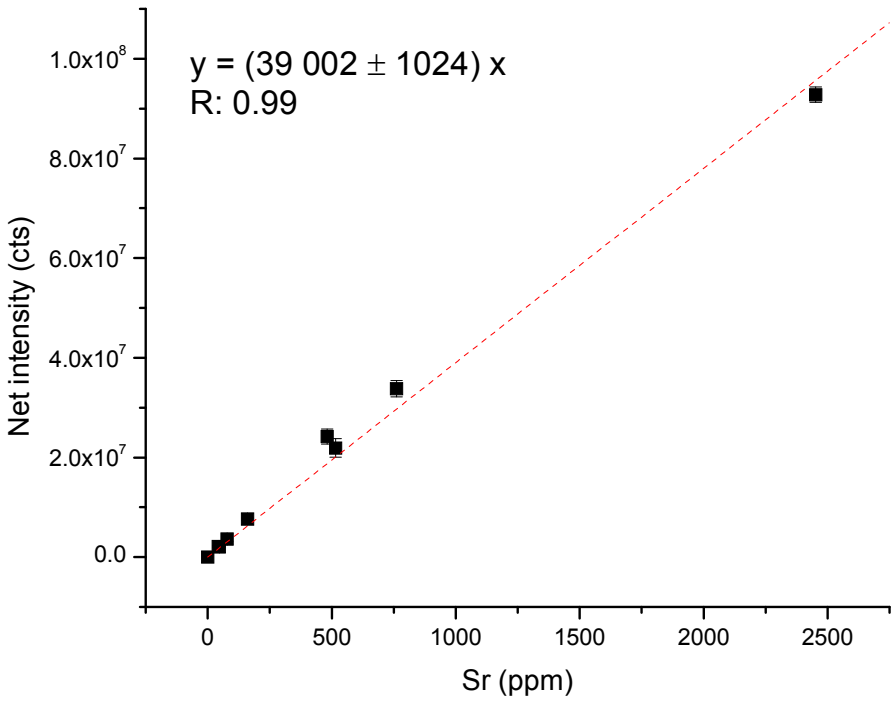

Figure 5-16. Calibration plot for Sr ionic line at 407.77 nm.

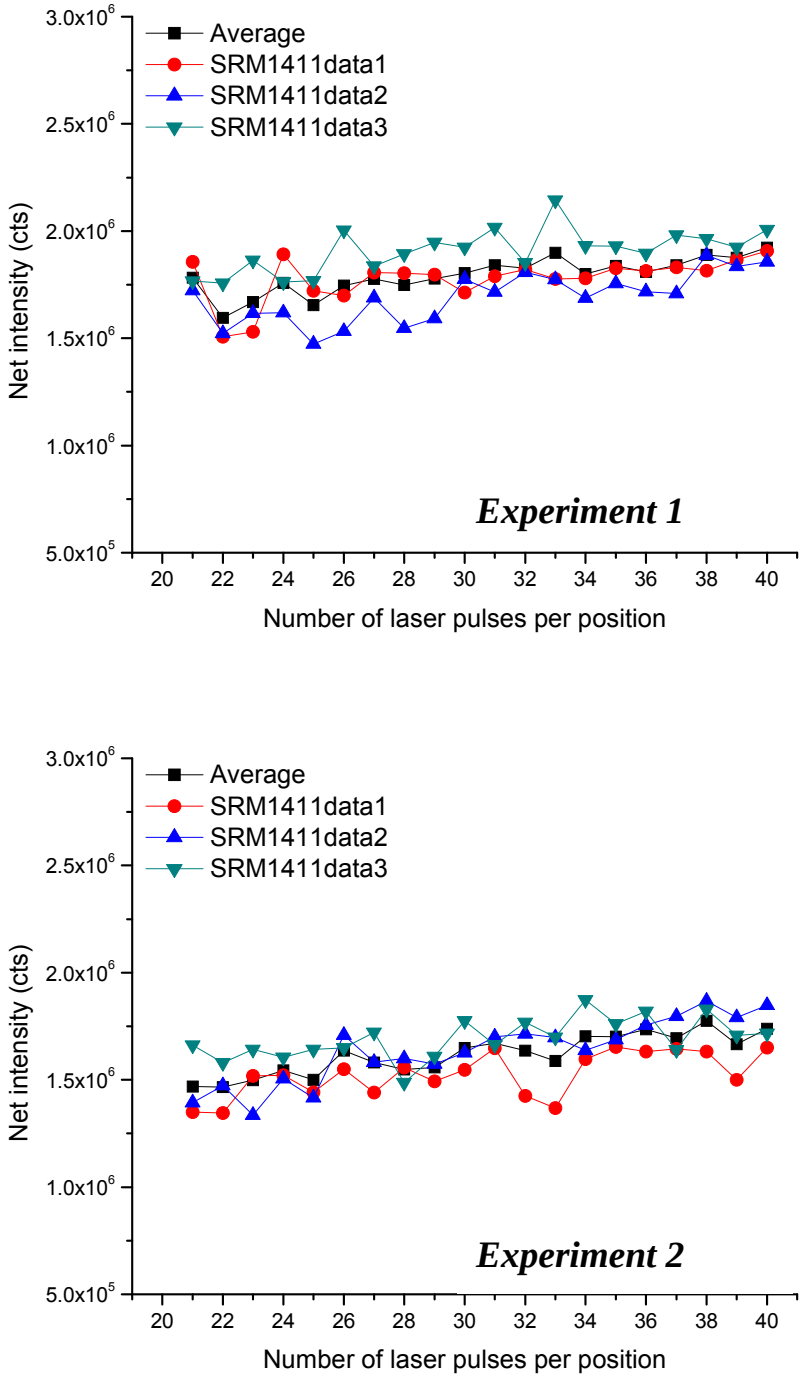

Figure 5-17. Strontium (460.73 nm) peak intensity variation with the number of laser pulses in SRM 1411.

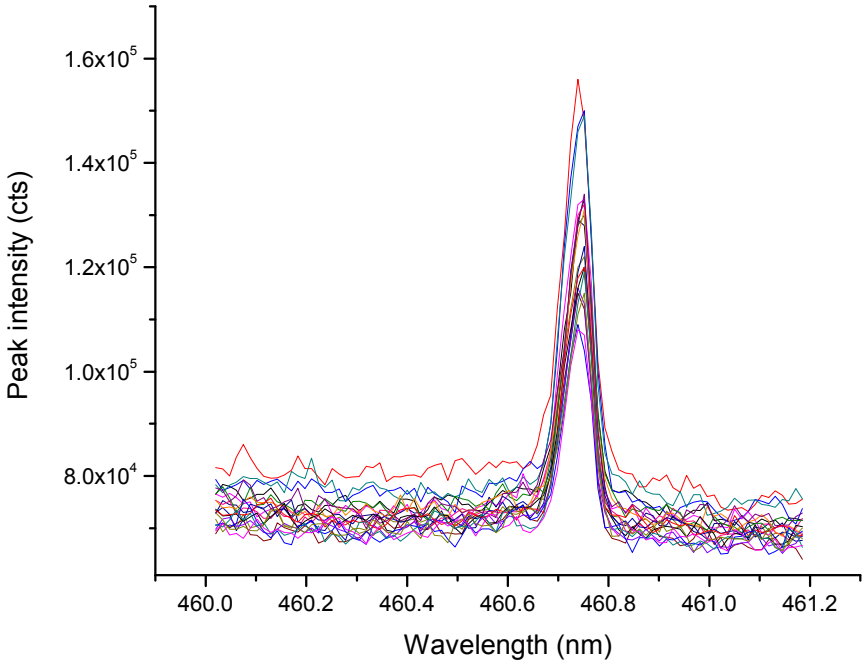

Figure 5-18. Strontium (460.73 nm) peak intensity dependence with the number of laser pulses for standards SRM 616.

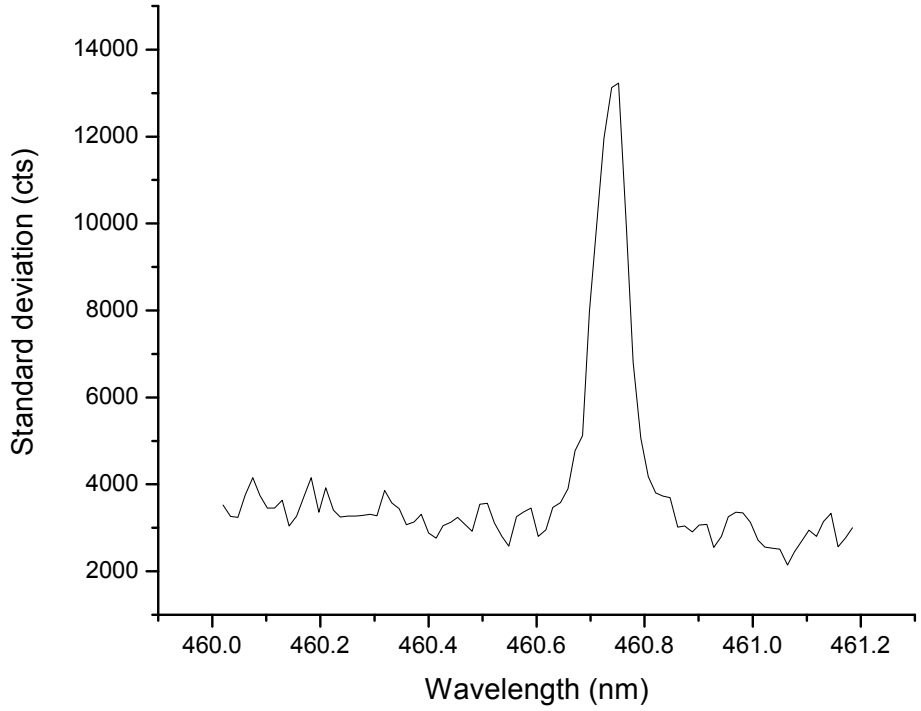

Figure 5-19. Standard deviation vs. wavelength around Sr I 460.73 nm for SRM 616

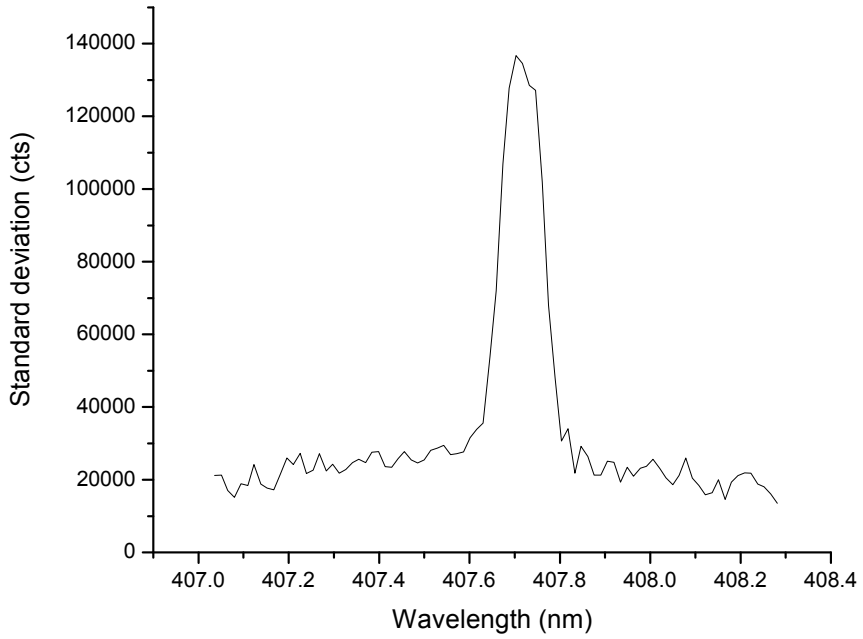

Figure 5-20. Standard deviation vs. wavelength around Sr II 407.77 nm for SRM 616

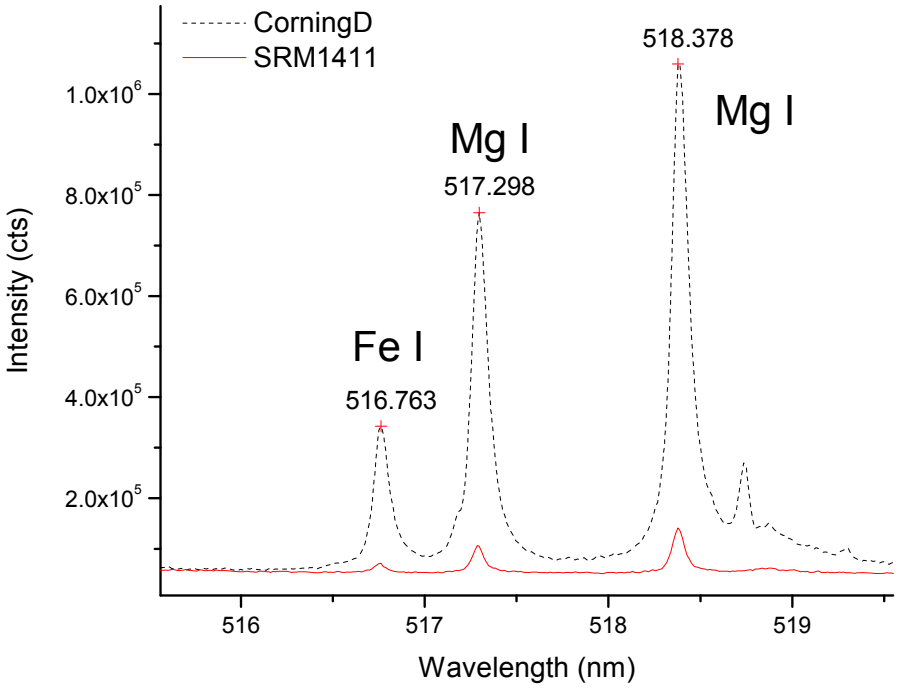

Figure 5-21. Magnesium peak at 517.27 nm.

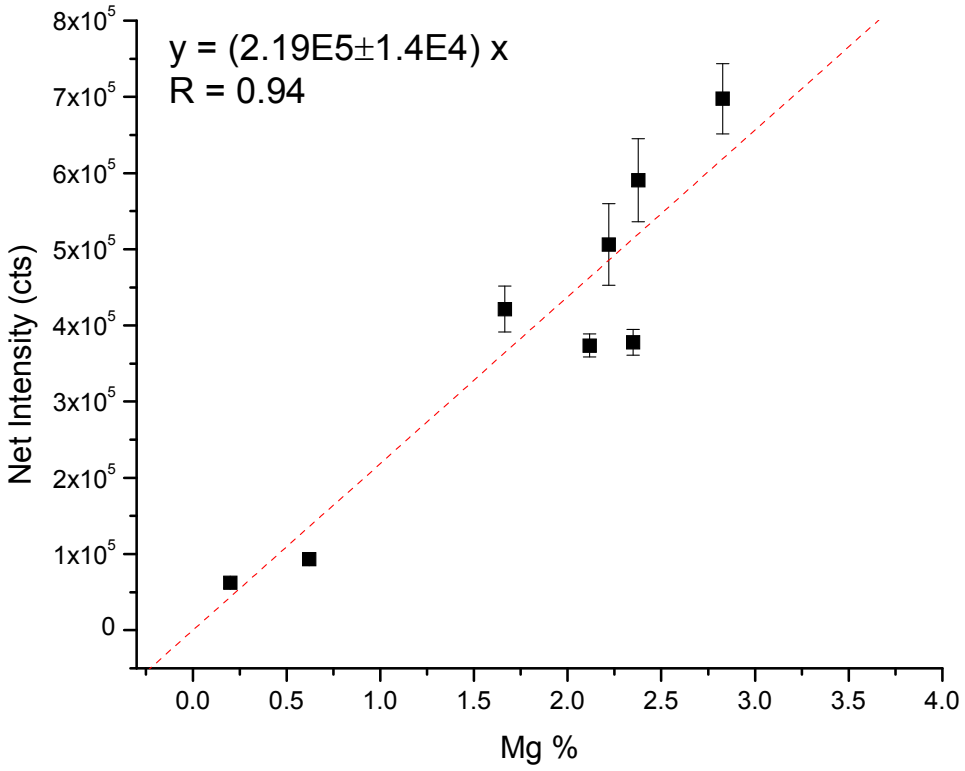

Figure 5-22. Calibration plot for Mg atomic line at 517.27 nm.

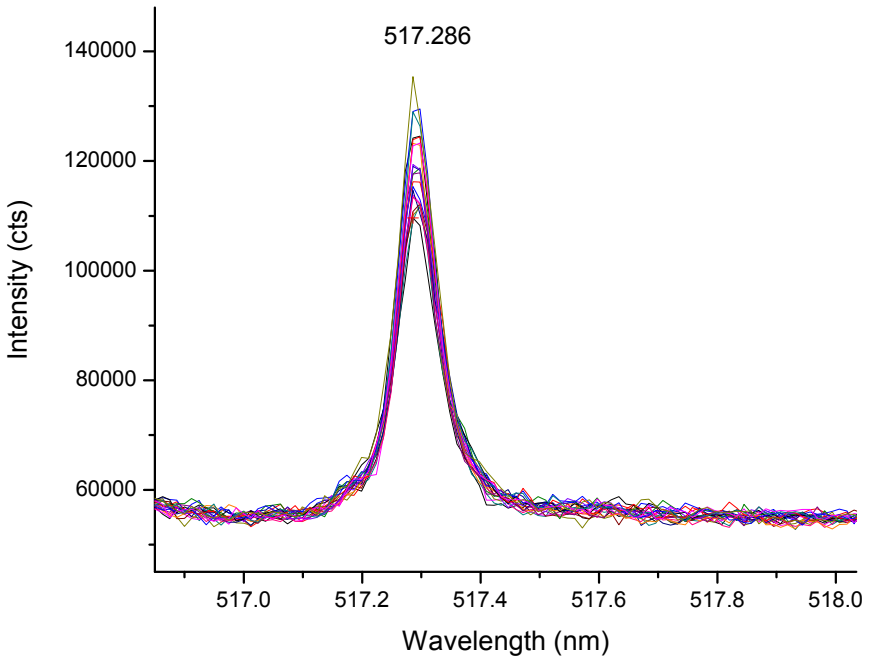

Figure 5-23. Magnesium peak intensity dependence with the number of laser pulses for standard SRM 610.

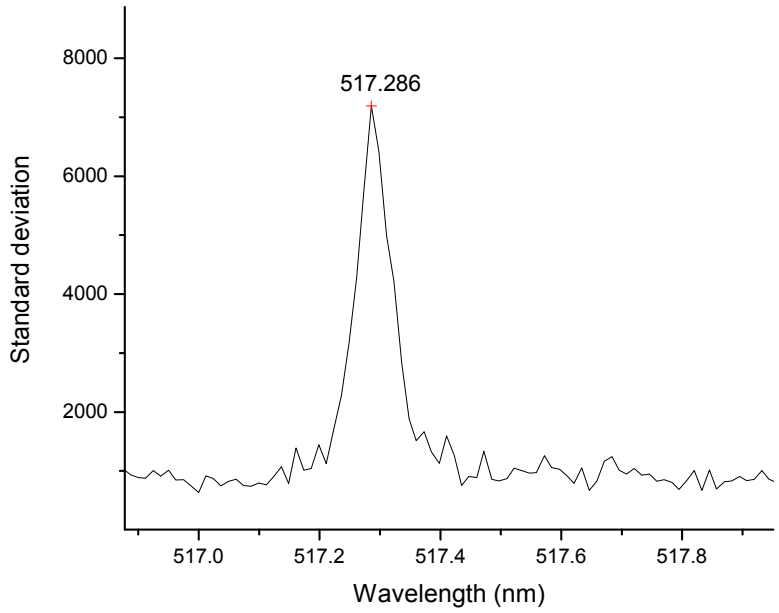

Figure 5-24. Standard deviation vs. wavelength for Mg 517.27 nm in SRM 1411.

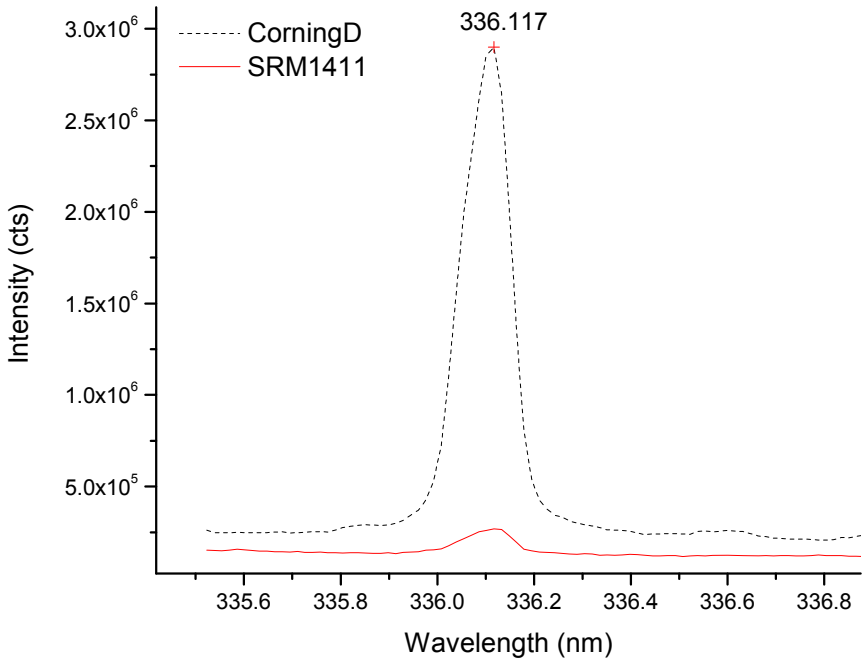

Figure 5-25. Titanium peak at 336.12 nm.

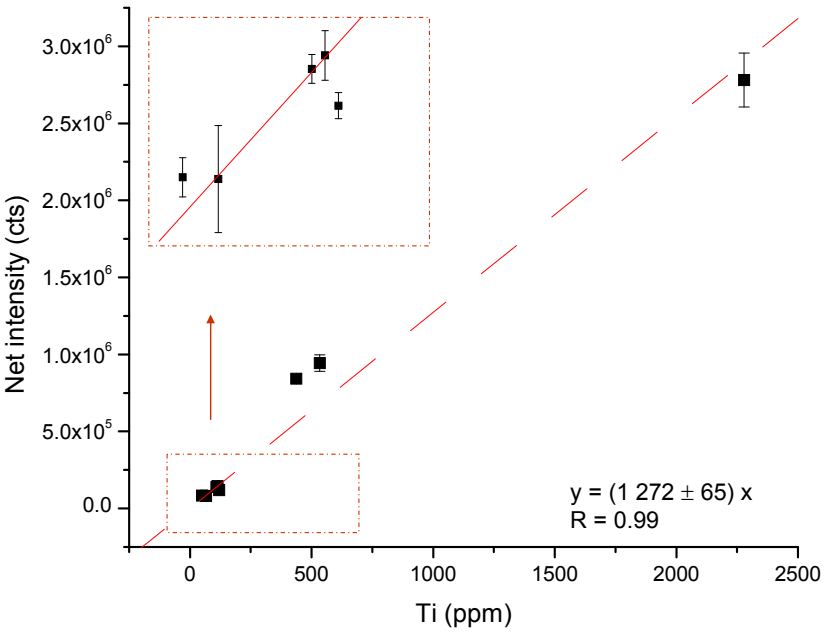

Figure 5-26. Calibration plot for Ti ionic line at 336.12 nm.

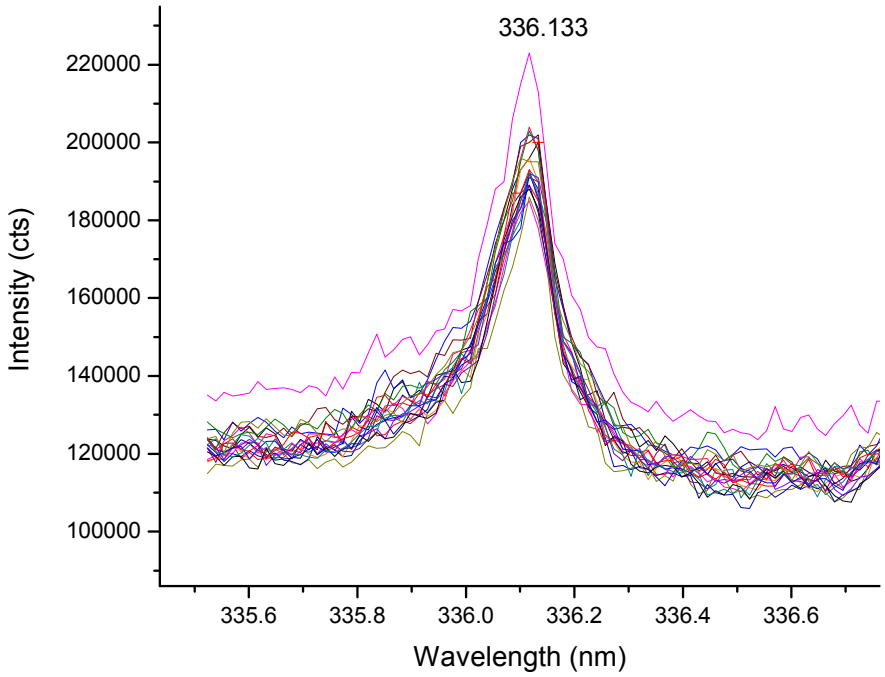

Figure 5-27. Titanium peak intensity dependence with the number of laser pulses for standard SRM 612.

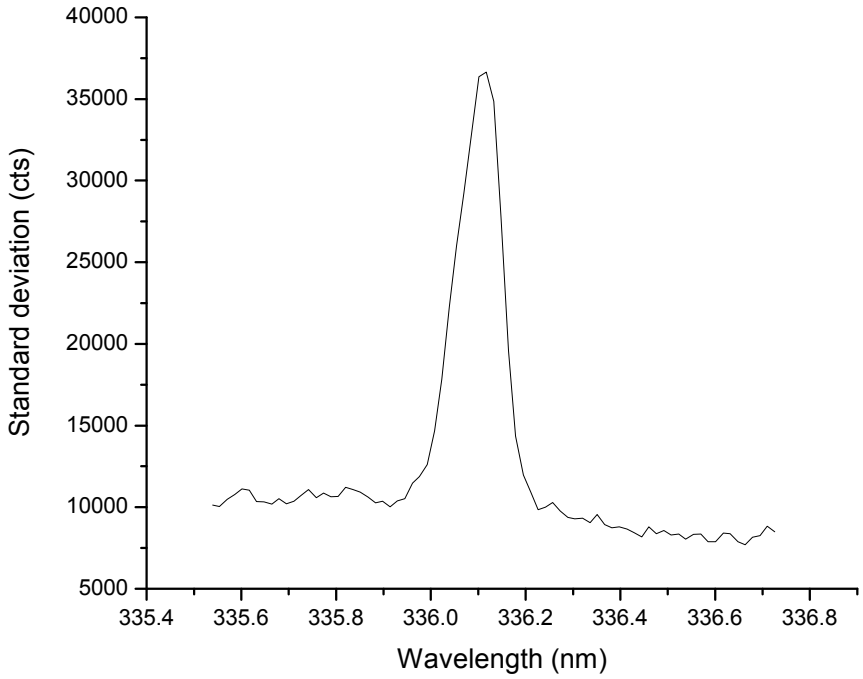

Figure 5-28. Standard deviation vs. wavelength for Ti 336.12 nm in SRM 612.

Table 5-1. Chemical composition of the studied soda-lime, soft-borosilicate and multi-component glass standards from NIST (SRM).

Concentration Wt. %	SRM620 Soda-Lime Flat	SRM1830 Soda-Lime Float	SRM1831 Soda-Lime Sheet	SRM1411 Soft-Borosilicate	SRM1412 Multi-component
SiO_2	72.1	73.1	73.1	58.0	42.4
PbO					4.40
Al_2O_3	1.80	0.120	1.21	5.68	7.52
FeO		0.032	0.025		
Fe_2O_3	0.0430	0.121	0.087	0.05	0.031
ZnO				3.85	4.48
CdO					4.38
TiO_2	0.018	0.011	0.019	0.02	
CaO	7.11	8.56	8.2	2.18	4.53
BaO				5	4.67
Li_2O					4.5
MgO	3.69	3.9	3.51	0.33	4.69
K_2O	0.41	0.04	0.33	2.97	4.14
Na_2O	14.4	13.7	13.3	10.1	4.69
B_2O_3				10.94	4.53
As_2O_3	0.056				
SO_3	0.28	0.26	0.25		
SrO				0.09	4.55

Table 5-2. Trace elements present in the glass standards NIST (SRM) used in this study.

Concentration	SRM 610-611	SRM 612-613	SRM 614-615	SRM 616-617
Pb	426	38.57	2.32	1.85
Fe	458	51	*13.3	*11
Zn	*433			
Cd			*0.55	
Ti	*437	*50.1	*3.1	*2.5
Ba		*41		
K	*461	*64	30	29
B	*351	*32	*1.3	*0.2
Sr	515.5	78.4	45.8	41.72
Cu	*444	*37.7	1.37	*0.80
Co	*390	*35.5	*0.73	
Au	*25	*5	*0.5	*0.18
Mn	485	*39.6		
Ni	458.7	38.8	*0.95	
Ru	425.7	*31.4	0.855	*0.100
Ag	*254	22	0.42	
U	461.5	37.38	0.823	0.0721
Ce		*39		
Sb			*1.06	*0.078

Unless stated otherwise, values are in parts-per-million (ppm).
* not certified values, information only

Table 5-3. Chemical composition in glass standards designed to be representative of ancient glass (Corning Inc).

Concentration Wt. %	Brill B	Brill C	Brill D
SiO_2	62.0	34.3	53.9
PbO	0.61	36.7	0.48
Al_2O_3	4.36	0.87	5.3
Fe_2O_3	0.34	0.34	0.52
ZnO	0.19	0.052	0.1
TiO_2	0.089	0.79	0.38
CaO	8.56	5.07	14.8
BaO	0.12	11.4	0.51
MgO	1.03	2.76	3.94
K_2O	1	2.84	11.3
Na_2O	17	1.07	1.2
P_2O_5	0.82	0.14	3.93
SrO	0.019	0.29	0.057
Cu	2.66	1.13	0.38
CoO	0.046	0.18	0.023
MnO	0.25		0.55
NiO	0.099		

Table 5-4. Percentage relative standard deviation (%RSD) variability with the number of laser pulses on the same spot

Number of laser pulses	SRM 620	Corning B
1-10	77	6.4
1-20	47	6.3
1-30	39	5.9
1-40	34	6.0
1-50	34	5.9
1-60	28	6.3
1-70	26	6.3
1-80	25	6.3
1-90	23	6.2
1-100	22	6.2
20-30	6.3	7.2
20-40	6.0	6.7
20-50	6.0	6.6
20-60	6.6	6.6
20-70	6.5	6.4
20-80	6.3	6.3
20-90	6.1	6.3
20-100	5.8	6.3
30 - 40	2.7	6.4
30- 50	5.4	6.4
30 -60	5.4	6.4
30 - 70	5.7	6.2
30 -80	5.5	6.2
30-90	5.3	6.1
30-100	5.0	6.2
40 - 50	7.2	4.8
40 - 60	6.3	6.0
40 - 70	6.4	5.6
40 - 80	6.0	5.7
40 - 90	5.7	5.9
40 - 100	5.3	6.0
50 - 60	3.8	6.6
50 - 70	6.3	6.0
50 - 80	5.7	6.0
50 - 90	5.3	6.0
50 - 100	4.8	6.1

Table 5-5. List of spectral lines present in the vicinity of Sr I 460.73 nm [195].

Line	Wavelength (nm)
Ni I	460.50
Mn I	460.54
Lu I	460.54
Ni I	460.62
Cr I	460.64
Ce II	460.64
Sm II	460.65
Er I	460.66
Ne II	460.67
Nb I	460.68
Sc I	460.69
W I	460.70
Fe I	460.71
N II	460.72
Sr I	460.73
Li II	460.73
Au I	460.75
W I	460.76
Rh I	460.81
K II	460.85
Kr II	460.85
W I	460.88
Ti II	460.93
Ne I	460.94
Ti I	460.94

Table 5-6. Detection limits for various elements present in the studied glasses.

Element	Concentration (ppm)
Sr I 460.73 nm	21 ± 2.4
Sr II 407.77 nm	1.7 ± 0.30
Mg I 517.27 nm	120 ± 7.5
Ti II 336.12 nm	19 ± 0.98

CHAPTER 6
NORMALIZATION OF THE SIGNAL FOR QUANTITATIVE LIBS ANALYSIS

Introduction

Key features which make LIBS an attractive analytical technique include minimal sample preparation, *in situ*, rapid and real time analysis. Good detection limits and wide dynamic ranges have been demonstrated in a variety of sample matrices. However, the signal in LIBS is affected by a high continuum background which demands time resolved detection, and relatively poor precision caused by the very strong non-linear nature of the laser-material interaction [203]. Calibration can be a difficult task for many matrices.

The problem of matrix effects has been addressed in many publications. For example, Eppler et al.[204] reported the effects of analyte speciation and matrix composition on the determination of Pb and Ba in soil and sand with the use of LIBS. The form of the chemical compound (carbonate, oxide, sulfate, chloride, or nitrate) and, the bulk sample composition (different proportions of soil and sand in a soil/ sand mixture) were found as factors to influence the emissions from Pb and Ba in both matrices. In their study, the effects of speciation where not correlated to any physical property or with the absorptivity of the compounds. However, changes in the bulk sample composition were related to changes in the concentration of ionized species through perturbation of the electron density. Although some suggestions were made to correct for the matrix effect, no universal solution to the problem was proposed[204].

Later, a normalization procedure was presented by Chaleard et al.[205]. In this approach, quantification and correction for matrix effects is done assuming emission lines to be a function of two parameters: the vaporized mass and the plasma excitation temperature. In their studies, the ablation mass was determined using an acoustic signal, whereas the excitation temperature was measured by the two-line method. The two line method consists on the measurement of the

ratio between two lines of a given element used as a “temperature sensor”. The two lines chosen originate from two separate energy levels in order to give a ratio that is sensitive to variations in the excitation temperature. It was demonstrated that normalization of the net emission intensity by both the acoustic signal and the temperature allowed for a multi-matrix calibration curve with about 5% precision for Cu and Mn in various alloy matrices.

Panne et al.[138, 182] proposed the use of temperature-normalized intensity ratios. This method was proposed for the LIBS analysis of major constituents (Si, Al, and Ca) in glass and glass melts. The normalization resulted in linear calibration plots and improved analytical performance (8–20% accuracy).

Ko et al.[206] examined the possibility of using internal standardization in laser ablation-microwave-induced plasma (LA-MIP) experiments. In these experiments with binary alloys, the authors found that internal standardization could be successfully applied if the line intensities were measured after a sufficient time delay, allowing the atomization of the sample material to be completed. This delay time was found to be significantly longer for Cu/Zn alloys (~16 μs), where the elements involved have largely different vapor pressures, than, for instance, Fe/Cr alloys. Gornushkin et al. [155, 158] reported on the use of linear and rank correlation for reliable material identification. Galbacs et. al. [165] proposed a new calibration approach to analyze binary solid samples at the percentage level. The method is based on the observed dependence of the linear correlation coefficient on the analyte concentration in a binary sample. The linear correlation coefficient is calculated between spectra of a range of certified standards and the spectrum of a reference sample (the analyte in the form of a pure metal), and the resulting curve is used as a calibration curve. Their method provided 1–5% accurate results for major components. Later, they report on a matrix-free calibration based on the normalization of the

emission intensities by surface density for correction of matrix effects in the detection of magnesium in powdered samples[203].

In 1999, Ciucci et al. [207] proposed a new method for standard-less LIBS analysis. The so-called calibration-free laser-induced breakdown spectroscopy (CF-LIBS) is as an alternative method to quantitative analysis by conventional calibration curves. This method compensates for matrix effects by applying basic equations derived from the local thermodynamic equilibrium assumption. The method relies on the assumptions of stoichiometric ablation, local thermal equilibrium and, in its initial formulation, optically thin plasmas [2, 207]. Several research groups have applied this and variants of this method to the analysis of different types of samples [122, 207-219].

This research aims to a further insight into normalization of the signal for quantitative LIBS analysis; the procedure looks into a possible correlation between the background fluctuation (or plasma continuum) and the analytical signal in single-shot measurements. This method has been proposed by Xu et al. for the detection of Zn in aerosol samples[220]. The basic idea behind this method is that shot-to-shot signal fluctuations can be described as a multiplicative effect, for both the spectral peaks and the background fluctuation. In the practical implementation of the approach, numerous single-shot spectra were recorded, and spectral line intensities were found to correlate with the continuum plasma background. A simple algebraic model was proposed [220]in which the background (B_i) for each laser shot i was given as the sum of a constant (b_o) and a fluctuating ($k_1 f_i$) term, where k_1 is a proportionality factor and f_i is responsible for the signal and baseline fluctuations. The peak height measured for shot i, can be expressed as

$$P_i = B_i(1 + kC) - kCb_o \tag{6.1}$$

where k is a proportionality factor that correlates the fluctuations with the peak intensity and C is the element concentration. A plot of the peak intensity versus the background baseline intensity should then yield a straight line with a slope (α) equal to $1+kC$, and a plot of (α-1) vs. C would therefore result in a linear calibration curve passing through the origin and free of fluctuation effects. This plot can be used instead of a traditional calibration curve[220].

Gornushkin et al.[221] applied this method to the analysis of iron, aluminum, phosphorous, silicon in phosphate rock, zinc in brass, and chromium in stainless steel. Although they found some degree of correlation, the correlation coefficients were somewhat uncertain due to the large scatter of the experimental points; the plot of (α-1) vs. C was not linear and therefore no improvements were obtained when using this methodology. Nevertheless, this method seems to be simple to apply and has given good results in the case of aerosol samples[220], and it was therefore considered worth of being revisited. Its usefulness in the case of solid samples would be assessed in comparison to conventional calibration plots.

Experimental

The experimental system and spectral data acquisition used in all measurements have already been described in detail in Chapter 5. The schematic of the setup is illustrated in Fig. 5-4. Aluminum alloys and steel standards were used in these experiments. The aluminum alloy standard disks came from:

- National Research Council Industrial Materials Institute (NRC-IMI) in Canada
- APEX Smelter Co. in South Africa, and
- Federal Institute for Materials Research and Testing (BAM) in Germany

The elemental compositions for these standards are given in tables 6-1 to 6-3, respectively. Besides aluminum alloys, a silicon wafer was used to monitor the relationship between the signal

and the background. The composition of the steel standards (C1-C10) from BAM is presented in Table 6-4.

For all the experiments, pulse energy of 90 mJ and a repetition rate of 1 Hz were used. The detector delay time and gate width values were selected according to the emission lines to be analyzed.

Results and Discussion

To date, most of the research devoted to enhance LIBS sensitivity and precision is based on averaging of spectra (including data filtering algorithms) as a means to overcome the extensive spectral fluctuations observed on a laser shot-to-shot basis[222]. There are some industrial tasks, e.g. *in situ* analysis of metallurgic specimens, requiring a fast, non-contact, and reliable method in where single-shot spectra acquisition by LIBS might become a reliable alternative for analysis[223].

As described in the chapter introduction, if there is an association between the spectral peak and the background fluctuation the slope of this plot can be used to normalized the signal for single-shot experiments. Several experiments were carried out to confirm this association. In the top part of Figure 6-1, a 10 nm spectral window from 246 to 256 nm is presented for steel with an approximate content of 0.5% Si (BAM-C1). In the bottom part, a positive zoom of the Si peak at 251.61 nm is shown. This peak is selected for the subsequent analysis. It is observed in Fig 6-1 that the spectrum is very rich in lines and the background around the selected Si line is not as uniform as desired. To avoid using the wings of the line itself when calculating the true background, several so-called "backgrounds" were tested (Figure 6-2):

- Vicinity of the line, $B_{i.}$
- Left of the peak, B_{left}. For this line, B_{left} is of relatively lower intensity than the background at the right (Fig. 6-1).

- Spectral window (~ 10 nm), $B_{i,average.}$
- Net background, $B_{i,net}$; ($B_{i,net} = B_i - B_m$) where B_m refers to the minimum number of counts present in the spectral window.

Figure 6-3 presents the plots of the peak intensity (P_i) vs. the four backgrounds described above for 50 individual measurements (50 spectra) in steel C1 taken at 6μs delay time and 6μs integration time for the detector. Good linear correlation is observed in all four cases, with correlation coefficients higher than 0.96. In addition, Figure 6-4 shows a good correlation between B_i and $B_{i,average}$. Consequently, the background around the line, B_i, is used for all succeeding experiments. The fluctuation of the peak intensity for Si at 251.61 nm in steel with the number of individual laser pulses is presented in Figure 6-5. The calculated %RSD for these 50 spectra is ~ 40%. Figure 6-6 shows the fluctuation of the background, B_i, vs. the number of individual spectra. If these two plots are compared against each other (Fig. 6-5 and 6-6), no immediate similarities arise. However, if a constant arbitrary value, which can be identified with b_o in equation 6-1, δ, is subtracted in Fig. 6-6, a similar fluctuation trend is observed for both, intensity and background (Fig. 6-7). This information is utilized in the forthcoming data analysis.

Calibration plot for silicon in steel

For most of the 10 steel standards, the plot of P_i vs. B_i for Si at 251.61 nm is linear when all 50 single-shot spectra are used (Figure 6-8). There were some cases in which linearity is present for most spectra but for some points of higher background values, the signal doesn't increase accordingly (Figure 6-9). This behavior was only present in some of the standards and for less than five points (spectra) in the plots.

Spectra were acquired to build a conventional (similar to Chapter 5 calibration plots) and a normalized calibration plot for Si using the 10 steel standards. For this spectral line, a detector

delay and a gate width of 6 μs were chosen. Fifty single-shot spectra were acquired per triplicate per sample.

For a conventional calibration plot, the average of the net peak intensity (P_i) minus B_i is plotted as a function of the Si % concentration (Figure 6-10). For the normalized calibration, (α-1) is plotted vs. the Si % concentration (Figure 6-11). By comparing these two plots, the spread of the data is considerably higher for the conventional calibration scheme shown in Fig. 6-10. For the normalized approach, one of the points (~1.5% Si) is an outlier to the linear fit. The reasons for this anomaly are not understood: apparently, the normalized approach presents a smaller linear dynamic range than the conventional approach. However, it is clear that the normalized calibration plot has a higher accuracy than the conventional one.

Calibration plots in aluminum alloys

This model was also applied to the LIBS analysis of aluminum alloys, seven emission lines corresponding to the elements Cr, Mg, Fe, Sn, Mn and Si were used in these experiments (Table 6-5). For each aluminum alloy, 50 single-shot spectra were acquired per triplicate. For all the lines, a detector delay of 2 μs and a gate width of 0.5 μs were chosen. Figures 6-12 to 6-18 present a comparison of the performance of the conventional calibration approach vs. the normalized method. For both methods, there is a linear correspondence with the element concentration. Nevertheless, for Si in aluminum (Fig. 6-18), the normalized method is more susceptible to higher Si concentrations and two points are outliers for the linear fit.

In each figure, the calibration equation: $y = (m \pm \Delta m).\ x$ together with the correlation coefficient of the linear fit is presented. The correlation coefficient, the value of the slope, m, and its associated error, Δm, are used to compare the accuracy of the two plots for each line. Table 6-6 is a summary of the results present in Fig 6-10 to 6-18. For most cases, there are improvements

when using the normalized approach. The best improvement is for Si in steel (Figs. 6-11 and 6-12). However for Mg, Fe and Mn in aluminum alloys, the conventional method performs slightly better.

Correlation coefficient as a function of the detector delay time

To better understand the conditions for the existence of a correlation between the background (or plasma continuum) fluctuations and those of the analytical signal the following experiment was envisaged. The intensity of a Si peak at 298.76 nm present in silicon wafer (Figure 6-19) was monitored at different detector delay times in the range of 0.5 to 50 μs. The gate width of the detector was fixed to 1μs. 200 single-shot spectra were acquired per delay time. A correlation plot is then obtained for each delay time (Figure 6-20). As expected, the intensity of the background or *continuum* decreases with the increasing delay time; the linear correspondence between the peak intensity and the background is practically lost for delay times higher than 6μs. A plot of the correlation coefficient as a function of the detector delay time is shown in Figure 6-21. The experimental conditions used for spectra acquisition affect this normalized approach. There is no correlation between signal and background for higher delay times.

Conclusions

The feasibility of constructing normalized calibration plots based on the use of the relationship between the peak and background intensity was evaluated for Si (in steel) and Cr, Mg, Fe, Sn, Mn and Si in aluminum alloys. The normalized plots were compared to the conventional calibration plots obtained by averaging the 50 individual spectra. When using the normalized approach, some improvements were observed especially in the case of Si in steel. However, the improvements observed were not systemic and general for all the cases investigated: this seems to indicate that the approach has to be considered case by case. Our

research indicate, however, that the correlation between the peak signal and the background depends strongly upon the delay time chosen for the measurement (see Figure 6-21) and upon the availability of spectrally well isolated lines to allow a correct measurement of the background.

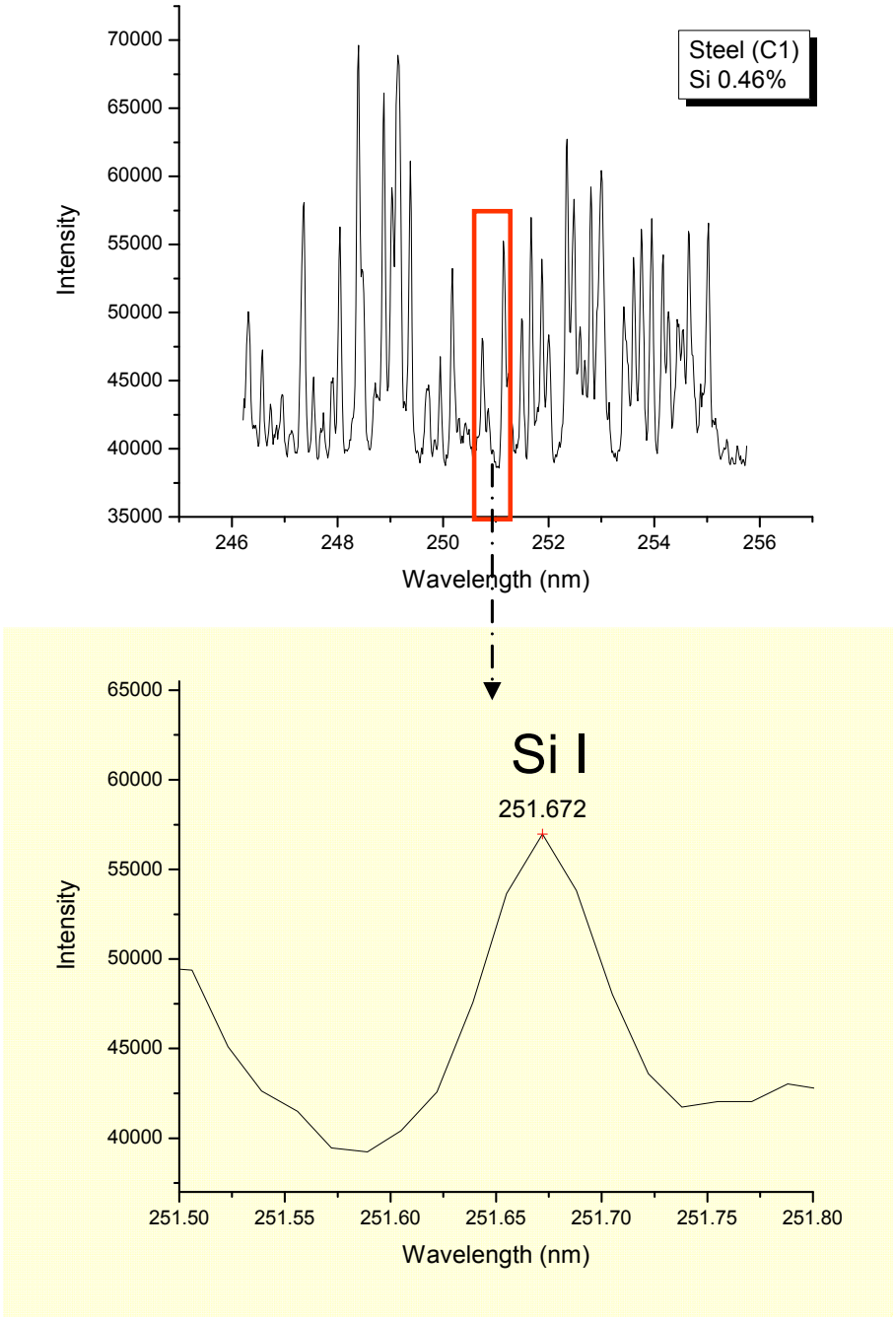

Figure 6-1. Spectrum of steel in the wavelength range 246-256 nm

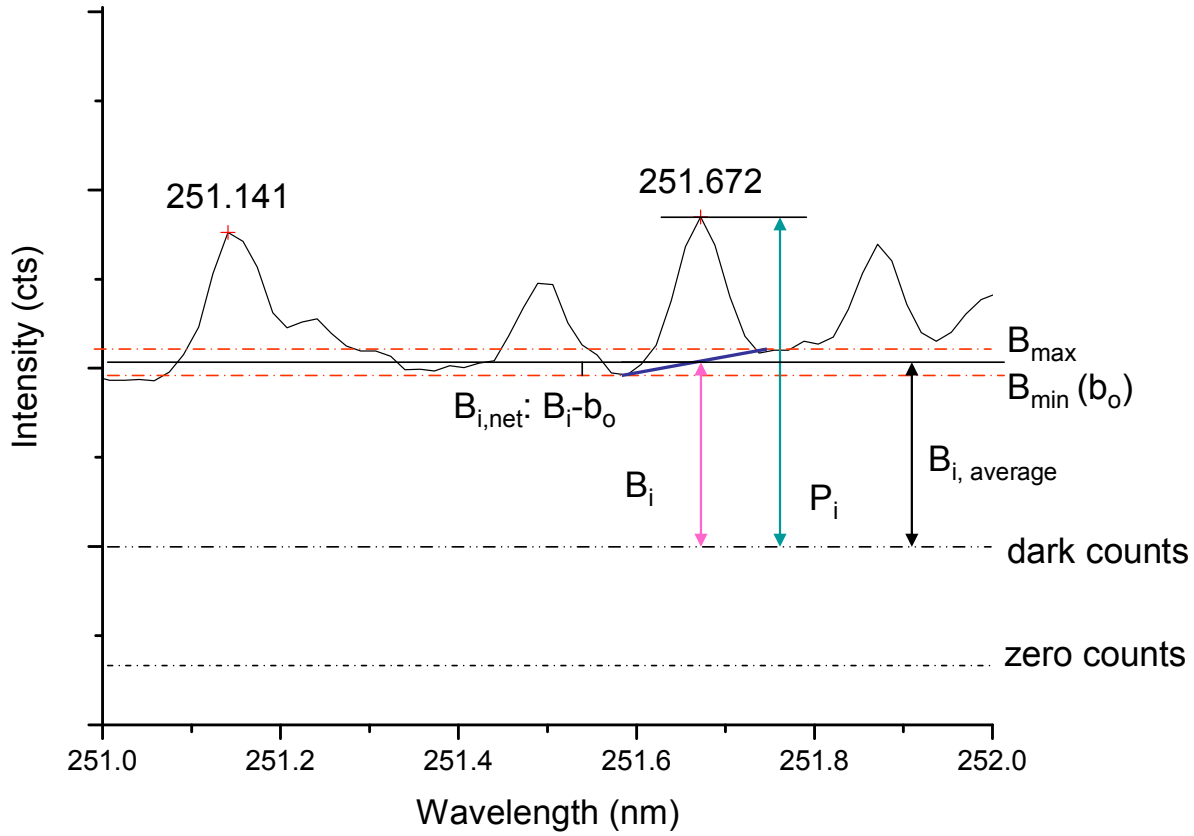

Figure 6-2. Background(s) for Si I 251.61 nm in steel

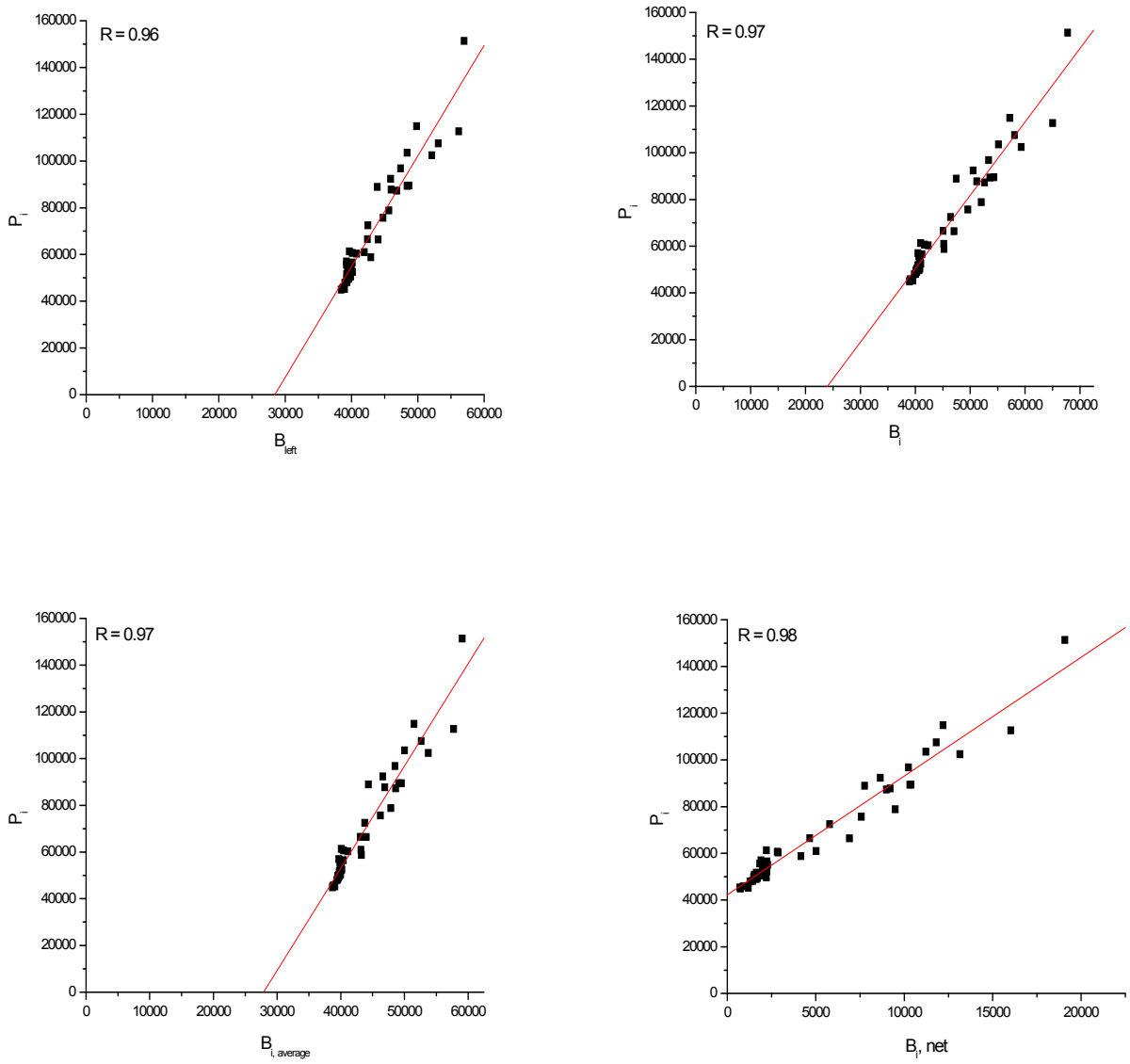

Figure 6-3. Linear correlation between P_i for Si at 251.61 nm in steel C1 and the correspondent background.

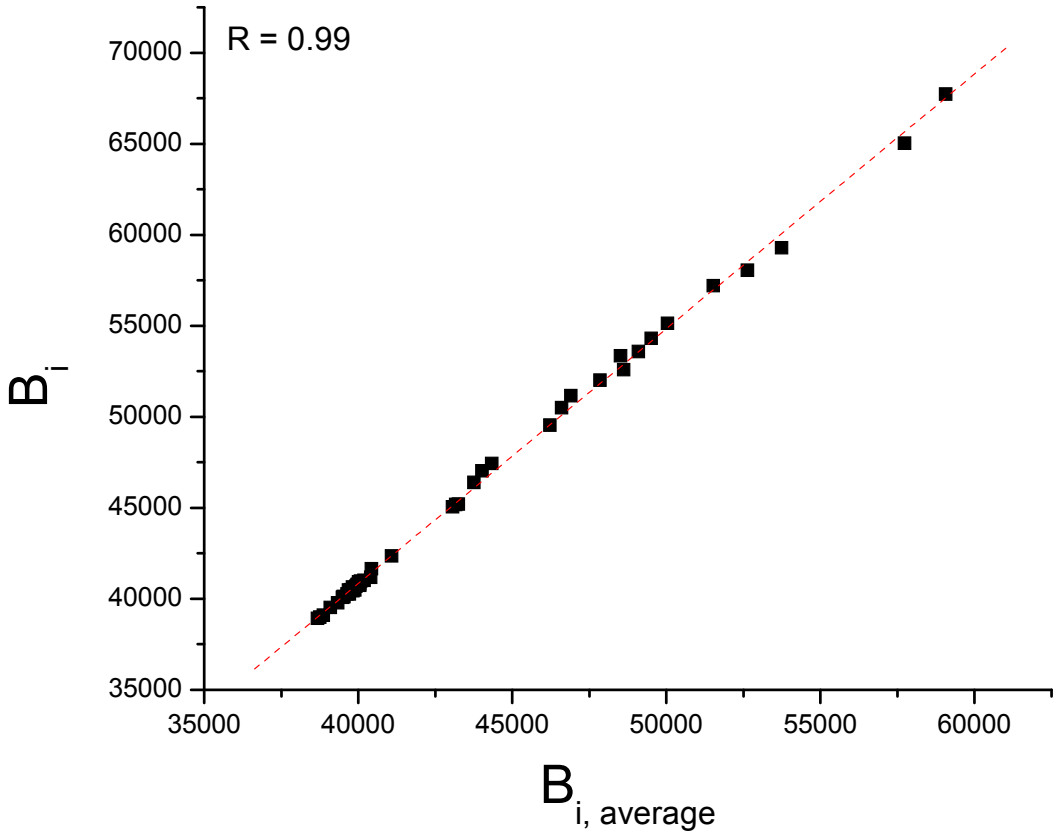

Figure 6-4. Linear correlation between background around the Si 251.61 nm (B_i) and in the spectral window from 246-256 nm ($B_{i,average}$).

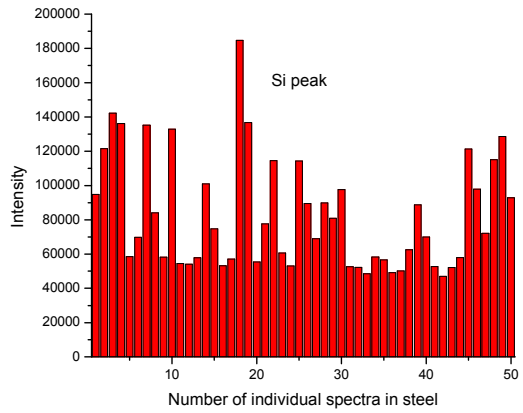

Figure 6-5. Fluctuations of intensity of Si at 251.61 nm in steel for 50 individual spectra.

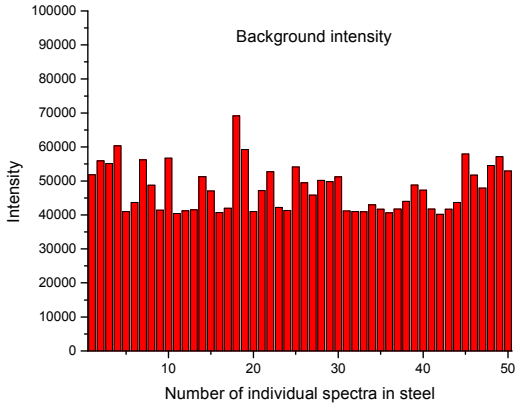

Figure 6-6. Fluctuations of background intensity of Si at 251.61 nm in steel for 50 individual spectra.

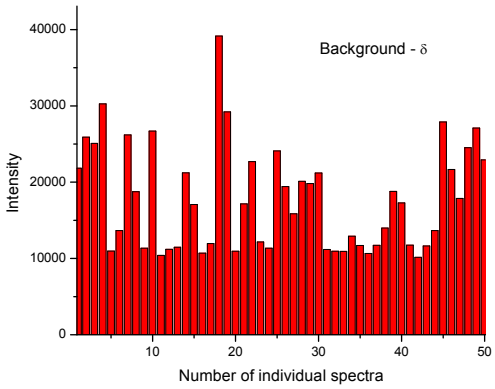

Figure 6-7. Fluctuations of intensity of background minus an arbitrary constant value in steel for 50 individual spectra

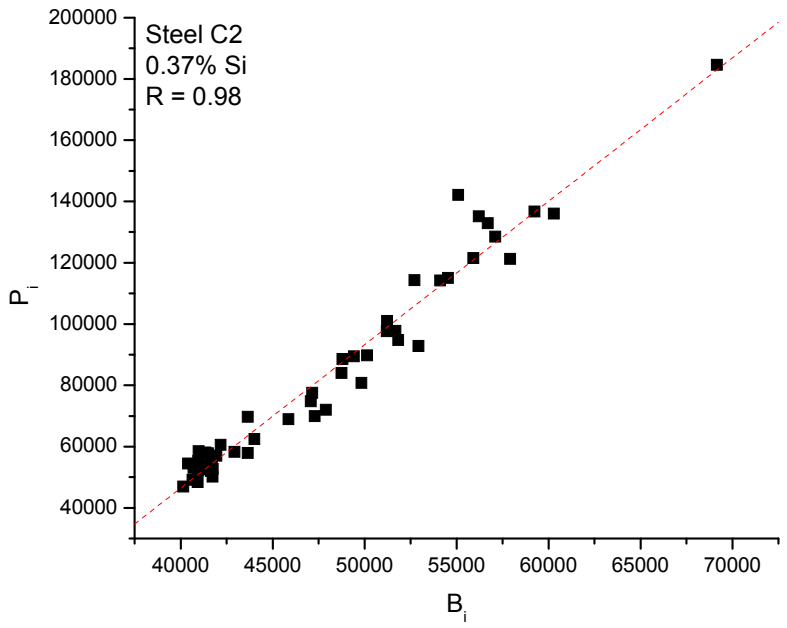

Figure 6-8. Peak intensity as a function of the background. Linear correlation is observed for Si at 251.61 nm in steel C2

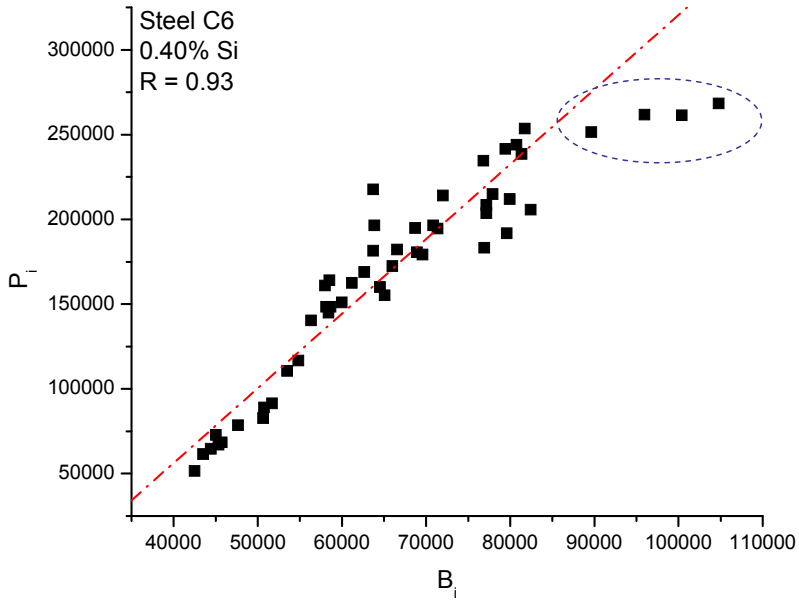

Figure 6-9. Peak intensity as a function of the background. Linear correlation is not achieved in all spectra for Si at 251.61 nm in steel C6

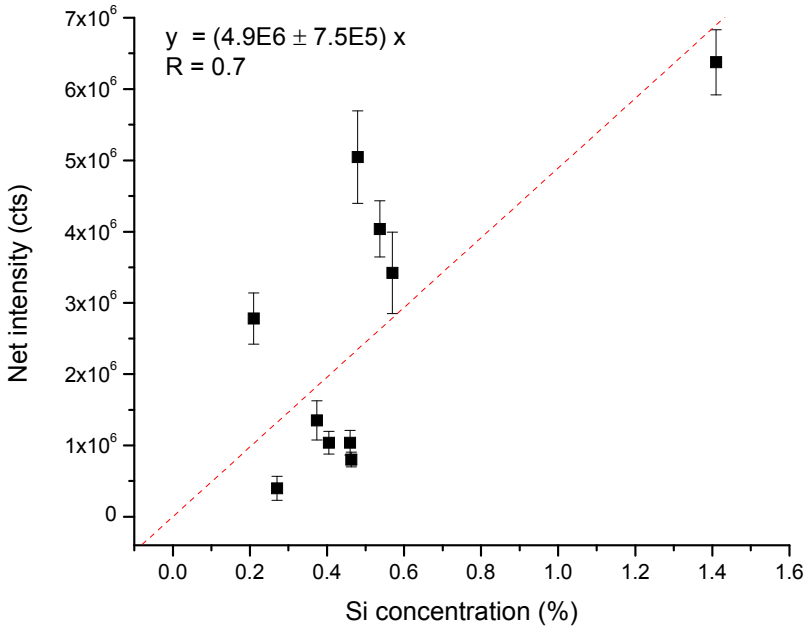

Figure 6-10. Calibration plot for Si atomic line at 251.61 nm in steel

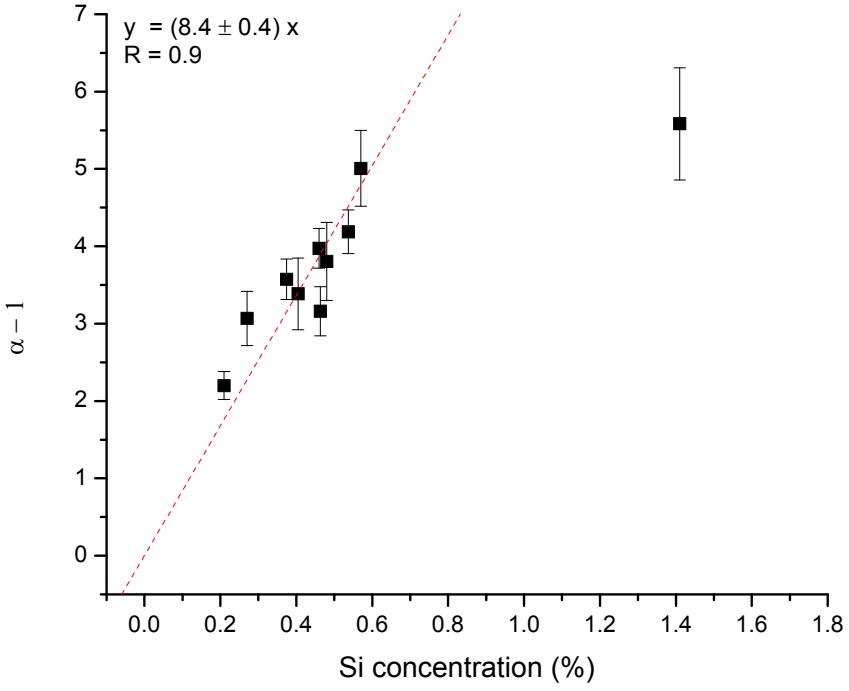

Figure 6-11. Plot of α-1 against Si concentration in steel

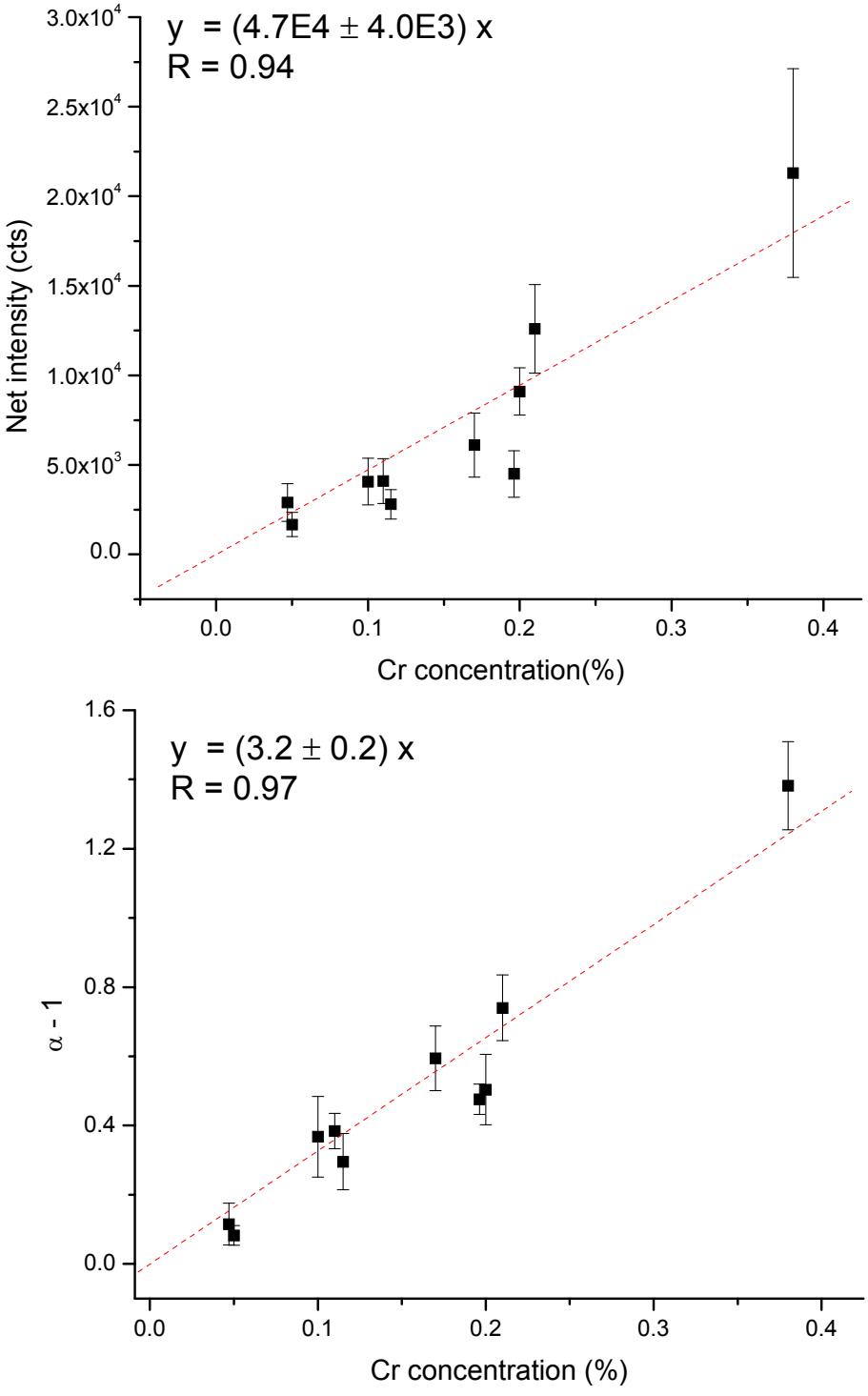

Figure 6-12. Comparison of conventional and normalized calibration plots for Cr at 301.52 nm in aluminum alloys.

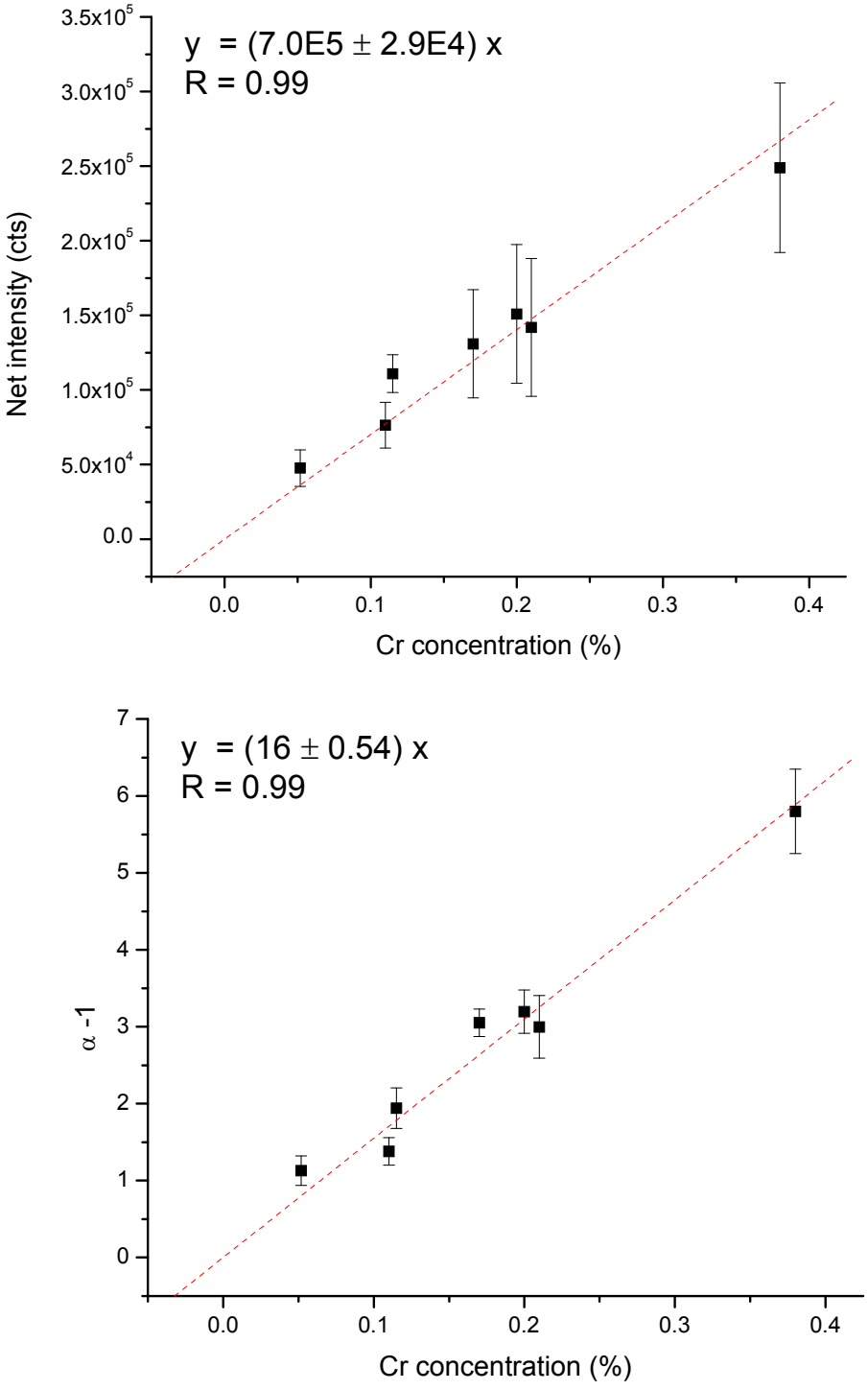

Figure 6-13. Comparison of conventional and normalized calibration plots for Cr at 283.56 nm in aluminum alloys.

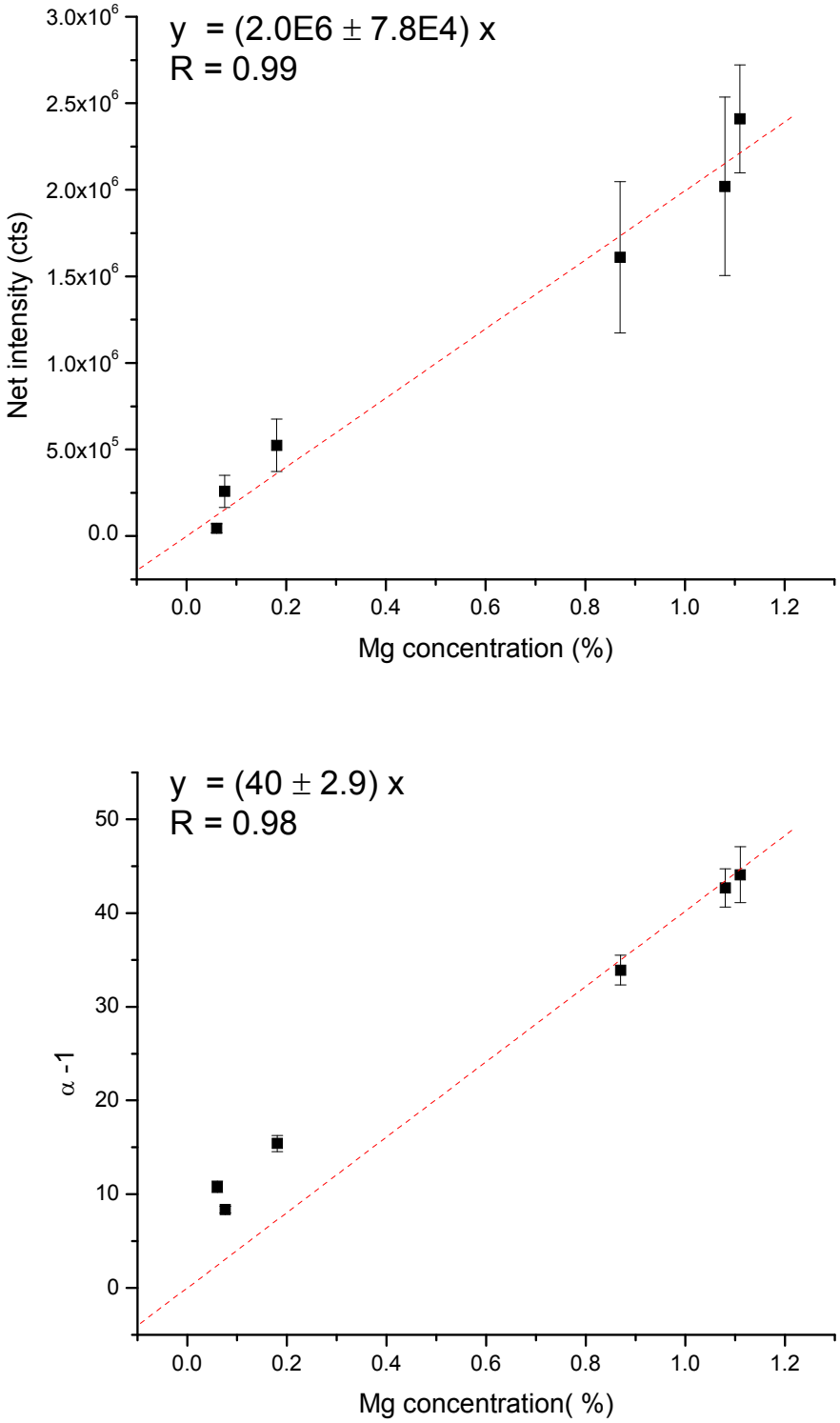

Figure 6-14. Comparison of conventional and normalized calibration plots for Mg at 285.21 nm in aluminum alloys.

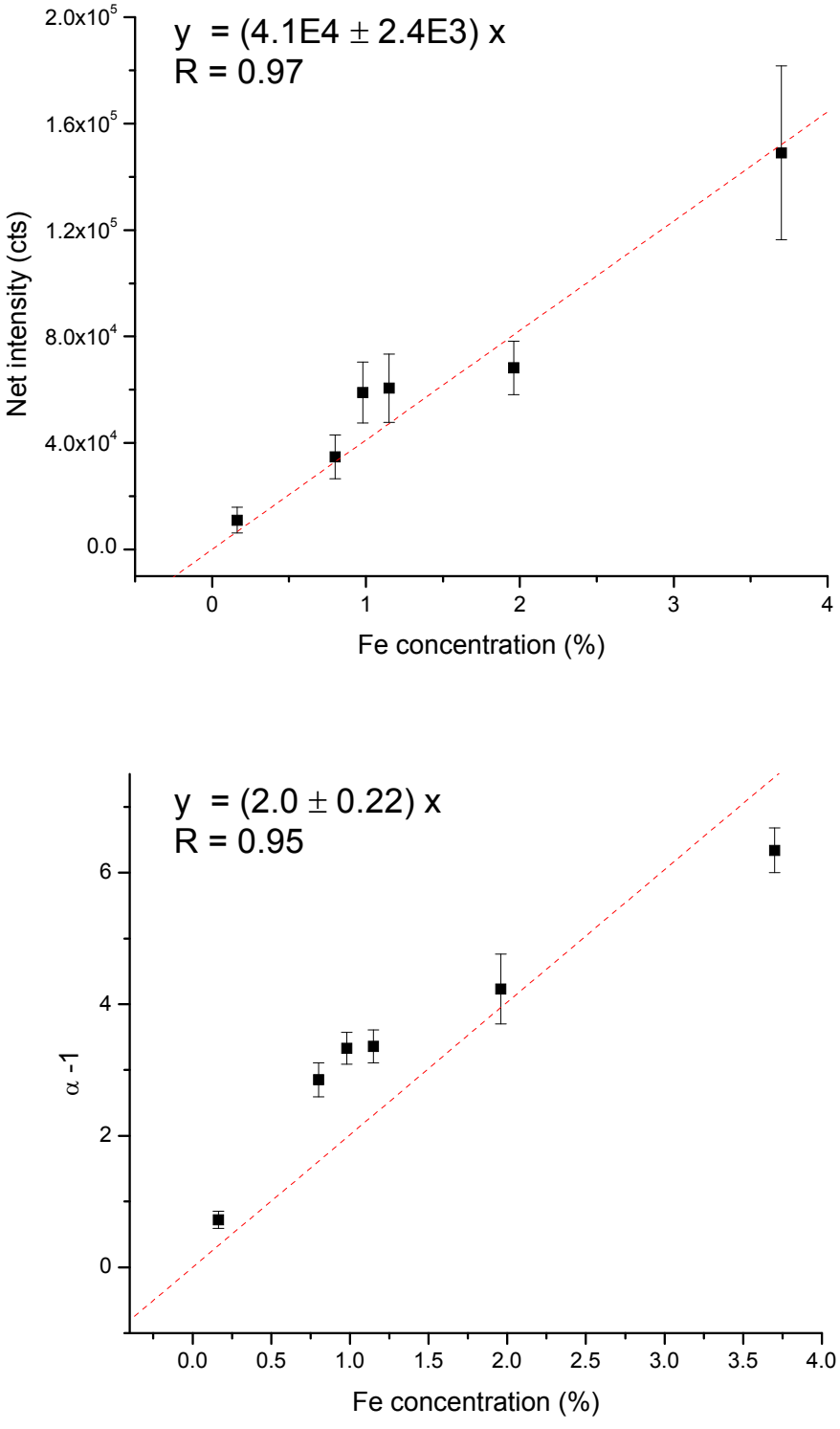

Figure 6-15. Comparison of conventional and normalized calibration plots for Fe at 302.11 nm in aluminum alloys.

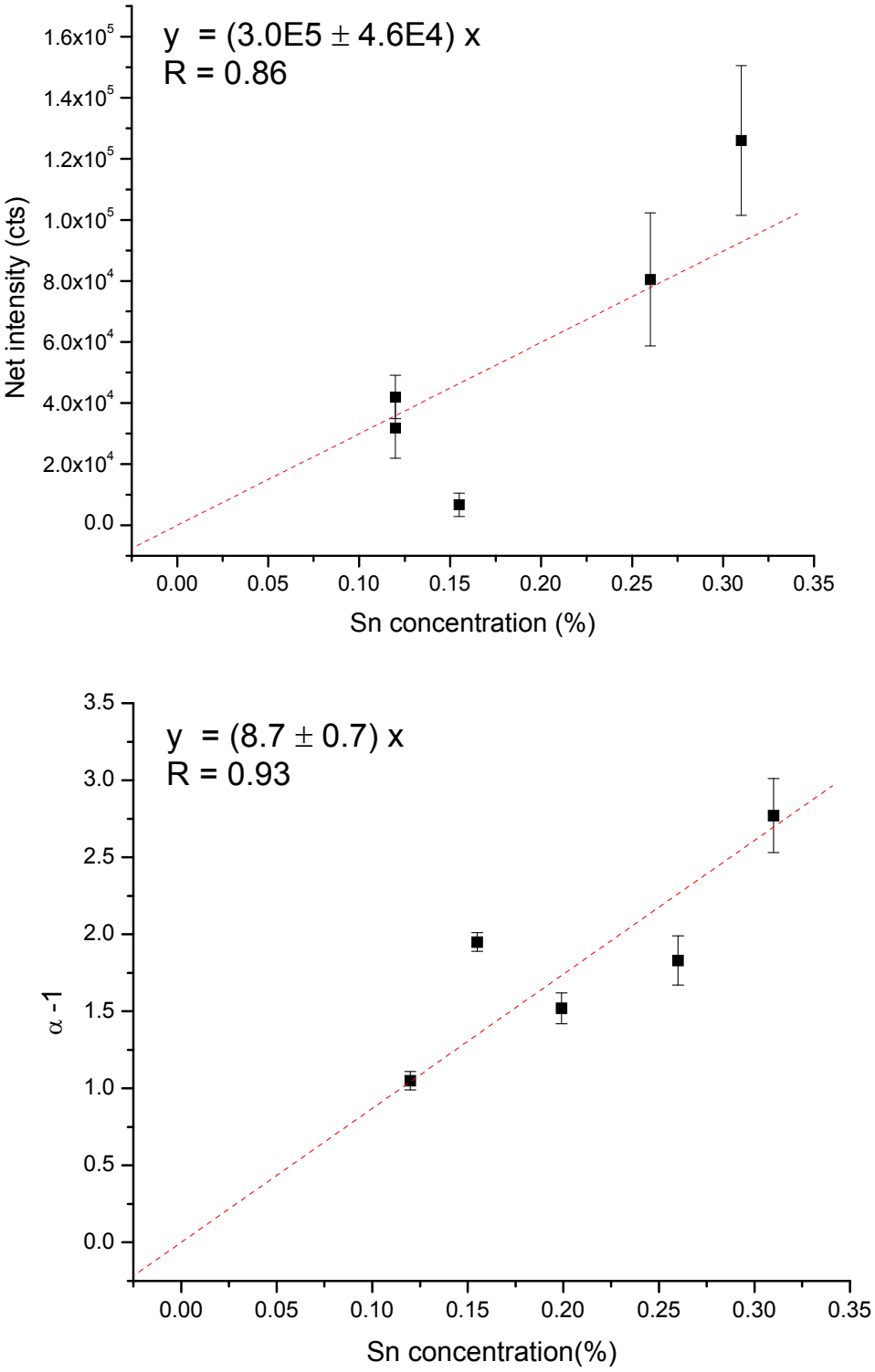

Figure 6-16. Comparison of conventional and normalized calibration plots for Sn at 283.99 nm in aluminum alloys.

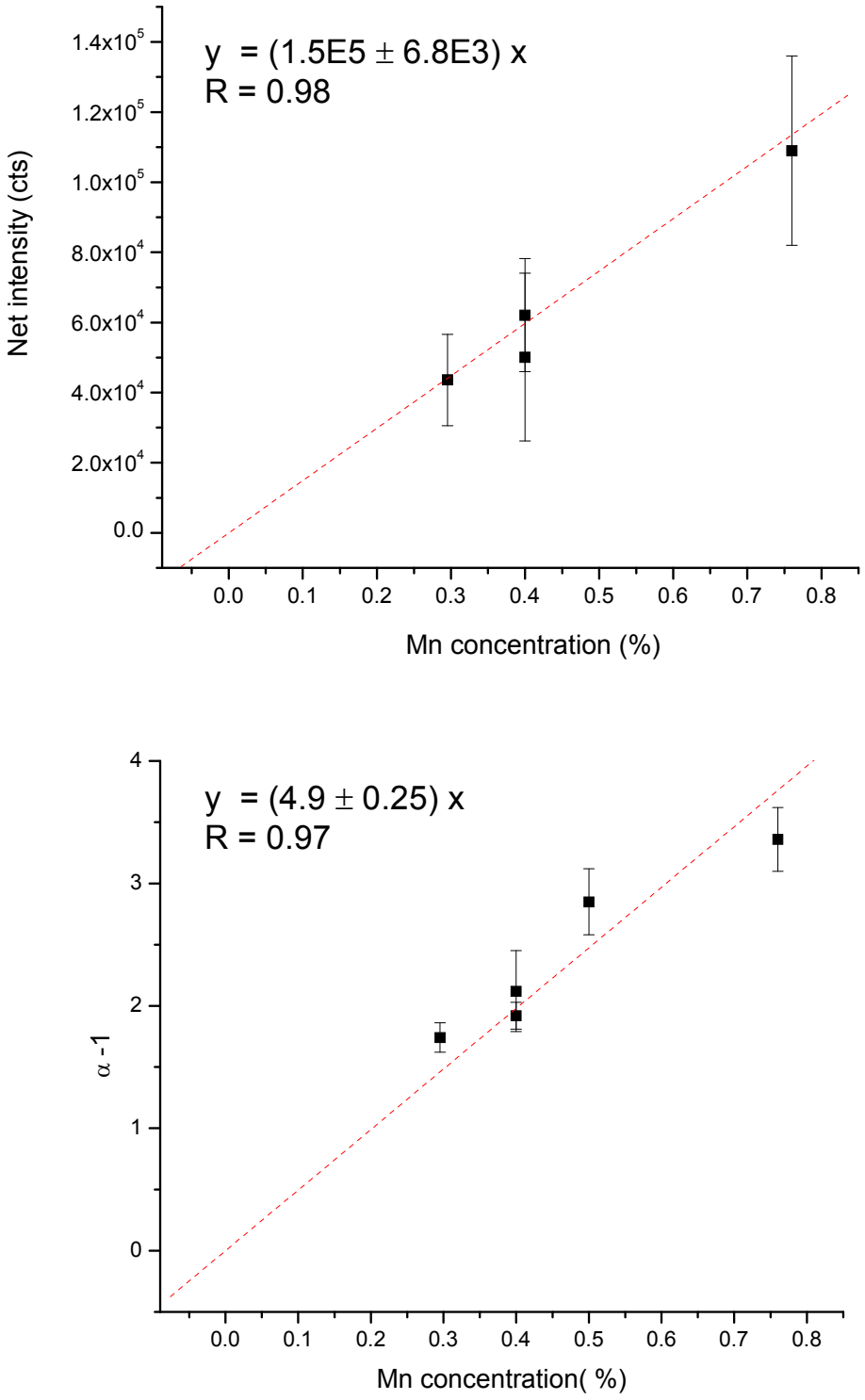

Figure 6-17. Comparison of conventional and normalized calibration plots for Mn at 288.96 nm in aluminum alloys.

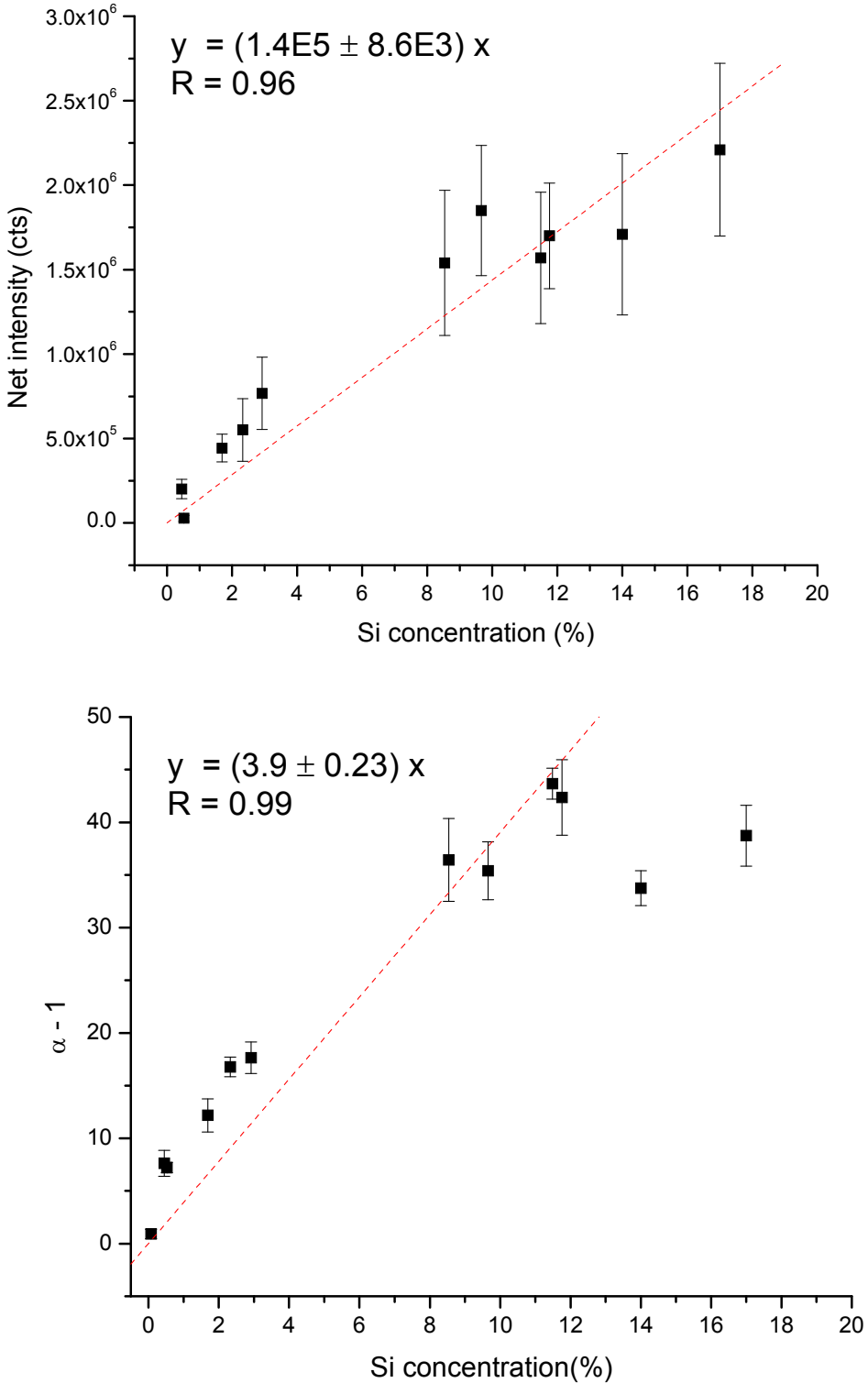

Figure 6-18. Comparison of conventional and normalized calibration plots for Si at 288.16 nm in aluminum alloys.

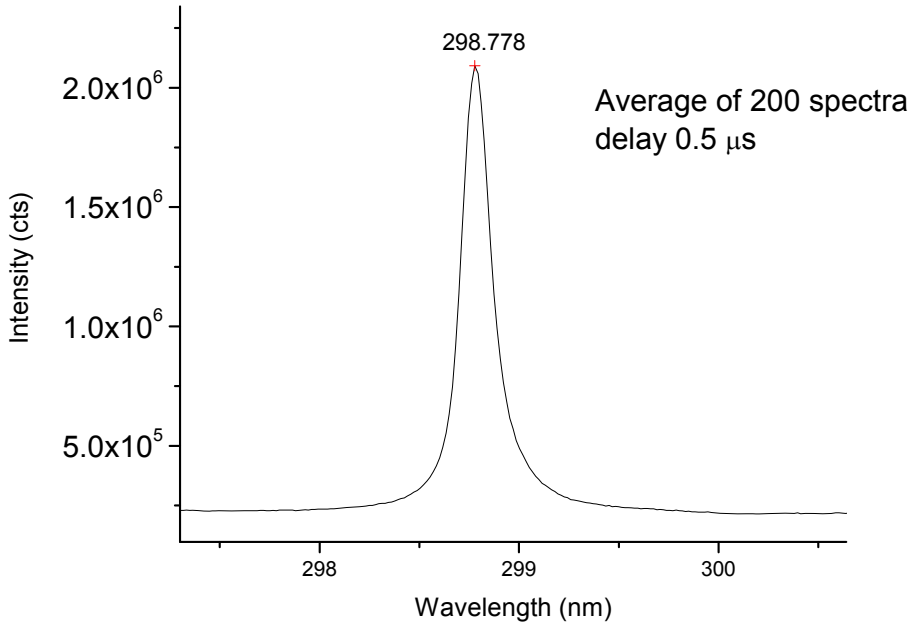

Figure 6-19. Spectrum of Si at 298.76 nm in silicon wafer.

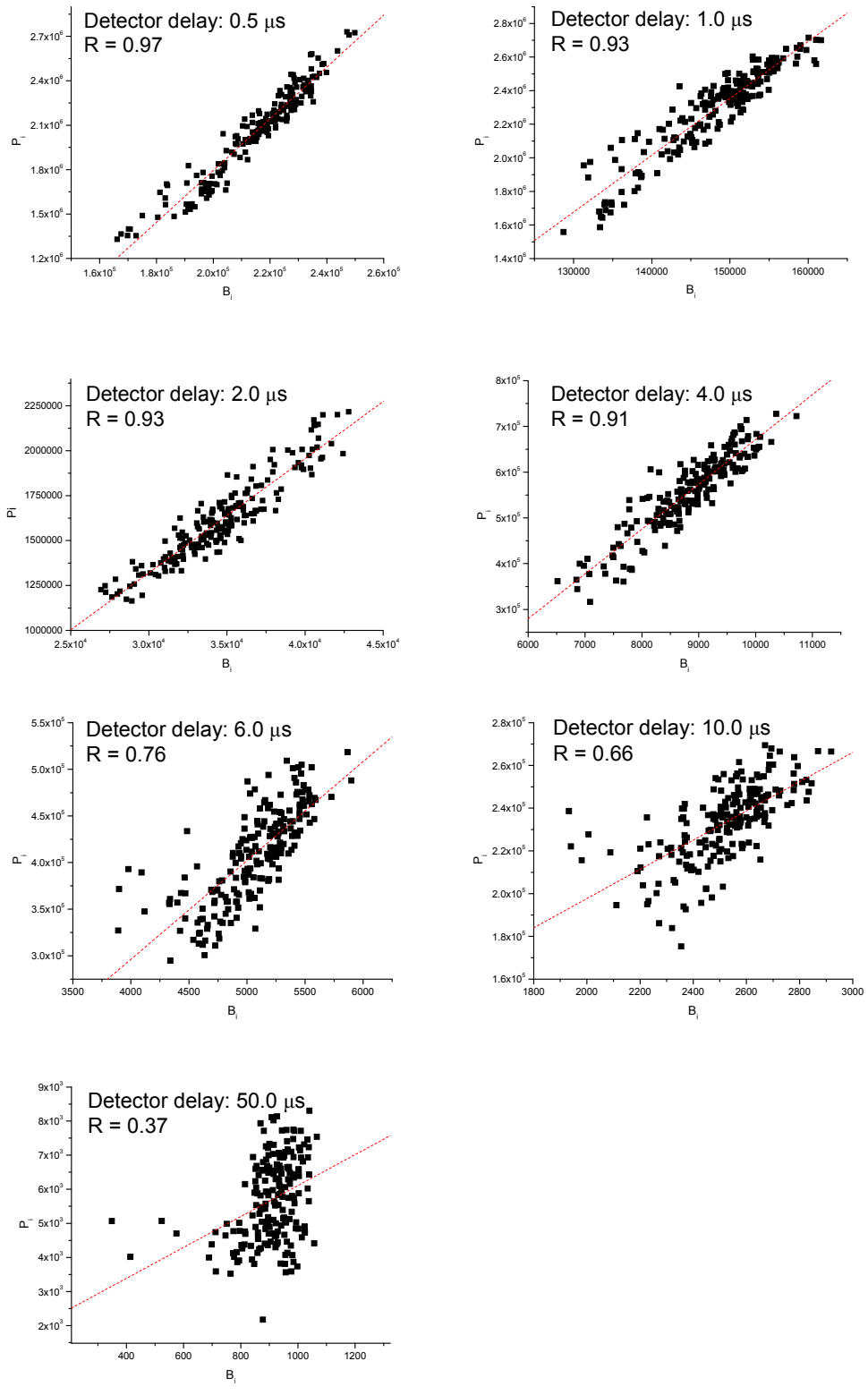

Figure 6-20. Peak intensity as a function of the background for Si at different delay times.

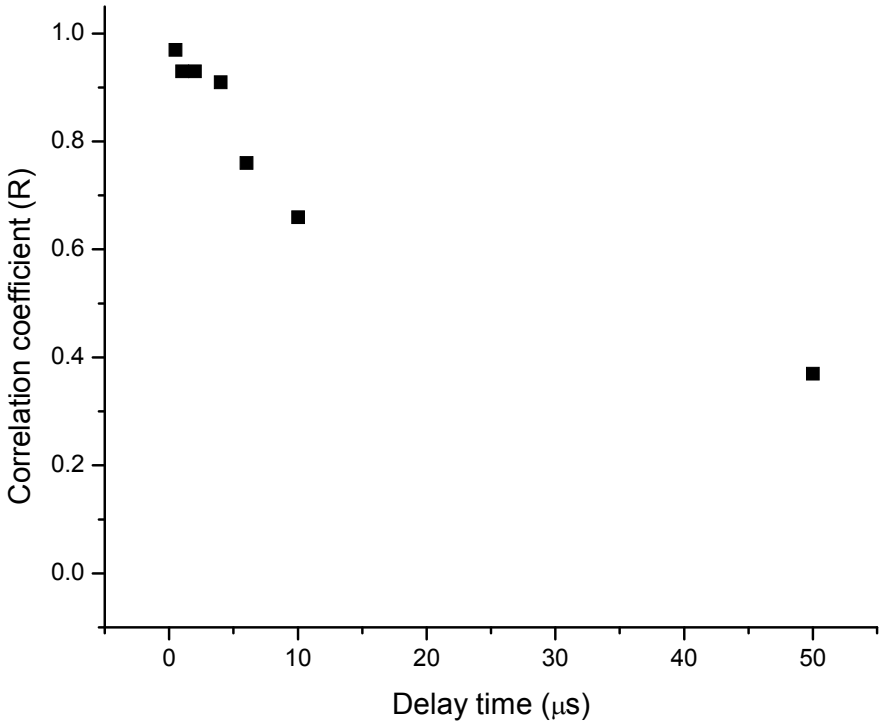

Figure 6-21. Correlation coefficient as a function of the delay time.

Table 6-1. Chemical composition in aluminum alloys NRC-IMI

Concentration Wt. %	N3005	N1075	N4104	MN397
Al	97.6	99.7	87.9	98.8
Si	0.084	0.079	9.67	0.049
Mg	0.37	0.004	1.33	0.012
Cu	0.44	0.007	0.15	0.0008
Zn	0.041	0.014	0.088	0.24
Fe	0.2	0.15	0.6	0.095
Mn	1.13	0.007	0.052	0.6
Ni	0.026	0.006	0.026	0.008
Ti	0.05	0.011	0.024	0.14
Cr	0.026	0.006	0.026	0.008
Sn	0.005	0.003	0.005	0.006
Pb	0.005	0.003	0.005	0.006
Bi	0.006	0.003	0.09	0.007
Zr	0.006	0.004	0.005	0.007

Table 6-2. Chemical composition in aluminum alloys APEX Smelter Co.

Concentration Wt. %	B8	D33	M7	R14	AA3	D28	SM9	SM10	S11
Al	87.9	84.9	85.47	79.59	69.14	81.55	85.34	84.67	89.20
Si	2.33	8.54	0.52	14	17	9.66	1.69	2.92	0.45
Mg	0.076	0.038	0.06	0.87	0.2	0.004	0.43	1.08	1.11
Cu	6.95	2.89	11.12	2.05	8	1.76	3	2.8	0.98
Zn	0.52	0.59	0.51	0.48	3.2	3.6	3.7	5.45	6.85
Fe	0.8	1.15	1.28	0.63	1.77	0.98	3.7	1.96	0.57
Mn	0.4	0.4	0.34	0.92	0.21	0.59	0.76	0.295	0.5
Ni	0.2	0.5	0.205	0.97	0.106	0.43	0.2	0.065	0.1
Ti	0.16	0.055	0.065	0.16	0.078	0.033	0.07	0.055	0.065
Cr	0.17	0.047	0.05	0.11	0.1	0.21	0.38	0.2	0.115
Sn	0.155	0.048	0.105	0.12	0.12	0.3	0.31	0.26	
Pb	0.165	0.14	0.11	0.1	0.08	0.34	0.32	0.245	
Bi	0.099	0.68				0.54			
Zr			0.17			0.123			

Table 6-3. Chemical composition in aluminum alloys BAM

Concentration Wt. %	308	309	314
Si	0.0707	11.76	11.49
Mg	2.29	0.00068	0.18
Cu	1.315	0.0048	2.07
Zn	5.67	0.0038	1.19
Fe	0.1634	0.0883	0.76
Mn	0.0342	0.0548	0.4
Ni	0.0122	0.00087	0.22
Ti	0.0285	0.0556	0.16
Cr	0.1962	0.00047	0.05
Sn			0.199
Pb			0.221
Bi			94 µg/g
Zr	0.0078		55 µg/g

Table 6-4. Chemical composition in steel standards BAM

Concentration Wt. %	C	Si	Mn	Cr	Ni	Mo	Co
C1	0.092	0.46	0.74	12.35	12.55	--	--
C2	0.0103	0.374	0.686	14.727	6.124	0.0138	--
C3	0.0345	0.463	0.722	11.888	12.85	0.0304	--
C4	0.019	0.27	1.4	18.46	10.2	0.265	0.116
C5	0.086	0.57	0.791	25.39	20.05	--	0.054
C6	0.066	0.405	1.38	17.31	9.24	0.092	0.053
C7	0.0141	0.48	1.311	17.84	10.2	2.776	0.0184
C8	0.143	1.41	1.7	17.96	8.9	--	0.018
C9	0.05	0.21	0.89	14.14	5.66	1.59	0.22
C10	0.0201	0.537	1.745	16.811	10.72	2.111	0.0525

Table 6-5. Spectral emission lines for the analysis of aluminum alloys

Element	Wavelength (nm)
Cr I	301.52
Cr II	283.56
Mg I	285.21
Fe I	302.11
Sn I	283.99
Mn II	288.96
Si I	288.16

Table 6-6. Results for the calibration curves and the analysis of Si, Cr, Mg, Fe, Sn and Mn

Element	Wavelength (nm)	Conventional	Normalized
Si I in steel	251.61	y = (4.9E6 ± 7.5E5) x %RSD = 15.3 R = 0.72	y = (8.4 ± 0.4) x %RSD = 4.76 R = 0.89
Cr I in aluminum alloys	301.52	y = (4.7E4 ± 4.0E3) x %RSD = 8.51 R = 0.94	y = (3.2 ± 0.2) x %RSD = 6.25 R = 0.97
Cr II in aluminum alloys	283.56	y = (7.0E5 ± 2.9E4) x %RSD = 4.14 R = 0.99	y = (16 ± 0.54) x %RSD = 3.37 R = 0.99
Mg I in aluminum alloys	285.21	y = (2.0E6 ± 7.8E4) x %RSD = 3.92 R = 0.99	y = (40 ± 2.9) x %RSD = 7.25 R = 0.98
Fe I in aluminum alloys	302.11	y = (4.1E4 ± 2.4E3) x %RSD = 5.85 R = 0.97	y = (2.0 ± 0.22) x %RSD = 11.00 R = 0.95
Sn I in aluminum alloys	283.99	y = (3.0E5 ± 4.6E4) x %RSD = 15.3 R = 0.86	y = (8.7 ± 0.7) x %RSD = 8.05 R = 0.93
Mn II in aluminum alloys	288.96	y = (1.5E5 ± 6.8E3) x %RSD = 4.53 R = 0.98	y = (4.9 ± 0.25) x %RSD = 5.10 R = 0.97
Si I in aluminum alloys	288.16	y = (1.4E5 ± 8.6E3) x %RSD = 6.14 R = 0.96	y = (3.9 ± 0.23) x %RSD = 5.90 R = 0.99

CHAPTER 7
CONCLUSIONS AND FUTURE WORK

Summary and Concluding Remarks

An extensive experimental procedure for the characterization of solid samples, glasses in particular, by LIBS was carried out in this research. There are a number of satisfactory techniques available for the elemental analysis of glass fragments for forensic purposes. In the first part of this is work, linear and rank correlation techniques were applied for discrimination of LIBS spectra from glass samples with similar chemical composition, some of them from the same source. The robustness of this technique was demonstrated by the 100% correct identification (95% confidence level for a type 1 error) obtained by linear correlation when used in combination with a spectral mask. The identification was reliable even when experiments were performed on different days when ambient conditions might be different and affect the line intensities in the LIBS spectra. The rationale of using spectral masking is to eliminate regions of the spectra containing several intense lines common to all samples and to take advantage of the trace element impurities present in these glasses. We are aware of the fact that there are more sophisticated ways to generate a mask than the one used in this study. However, it was felt useful to focus at first on a simple masking procedure to see whether any further elaboration of this concept was worth pursuing. More refined procedures are planned for the future.

The elemental analysis of glass by LIBS has the potential of becoming a useful technique for the discrimination of forensic glasses. Its usefulness as an analytical method for legal purposes will be determined by its general acceptance in the relevant scientific community. Evidence of "general acceptance" normally includes known error rates and publication of the methods in peer-reviewed journals[168]. These legal aspects and corresponding implications, which would require more in-depth statistical analysis, have not been considered in this work.

In the course of this study, several key instrumental parameters were identified and investigated, and a comparative study regarding the performance of up to four different commercial instruments for LIBS analysis of solids has been made. Results indicate that the *spectral resolution* and *sensitivity* of the systems are linked to the performance and suitability of the technique for material identification by correlation methods, especially when samples are of very similar composition.

While the qualitative characterization of materials without sample preparation is certainly one of the main advantages of LIBS, the possibility of performing accurate quantitative analysis relies on the use of calibration curves made with matrix-matched standards[1, 2]. Such quantitative analysis would also improve the discrimination capability of the technique in the case of the glass samples analyzed. The feasibility of constructing calibration plots for NIST and Corning glass samples was evaluated for Sr, Mg, and Ti. These three elements are common to most types of glasses and their determination can provide useful information for discrimination studies. All constructed calibration plots were linear ($R > 0.9$) over the studied range of concentrations. In most cases, relative errors of less than ±10% were obtained. The delay time and gate width chosen for the detector was also an essential parameter to conclude on the efficiency of these measurements. The obtained LODs were significantly lower than those required for the analysis of glass; therefore, these calibration plots could be used as to determine the quantitative composition of unknown glass fragments.

In addition to the conventional analytical procedures followed in LIBS analysis, a normalization procedure of the signal [220] was investigated in this research. The viability of constructing normalized calibration plots based on the use of the relationship between the peak and background intensity was evaluated for Si (in steel) and Cr, Mg, Fe, Sn, Mn and Si in

aluminum alloys. The normalized plots were compared to the conventional calibration plots obtained by averaging the 50 individual spectra. When using the normalized approach, improvements were obtained for most lines especially in the case of Si in steel. The correlation between signal and background decreases with the increasing detector delay time.

The results of all these investigations have allowed a fair assessment of the applicability of LIBS for discrimination and quantitative characterization of solid samples in general, and glasses in particular.

Future Research Directions

As an addendum to the research carried out in this dissertation, it is suggested that, for the discrimination analysis, masks for spectral regions instead of lines should be used. It would also be beneficial to focus the analysis to the lines of the minor components common to these glasses instead of blocking the lines of the ones present in higher concentration. To improve the discrimination capability of the technique, the constructed calibration plots can be used to calculate the concentration of unknown glass fragments.

The normalization based on the correlation of intensity and background should also be applied to the analysis of glasses and the results can be compared to the conventional curves.

Some preliminary results, not reported in this Dissertation, suggest the use of another normalization procedure based on the observed behavior of the signals obtained for selected elements, present in the same concentration (or in a narrow range of concentrations) in different matrices, as a function of the energy of the excited state of the transitions investigated. This approach is similar to that used in double-pulse LIBS to interpret the enhancements observed[202], and has not been tested so far with the LIBS technique. Two matrices are used to construct independent calibration curves for each element investigated. For any given element, the plot of the intensity ratio in the two matrices versus the excitation energy will reveal whether

matrix effects are present as well which physical parameter (temperature, ablated mass) is involved.

Finally, as shown in a recent publication [196], by analyzing many spectra obtained under the same conditions, the noise characteristics of the measurements could be investigated by plotting the standard deviation (SD) and the relative standard deviation (RSD), calculated at every spectral element (pixel) of the selected spectral range, as a function of wavelength, for different delay times [196]. This procedure, which would complement our correlation analysis, appears to be useful to characterize the *limiting* type of noise present in our experiments.

LIST OF REFERENCES

[1] Cremers DA, Radziemski LJ. Handbook of laser-induced breakdown spectroscopy. Chichester: John Wiley 2006.

[2] Miziolek AW, Palleschi V, Schechter I. Laser-induced breakdown spectroscopy (LIBS): fundamentals and applications. Cambridge: Cambridge University Press 2006.

[3] Lee Y-I, Song K, Sneddon J. Laser-induced breakdown spectrometry. Huntington: Nova Science Publishers 2000.

[4] Singh JP, Thakur SN. Laser-induced breakdown spectroscopy. Amsterdam: Elsevier 2007.

[5] Bogue RW. Boom time for LIBS technology. Sensor Review. 2004; 24:353.

[6] DeMichelis C. Laser induced gas breakdown: A bibliographical review. IEEE Journal of Quantum Electronics. 1969; 5(4):188-202.

[7] Lee WB, Wu JY, Lee YI, Sneddon J. Recent applications of laser-induced breakdown spectrometry: A review of material approaches. Appl Spectrosc Rev. 2004; 39(1):27-97.

[8] Lee YI, Yoo YJ, Sneddon J. Recent advances in laser-induced breakdown spectrometry. Spectroscopy. 1998; 13(7):14.

[9] Majidi V, Joseph MR. Spectroscopic applications of laser-induced plasmas. Crit Rev Anal Chem. 1992; 23(3):143-62.

[10] Radziemski LJ. From laser to LIBS, the path of technology development. Spectrochim Acta, Part B. 2002; 57(7):1109-13.

[11] Rusak DA, Castle BC, Smith BW, Winefordner JD. Recent trends and the future of laser-induced plasma spectroscopy. TrAC, Trends Anal Chem. 1998; 17(8-9):453-61.

[12] Scott RH, Strasheim A. Laser induced plasmas for analytical spectroscopy. Spectrochim Acta, Part B. 1970; 25(7):311-16.

[13] Sneddon J, Lee Y-I. Laser-induced breakdown spectrometry. The Chemical Educator. 1998; 3(6):1-7.

[14] Song K, Lee Y-I, Sneddon J. Applications of laser-induced breakdown spectrometry. Appl Spectrosc Rev. 1997; 32(3):183 - 235.

[15] Winefordner JD, Gornushkin IB, Correll T, Gibb E, Smith BW, Omenetto N. Comparing several atomic spectrometric methods to the super stars: special emphasis on laser induced breakdown spectrometry, LIBS, a future super star. J Anal At Spectrom. 2004; 19(9):1061-83.

[16] Sneddon J, Lee YI. Novel and recent applications of elemental determination by laser-induced breakdown spectrometry. Anal Lett. 1999; 32(11):2143-62.

[17] Song K, Lee YI, Sneddon J. Recent developments in instrumentation for laser induced breakdown spectroscopy. Appl Spectrosc Rev. 2002; 37(1):89-117.

[18] Tognoni E, Palleschi V, Corsi M, Cristoforetti G. Quantitative micro-analysis by laser-induced breakdown spectroscopy: a review of the experimental approaches. Spectrochim Acta, Part B. 2002; 57(7):1115-30.

[19] Kaiser J, Galiová M, Novotný K, Cervenka R, Reale L, Novotný J, Liska M, Samek O, Kanický V, Hrdlicka A, Stejskal K, Adam V, Kizek R. Mapping of lead, magnesium and copper accumulation in plant tissues by laser-induced breakdown spectroscopy and laser-ablation inductively coupled plasma mass spectrometry. Spectrochim Acta, Part B. 2009; 64(1):67-73.

[20] Rusak DA, Castle BC, Smith BW, Winefordner JD. Fundamentals and applications of laser-induced breakdown spectroscopy. Crit Rev Anal Chem. 1997; 27(4):257 - 90.

[21] Vadillo JM, Laserna JJ. Laser-induced plasma spectrometry: truly a surface analytical tool. Spectrochim Acta, Part B. 2004; 59(2):147-61.

[22] Martin MZ, Cheng MD, Martin RC. Aerosol measurement by laser-induced plasma technique: A review. Aerosol Sci Technol. 1999; 31(6):409-21.

[23] Maiman TH. Stimulated optical emission in ruby. J Opt Soc Am. 1960; 50(11):1134-34.

[24] Maiman TH. Optical and microwave-optical experiments in ruby. Phys Rev Lett. 1960; 4(11):564-66.

[25] Maiman TH, Evtuhov V, Hoskins RH, Dhaenens IJ, Asawa CK. Stimulated optical emission in fluorescent solids, spectroscopy and stimulated emission in ruby. Physical Review. 1961; 123(4):1151-57.

[26] Brech F, Cross L. Optical microemission stimulated by a ruby laser. Appl Spectrosc. 1962; 16:59.

[27] Debras-Guédon J, Liodec N. De l'utilisation du faisceau d'un amplificateur a ondes lumineuses par émission induite de rayonnement (laser á rubis), comme source énergétique pour l'excitation des spectres d'émission des éléments. CR Acad Sci. 1963; 257:3336-39.

[28] Maker PD, Terhune RW, Savage CM. Optical third harmonic generation. Quantum Electronics. 1964; 2.

[29] Runge EF, Minck RW, Bryan FR. Spectrochemical analysis using a pulsed laser source. Spectrochim Acta, Part B.1964; 20:733-35.

[30] Young M, Hercher M, Wu CY. Some characteristics of laser-induced air sparks. J Appl Phys. 1966; 37(13):4938.

[31] Felske A, Hagenah WD, Laqua K. Über einige erfahrungen bei der makrospektralanalyse mit laserlichtquellen: durchschnittsanalyse metallischer proben. Spectrochim Acta, Part B. 1972; 27(1):1-4.

[32] Afanasev YV, Krokhin ON. Vaporization of matter exposed to laser emission. Soviet Physics JETP. 1967; 25:639-45.

[33] Biberman LM, Norman GE. Continuous spectra of atomic gases and plasma. Sov Phys Uspekhi. 1967; 10:52-54.

[34] Raizer IUP. Laser-induced discharge phenomena. New York: Consultants Bureau 1977.

[35] Raizer YP. Breakdown and heating of gases under the influence of a laser beam. Sov Phys Uspekhi. 1966; 8:650-73.

[36] Zel'dovich YB, Raizer YP. Physics of shock waves and high-temperature hydrodynamic phenomena. Mineola: Dover 2002.

[37] Buzukov AA, Popov YA, Teslenko VS. Experimental study of explosion caused by focusing monopulse laser radiation in water. J Appl Mech Tech Phys. 1969; 10(5): 701-08.

[38] Lauterborn W. High-speed photography of laser-induced breakdown in liquids. Appl Phys Lett. 1972; 21:27-29.

[39] Teslenko VS. Investigation of photoacoustic and photohydrodynamic parameters of laser breakdown in liquids. Sov J Quantum Electron. 1977; 7:981-84.

[40] Belyaev EB, Godlevskiĭ AP, Kopytin YD. Laser spectrochemical analysis of aerosols. Sov J Quantum Electron. 1978; 8:1459-63.

[41] Edwards AL, J. A. Fleck, Jr. Two-dimensional modeling of aerosol-induced breakdown in air. J Appl Phys. 1979; 50(6):4307-13.

[42] Ivanov YV, Kopytin YD. Selective interaction of a train of laser pulses with an aerosol medium. J Quantum Electron. 1982; 12:355-57.

[43] Lencioni DE. The effect of dust on 10.6-mu m laser-induced air breakdown. Appl Phys Lett. 1973; 23(1):12-14.

[44] Cerrai E, Trucco R. On the matrix effect in laser sampled spectrochemical analysis. Energia Nucleare. 1968; 15:581-85.

[45] Marich KW, Carr PW, Treytl WJ, Glick D. Effect of matrix material on laser-induced elemental spectral emission. Anal Chem. 1970; 42:1775-79.

[46] Treytl WJ, Saffir AJ, Glick D, Marich KW, J. B. Orenberg. Detection limits in analysis of metals in biological materials by laser microprobe optical emission spectrometry. Anal Chem. 1972; 44:1903-04.

[47] Fichet P, Mauchien P, Moulin C. Determination of impurities in uranium and plutonium dioxides by laser-induced breakdown spectroscopy. Appl Spectrosc. 1999; 53:1111-17.

[48] Sneddon J, Lee YI. Application of laser-induced breakdown spectrometry in urban health. Microchem J. 2000; 67(1-3):201-05.

[49] Stratis DN, Eland KL, Carter JC, Tomlinson SJ, Angel SM. Comparison of acousto-optic and liquid crystal tunable filters for laser-induced breakdown spectroscopy. Appl Spectrosc. 2001; 55:999-1004.

[50] Gonzaga FB, Pasquini C. A new detection system for laser induced breakdown spectroscopy based on an acousto-optical tunable filter coupled to a photomultiplier: application for manganese determination in steel. Spectrochim Acta, Part B. 2008; 63(11):1268-73.

[51] Houck MM. Mute witnesses: trace evidence analysis. San Diego, London: Academic Press 2001.

[52] Caddy B. Forensic examination of glass and paint analysis and interpretation. London-New York: Taylor & Francis 2001.

[53] Zadora G. Glass analysis for forensic purposes - a comparison of classification methods. J Chemom. 2007; 21(5-6):174-86.

[54] Curran JM, Hicks TN, Buckleton JS. Forensic interpretation of glass evidence. Boca Raton: CRC Press 2000.

[55] Tsach T, Wiesner S, Shor Y. Empirical proof of physical match: systematic research with tensile machine. Forensic Sci Int. 2007; 166(1):77-83.

[56] Winchell AN, Emmons RC. Some methods for determining refractive indices American Mineral. 1926; 11:115-19.

[57] Almirall JR, Cole MD, Gettinby G, Furton KG. Discrimination of glass sources using elemental composition and refractive index: development of predictive models. Science & Justice. 1998; 38(2):93-100.

[58] Bennett RL, Kim ND, Curran JM, Coulson SA, Newton AWN. Spatial variation of refractive index in a pane of float glass. Science & Justice. 2003; 43(2):71-76.

[59] Koons RD, Buscaglia J. Distribution of refractive index values in sheet glasses. Forensic Science Communications. 2001; 3(1).

[60] Koons RD, Buscaglia JA. The forensic significance of glass composition and refractive index measurements. J Forensic Sci. 1999; 44(3):496-503.

[61] Koons RD, Peters CA, Rebbert PS. Comparison of refractive-index, energy dispersive-x-ray fluorescence and inductively coupled plasma atomic emission-spectrometry for forensic characterization of sheet glass fragments. J Anal At Spectrom. 1991; 6(6):451-56.

[62] Lambert JA, Evett IW. The refractive-index distribution of control glass samples examined by the forensic-science laboratories in the United Kingdom. Forensic Sci Int. 1984; 26(1):1-23.

[63] Newton AWN, Buckleton JS. An investigation into the relationship between edge counts and the variability of the refractive index of glass. Forensic Sci Int. 2008; 177(1):24-31.

[64] Newton AWN, Curran JM, Triggs CM, Buckleton JS. The consequences of potentially differing distributions of the refractive indices of glass fragments from control and recovered sources. Forensic Sci Int. 2004; 140(2-3):185-93.

[65] Pawluk-Kolc M, Zigba-Palus J, Parczewski A. The effect of re-annealing on the distribution of refractive index in a windscreen and a windowpane classification of glass samples. Forensic Sci Int. 2008; 174(2-3):222-28.

[66] Stoney DA, Thornton JI. The forensic significance of the correlation of density and refractive-index in glass evidence. Forensic Sci Int. 1985; 29(3-4):147-57.

[67] Suzuki Y, Kasamatsu M, Suzuki S, Nakanishi T, Takatsu M, Muratsu S, Shimoda O, Watanabe S, Nishiwaki Y, Miyamoto N. Forensic discrimination of sheet glass by a refractive-index measurement and elemental analysis with synchrotron radiation x-ray fluorescence spectrometry. Anal Sci. 2005; 21(7):855-59.

[68] Suzuki Y, Sugita R, Suzuki S, Marumo Y. Forensic discrimination of bottle glass by refractive index measurement and analysis of trace elements with ICP-MS. Anal Sci. 2000; 16(11):1195-98.

[69] Buscaglia JA. Elemental analysis of small glass fragments in forensic science. Anal Chim Acta. 1994; 288(1-2):17-24.

[70] Zurhaar A, Mullings L. Characterization of forensic glass samples using inductively coupled plasma mass-spectrometry. J Anal At Spectrom. 1990; 5(7):611-17.

[71] Hughes JC, Catterick T, Southeard G. The quantitative analysis of glass by atomic absorption spectroscopy. Forensic Science. 1976; 3:217-27.

[72] Blacklock EC, Rogers A, Wall C, Wheals BB. The quantitative analysis of glass by emission spectrography: a six element survey. Forensic Science. 1976; 2:121-30.

[73] Ducreux-Zappa M, Mermet JM. Analysis of glass by UV laser ablation inductively coupled plasma atomic emission spectrometry. Effects of the laser parameters on the amount of ablated material and the temporal behavior of the signal for different types of laser. Spectrochim Acta, Part B. 1996; 51(3):321-32.

[74] Ducreux-Zappa M, Mermet JM. Analysis of glass by UV laser ablation inductively coupled plasma atomic emission spectrometry. Analytical figures of merit. Spectrochim Acta, Part B. 1996; 51(3):333-41.

[75] Hickman DA. A classification scheme for glass. Forensic Sci Int. 1981; 17:265-81.

[76] Koons RD, Fiedler C, Rawalt RC. Classification and discrimination of sheet and container glasses by inductively coupled plasma-atomic emission-spectrometry and pattern-recognition. J Forensic Sci. 1988; 33(1):49-67.

[77] Ohsaki H, Kasamatsu M, Suzuki Y, Suzuki S. Forensic discrimination of steel wire by determination of trace elements with ICP-AES. Bunseki Kagaku. 2007; 56(12):1191-95.

[78] Suzuki Y, Kasamatsu M, Suzuki S, Marumo Y. Forensic discrimination of lead-tin solder based on the trace impurity analysis by ICP-AES. Anal Sci. 2003; 19(3):415-18.

[79] Suzuki Y, Kasamatsu M, Suzuki S, Ohashi K, Kawase A. Forensic discrimination of arsenous acid by the analysis of trace impurities with ICP-AES. Bunseki Kagaku. 2001; 50(5):335-39.

[80] Wolnik KL, Gaston CM, Fricke FL. Analysis of glass in product tampering investigations by inductively coupled plasma atomic emission-spectrometry with a hydrofluoric-acid resistant torch. J Anal At Spectrom. 1989; 4(1):27-31.

[81] Verita M, Basso R, Wypyski MT, Koestler RJ. X-ray microanalysis of ancient glassy materials: a comparative study of wavelength dispersive and energy dispersive techniques. Archaeometry. 1994; 36(2):241-51.

[82] Falcone R, Sommariva G, Verita M. WDXRF, EPMA and SEM/EDX quantitative chemical analyses of small glass samples. Microchim Acta. 2006; 155(1-2):137-40.

[83] Falcone R, Renier A, VeritÃ M. Wavelength–dispersive x–ray fluorescence analysis of ancient glasses. Archaeometry. 2002; 44(4):531-42.

[84] Furukawa K, Fukushima S. Discrimination of beer bottle glass fragments by wavelength dispersive electron probe microanalyzer. Reports of National Research Institute of Police Science Research on Forensic Science. 1999; 52:89-98.

[85] Falcone R, Galinetto P, Messiga B, Negri E, Riccardi MP, Sommariva G, Verita M. Combined SEM-EDX and mu-raman spectroscopy for the characterisation of glass/Al-rich refractory interfaces. Microchim Acta. 2008; 161(3-4):381-86.

[86] Andrasko J, Maehly AC. The discrimination between samples of window glass by combining physical and chemical techniques. J Forensic Sci. 1978; 22:250-62.

[87] Dudley RJ, Howden CR, Taylor TJ, Smalldon KW. The discrimination and classification of small fragments of window and non-window glasses using energy-dispersive x-ray fluorescence spectrometry. X-Ray Spectrom. 1980; 9(3):119-22.

[88] Howden CR, Dudley RJ, Smalldon KW. The analysis of small glass fragments using energy dispersive x-ray fluorescence spectrometry. J Forensic Sci Soc. 1978; 18(1-2):99-112.

[89] Reeve V, Mathiesen J, Fong W. Elemental analysis by energy dispersive X-ray: A significant factor in the forensic analysis of glass. J Forensic Sci. 1976; 21:291-306.

[90] Nakanishi T, Nishiwaki Y, Miyamoto N, Shimoda O, Watanabe S, Muratsu S, Takatsu M, Terada Y, Suzuki Y, Kasamatsu M, Suzuki S. Lower limits of detection of synchrotron radiation high-energy x-ray fluorescence spectrometry and its possibility for the forensic application for discrimination of glass fragments. Forensic Sci Int. 2008; 175(2-3):227-34.

[91] Nishiwaki Y, Nakanishi T, Terada Y, Ninomiya T, Nakai I. Nondestructive discrimination of small glass fragments for forensic examination using high energy synchrotron radiation x-ray fluorescence spectrometry. X-Ray Spectrom. 2006; 35(3):195-99.

[92] Suzuki Y, Kasamatsu M, Sugita R, Ohta H, Suzuki S, Marumo Y. Forensic discrimination of headlight glass by analysis of trace impurities with synchrotron radiation x-ray fluorescence spectrometry and ICP-MS. Bunseki Kagaku. 2003; 52(6):469-74.

[93] Suzuki S, Suzuki Y, Ohta H, Kasamatsu M, Nakanishi T. Evaluation of a quantitative method for trace impurities in arsenous acids by synchrotron radiation x-ray fluorescence spectrometry and inductively coupled plasma-atomic emission spectrometry. Anal Sci. 2005; 21(7):775-78.

[94] Nishiwaki Y, Shimoyama M, Nakanishi T, Ninomiya T, Nakai I. Application of total reflection x-ray fluorescence spectrometry to small glass fragments. Anal Sci. 2006; 22(10):1297-300.

[95] Suzuki Y, Kikkawa HS, Kasamatsu M, Higashikawa Y, Suzuki S. Forensic discrimination of sheet glass exposed to high temperature by the determination of trace impurities using ICP-MS. Anal Sci. 2008; 24(6):745-49.

[96] Umpierrez S, Trejos T, Neubauer K, Almirall J. Determination of iron in glass by solution and laser ablation DRC-ICP-MS. At Spectrosc. 2006; 27(3):76-79.

[97] Suzuki Y, Sugita R, Suzuki S, Marumo Y. Determination of trace impurities in windshield glass by ICP-MS. Bunseki Kagaku. 1997; 46(10):825-30.

[98] Duckworth DC, Morton SJ, Bayne CK, Koons RD, Montero S, Almirall JR. Forensic glass analysis by ICP-MS: a multi-element assessment of discriminating power via analysis of variance and pairwise comparisons. J Anal At Spectrom. 2002; 17(7):662-68.

[99] Montero S, Hobbs AL, French TA, Almirall AR. Elemental analysis of glass fragments by ICP-MS as evidence of association: Analysis of a case. J Forensic Sci. 2003; 48(5):1101-07.

[100] Neufeld LM. Application of laser ablation ICP-MS to the analysis of forensic glass samples. Spectroscopy. 2005; 20(7):31-36.

[101] Parouchais T, Warner IM, Palmer LT, Kobus H. The analysis of small glass fragments using inductively coupled plasma mass spectrometry. J Forensic Sci. 1996; 41(3):351-60.

[102] Duckworth DC, Bayne CK, Morton SJ, Almirall J. Analysis of variance in forensic glass analysis by ICP-MS: variance within the method. J Anal At Spectrom. 2000; 15(7):821-28.

[103] Ghazi AM, Millette JR. Environmental forensic application of lead isotope ratio determination: a case study using laser ablation sector ICP-MS. Environmental Forensics. 2004; 5(2):97-108.

[104] Aeschliman DB, Bajic SJ, Baldwin DP, Houk RS. Multivariate pattern matching of trace elements in solids by laser ablation inductively coupled plasma-mass spectrometry: Source attribution and preliminary diagnosis of fractionation. Anal Chem. 2004; 76(11):3119-25.

[105] Bajic SJ, Aeschliman DB, Saetveit NJ, Baldwin DP, Houk RS. Analysis of glass fragments by laser ablation-inductively coupled plasma-mass spectrometry and principal component analysis. J Forensic Sci. 2005; 50(5):1123-27.

[106] Becker JS, Tenzler D. Studies of LA-ICP-MS on quartz glasses at different wavelengths of a Nd:YAG laser. Fresenius J Anal Chem. 2001; 370(5):637-40.

[107] Berends-Montero S, Wiarda W, de Joode P, van der Peijl G. Forensic analysis of float glass using laser ablation inductively coupled plasma mass spectrometry (LA-ICP-MS): validation of a method. J Anal At Spectrom. 2006; 21(11):1185-93.

[108] Bridge CM, Powell J, Steele KL, Williams M, MacInnis JM, Sigman ME. Characterization of automobile float glass with laser-induced breakdown spectroscopy and laser ablation inductively coupled plasma mass spectrometry. Appl Spectrosc. 2006; 60(10):1181-87.

[109] Hobbs AL, Almirall JR. Trace elemental analysis of automotive paints by laser ablation-inductively coupled plasma-mass spectrometry (LA-ICP-MS). Anal Bioanal Chem. 2003; 376(8):1265-71.

[110] Ito M, Hokura A, Oishi M, Nishiwaki Y, Nakai I. Characterization of sheet glass based on trace elements analysis using LA-ICP-MS and their applications to forensic science. Bunseki Kagaku. 2007; 56(12):1115-25.

[111] Latkoczy C, Becker S, Ducking M, Gunther D, Hoogewerff JA, Almirall JR, Buscaglia J, Dobney A, Koons RD, Montero S, van der Peijl GJQ, Stoecklein WRS, Trejos T, Watling JR, Zdanowicz VS. Development and evaluation of a standard method for the quantitative determination of elements in float glass samples by LA-ICP-MS. J Forensic Sci. 2005; 50(6):1327-41.

[112] Scadding CJ, Watling RJ, Thomas AG. The potential of using laser ablation inductively coupled plasma time of fight mass spectrometry (LA-ICP-TOF-MS) in the forensic analysis of micro debris. Talanta. 2005; 67(2):414-24.

[113] Trejos T, Almirall JR. Sampling strategies for the analysis of glass fragments by LA-ICP-MS - Part II: Sample size and sample shape considerations. Talanta. 2005; 67(2):396-401.

[114] Trejos T, Almirall JR. Sampling strategies for the analysis of glass fragments by LA-ICP-MS - Part I. Micro-homogeneity study of glass and its application to the interpretation of forensic evidence. Talanta. 2005; 67(2):388-95.

[115] Trejos T, Montero S, Almirall JR. Analysis and comparison of glass fragments by laser ablation inductively coupled plasma mass spectrometry (LA-ICP-MS) and ICP-MS. Anal Bioanal Chem. 2003; 376(8):1255-64.

[116] Watling RJ, Lynch BF, Herring D. Use of laser ablation inductively coupled plasma mass spectrometry for fingerprinting scene of crime evidence. J Anal At Spectrom. 1997; 12(2):195-203.

[117] Becker S, Ducking M, Watzke P, Stoecklein W. Laser ablation in forensic glass analysis: The use of matrix matched standards for quantitative float glass analysis. Forensic Sci Int. 2003; 136:361-61.

[118] Hordijk M, Wiarda W, de Joode P, van der Peijl G, Montero S. LA-ICP-MS method for the elemental profiling of forensic glass: A study of a float glass sample set collected in the Netherlands. Forensic Sci Int. 2003; 136:358-59.

[119] Neufeld L. Application of laser ablation ICP-MS to the analysis of forensic glass samples. Spectroscopy. 2005; 20(7).

[120] Russo RE, Mao XL, Chan WT, Bryant MF, Kinard WF. Laser ablation sampling with inductively coupled plasma atomic emission spectrometry for the analysis of prototypical glasses. J Anal At Spectrom. 1995; 10(4):295-301.

[121] Dockery CR, Goode SR. Laser-induced breakdown spectroscopy for the detection of gunshot residues on the hands of a shooter. Appl Opt. 2003; 42(30):6153-58.

[122] Corsi M, Cristoforetti G, Hidalgo M, Legnaioli S, Palleschi V, Salvetti A, Tognoni E, Vallebona C. Application of laser-induced breakdown spectroscopy technique to hair tissue mineral analysis. Applied Optics. 2003; 42(30):6133-37.

[123] Al-Jeffery MO, Telle HH. LIBS and LIFS for rapid detection of Rb traces in blood. In: Robert RA, editor.; 2002: SPIE; 2002. p. 152-61.

[124] Taschuk MT, Tsui YY, Fedosejevs R. Detection and mapping of latent fingerprints by laser-induced breakdown spectroscopy. Appl Spectrosc. 2006; 60:1322-27.

[125] Page D. Read our LIBS: crime scene wood analysis gets new bark. Forensic Magazine. 2005; 21(5):15-17.

[126] Martin MZ, Labbe N, Andre N, Harris R, Ebinger M, Wullschleger SD, Vass AA. High resolution applications of laser-induced breakdown spectroscopy for environmental and forensic applications. Spectrochim Acta, Part B. 2007; 62(12):1426-32.

[127] Almirall J, Umpierrez S, Castro W, Gornushkin I, Winefordner J. Forensic elemental analysis of materials by laser induced breakdown spectroscopy (LIBS). In: Edward MC, editor.; 2005: SPIE; 2005. p. 657-66.

[128] Bridge CM, Powell J, Steele KL, Sigman ME. Forensic comparative glass analysis by laser-induced breakdown spectroscopy. Spectrochim Acta, Part B. 2007; 62(12):1419-25.

[129] Barnett C, Cahoon E, Almirall JR. Wavelength dependence on the elemental analysis of glass by laser induced breakdown spectroscopy. Spectrochim Acta, Part B. 2008; 63(10):1016-23.

[130] Naes BE, Umpierrez S, Ryland S, Barnett C, Almirall JR. A comparison of laser ablation inductively coupled plasma mass spectrometry, micro x-ray fluorescence spectroscopy, and laser induced breakdown spectroscopy for the discrimination of automotive glass. Spectrochim Acta Part B. 2008; 63(10):1145-50.

[131] Carmona N, Oujja M, Gaspard S, Garcia-Heras M, Villegas MA, Castillejo M. Lead determination in glasses by laser-induced breakdown spectroscopy. Spectrochim Acta, Part B. 2007; 62(2):94-100.

[132] Carmona N, Oujja M, Rebollar E, Romich H, Castillejo M. Analysis of corroded glasses by laser induced breakdown spectroscopy. Spectrochim Acta, Part B. 2005; 60(7-8):1155-62.

[133] Klein S, Hildenhagen J, Dickmann K, Stratoudaki T, Zafiropulos V. LIBS-spectroscopy for monitoring and control of the laser cleaning process of stone and medieval glass. Journal of Cultural Heritage. 2000; 1(Supplement 1):S287-S92.

[134] Klein S, Stratoudaki T, Zafiropulos V, Hildenhagen J, Dickmann K, Lehmkuhl T. Laser-induced breakdown spectroscopy for on-line control of laser cleaning of sandstone and stained glass. Appl Phys A: Mater Sci Process. 1999; 69(4):441.

[135] Lal BS, Yueh FY, Singh JP. Glass-batch composition monitoring by laser-induced breakdown spectroscopy. Appl Opt. 2005; 44(18):3668-74.

[136] Lazic V, Fantoni R, Colao F, Santagata A, Morone A, Spizzichino V. Quantitative laser induced breakdown spectroscopy analysis of ancient marbles and corrections for the variability of plasma parameters and of ablation rate. J Anal At Spectrom. 2004; 19(4):429-36.

[137] Muller K, Stege H. Evaluation of the analytical potential of laser-induced breakdown spectrometry (LIBS) for the analysis of historical glasses. Archaeometry. 2003; 45:421-33.

[138] Panne U, Clara M, Haisch C, Niessner R. Analysis of glass and glass melts during the vitrification of fly and bottom ashes by laser-induced plasma spectroscopy. Part II. Process analysis. Spectrochim Acta, Part B. 1998; 53(14):1969-81.

[139] Su CF, Feng SM, Singh JP, Yuen FY, Rigsby JT, Monts DL, Cook RL. Glass composition measurement using laser induced breakdown spectrometry. Glass Technology. 2000; 41(1):16-21.

[140] Yoon Y, Kim T, Yang M, Lee K, Lee G. Quantitative analysis of pottery glaze by laser induced breakdown spectroscopy. Microchem J. 2001; 68(2-3):251-56.

[141] Burakov V, Tarasenko N, Nedelko M, Isakov S. Time-resolved spectroscopy and imaging diagnostics of single pulse and collinear double pulse laser induced plasma from a glass sample. Spectrochim Acta, Part B. 2008; 63(1):19-26.

[142] Carmona N, Oujja M, Gaspard S, Garcia-Heras M, Villegas MA, Castillejo M. Lead determination in glasses by laser-induced breakdown spectroscopy. Spectrochim Acta Part B. 2007; 62(2):94-100.

[143] Carmona N, Oujja M, Rebollar E, Romich H, Castillejo M. Analysis of corroded glasses by laser induced breakdown spectroscopy. Spectrochim Acta Part B. 2005; 60(7-8):1155-62.

[144] Craparo JC, Weisberg A, De Saro R. New technique developed to measure glass batch, sort cullet. Am Ceram Soc Bull. 2006; 85(3):33-37.

[145] Galiova M, Mozna V, Stankova A, Novotny K, Kanicky V. Study of laser-sample interactions of glasses and soils using laser-induced breakdown spectroscopy and optical emission spectroscopy with inductively coupled plasma. Chem Listy. 2006; 100(3):204-09.

[146] Gautier C, Fichet P, Menut D, Dubessy J. Applications of the double-pulse laser-induced breakdown spectroscopy (LIBS) in the collinear beam geometry to the elemental analysis of different materials. Spectrochim Acta, Part B. 2006; 61(2):210-19.

[147] Giakoumaki A, Melessanaki K, Anglos D. Laser-induced breakdown spectroscopy (LIBS) in archaeological science-applications and prospects. Anal Bioanal Chem. 2007; 387(3):749-60.

[148] Klein S, Stratoudaki T, Zafiropulos V, Hildenhagen J, Dickmann K, Lehmkuhl T. Laser-induced breakdown spectroscopy for on-line control of laser cleaning of sandstone and stained glass. Appl Phys A: Mater Sci Process. 1999; 69(4):441-44.

[149] Lal B, Zheng HB, Yueh FY, Singh JP. Parametric study of pellets for elemental analysis with laser-induced breakdown spectroscopy. Appl Opt. 2004; 43(13):2792-97.

[150] Laville S, Sabsabi M, Doucet FR. Multi-elemental analysis of solidified mineral melt samples by laser-induced breakdown spectroscopy coupled with a linear multivariate calibration. Spectrochim Acta, Part B. 2007; 62(12):1557-66.

[151] Loebe K, Uhl A, Lucht H. Microanalysis of tool steel and glass with laser-induced breakdown spectroscopy. Appl Opt. 2003; 42(30):6166-73.

[152] Stratis DN, Eland KL, Angel SM. Enhancement of aluminum, titanium, and iron in glass using pre-ablation spark dual-pulse LIBS. Appl Spectrosc. 2000; 54(12):1719-26.

[153] Tornari V, Zafiropulos V, Bonarou A, Vainos NA, Fotakis C. Modern technology in artwork conservation: a laser-based approach for process control and evaluation. Optics and Lasers in Engineering. 2000; 34(4-6):309-26.

[154] Yun JI, Klenze R, Kim JI. Laser-induced breakdown spectroscopy for the on-line multielement analysis of highly radioactive glass melt. Part 1: characterization and evaluation of the method. Appl Spectrosc. 2002; 56(4):437-48.

[155] Gornushkin IB, Smith BW, Nasajpour H, Winefordner JD. Identification of solid materials by correlation analysis using a microscopic laser-induced plasma spectrometer. Anal Chem. 1999; 71(22):5157-64.

[156] Anzano JM, Gornushkin IB, Smith BW, Winefordner JD. Laser-induced plasma spectroscopy for plastic identification. Polym Eng Sci. 2000; 40(11):2423-29.

[157] Anzano JM, Villoria MA, Gornushkin IB, Smith BW, Winefordner JD. Laser-induced plasma spectroscopy for characterization of archaeological material. Can J Anal Sci Spectros. 2002; 47(5):134-40.

[158] Gornushkin IB, Ruiz-Medina A, Anzano JM, Smith BW, Winefordner JD. Identification of particulate materials by correlation analysis using a microscopic laser induced breakdown spectrometer. J Anal At Spectrom. 2000; 15(6):581-86.

[159] Edwards L. Laser-induced breakdown spectroscopy for the determination of carbon in soil. Gainesville: University of Florida; 2007.

[160] Yalcin S, Crosley DR, Smith GP, Faris GW. Influence of ambient conditions on the laser air spark. Appl Phys B: Lasers Opt. 1999; 68(1):121-30.

[161] Wachter JR, Cremers DA. Determination of uranium in solution using laser-induced breakdown spectroscopy. Appl Spectrosc. 1987; 41:1042-48.

[162] Multari RA, Foster LE, Cremers DA, Ferris MJ. Effect of sampling geometry on elemental emissions in laser-induced breakdown spectroscopy. Appl Spectrosc. 1996; 50(12):1483-99.

[163] Kempenaers L, Janssens K, Jochum KP, Vincze L, Vekemans B, Somogyi A, Drakopoulos M, Adams F. Micro-heterogeneity study of trace elements in USGS, MPI-DING and NIST glass reference materials by means of synchrotron micro-XRF. J Anal At Spectrom. 2003; 18(4):350-57.

[164] Ott RL, Longnecker MT. A first course in statistical methods. Belmont: Duxbury Press 2003.

[165] Galbács G, Gornushkin IB, Smith BW, Winefordner JD. Semi-quantitative analysis of binary alloys using laser-induced breakdown spectroscopy and a new calibration approach based on linear correlation. Spectrochim Acta, Part B. 2001; 56(7):1159-73.

[166] Galbács G, Gornushkin IB, Winefordner JD. Generalization of a new calibration method based on linear correlation. Talanta. 2004; 63(2):351-57.

[167] Gornushkin IB, Mueller M, Panne U, Winefordner JD. Insights into linear and rank correlation for material identification in laser-induced breakdown spectroscopy and other spectral techniques. Appl Spectrosc. 2008; 62:542-53.

[168] Personal communication with Dr. Jose Almirall. March, 2008.

[169] De Lucia Jr FC, Gottfried JL, Munson CA, Miziolek AW. Double pulse laser-induced breakdown spectroscopy of explosives: Initial study towards improved discrimination. Spectrochim Acta, Part B. 2007; 62(12):1399-404.

[170] DeLucia FC, Samuels AC, Harmon RS, Walters RA, McNesby KL, LaPointe A, Winkel RJ, Miziolek AW. Laser-induced breakdown spectroscopy (LIBS): A promising versatile chemical sensor technology for hazardous material detection. IEEE Sens J. 2005; 5(4):681-89.

[171] Hybl JD, Lithgow GA, Buckley SG. Laser-induced breakdown spectroscopy detection and classification of biological aerosols. Appl Spectrosc. 2003; 57(10):1207-15.

[172] Munson CA, De Lucia JFC, Piehler T, McNesby KL, Miziolek AW. Investigation of statistics strategies for improving the discriminating power of laser-induced breakdown spectroscopy for chemical and biological warfare agent simulants. Spectrochim Acta, Part B. 2005; 60(7-8):1217-24.

[173] Samuels AC, DeLucia FC, McNesby KL, Miziolek AW. Laser-induced breakdown spectroscopy of bacterial spores, molds, pollens, and protein: initial studies of discrimination potential. Appl Opt. 2003; 42(30):6205-09.

[174] Jurado-Lopez A, De Castro MDL. Rank correlation of laser-induced breakdown spectroscopic data for the identification of alloys used in jewelry manufacture. Spectrochim Acta, Part B. 2003; 58(7):1291-99.

[175] Lopez AJ, Nicolas G, Mateo MP, Ramil A, Pinon V, Yanez A. LIPS and linear correlation analysis applied to the classification of roman pottery terra sigillata. Appl Phys A: Mater Sci Process. 2006; 83(4):695-98.

[176] Sattmann R, Monch I, Krause H, Noll R, Couris S, Hatziapostolou A, Mavromanolakis A, Fotakis C, Larrauri E, Miguel R. Laser-induced breakdown spectroscopy for polymer identification. Appl Spectrosc. 1998; 52(3):456-61.

[177] Rodriguez-Celis EM, Gornushkin IB, Heitmann UM, Almirall JR, Smith BW, Winefordner JD, Omenetto N. Laser induced breakdown spectroscopy as a tool for discrimination of glass for forensic applications. Anal Bioanal Chem. 2008; 391(5):1961-68.

[178] Ismail MA, Cristoforetti G, Legnaioli S, Pardini L, Palleschi V, Salvetti A, Tognoni E, Harith MA. Comparison of detection limits, for two metallic matrices, of laser-induced breakdown spectroscopy in the single and double-pulse configurations. Anal Bioanal Chem. 2006; 385(2):316-25.

[179] Ismail MA, Imam H, Elhassan A, Youniss WT, Harith MA. LIBS limit of detection and plasma parameters of some elements in two different metallic matrices. J Anal At Spectrom. 2004; 19(4):489-94.

[180] Sturm V, Peter L, Noll R. Steel analysis with laser-induced breakdown spectrometry in the vacuum ultraviolet. Appl Spectrosc. 2000; 54(9):1275-78.

[181] Sturm V, Vrenegor J, Noll R, Hemmerlin M. Bulk analysis of steel samples with surface scale layers by enhanced laser ablation and LIBS analysis of C, P, S, Al, Cr, Cu, Mn and Mo. J Anal At Spectrom. 2004; 19(4):451-56.

[182] Panne U, Haisch C, Clara M, Niessner R. Analysis of glass and glass melts during the vitrification process of fly and bottom ashes by laser-induced plasma spectroscopy. Part I: normalization and plasma diagnostics. Spectrochim Acta, Part B. 1998; 53(14):1957-68.

[183] Le Drogoff B, Margot J, Chaker M, Sabsabi M, Barthélemy O, Johnston TW, Laville S, Vidal F, von Kaenel Y. Temporal characterization of femtosecond laser pulses induced plasma for spectrochemical analysis of aluminum alloys. Spectrochim Acta, Part B. 2001; 56(6):987-1002.

[184] Aguilera JA, Bengoechea J, Aragon C. Spatial characterization of laser induced plasmas obtained in air and argon with different laser focusing distances. Spectrochim Acta, Part B. 2004; 59(4):461-69.

[185] Davison S, Newton RG. Conservation and restoration of glass. Oxford: Butterworth-Heinemann 2003.

[186] Teixeira S, Bernardin AM. Development of TiO2 white glazes for ceramic tiles. Dyes and Pigments. 2009; 80(3):292-96.

[187] Bray C. Dictionary of glass: materials and techniques. Tortola: Craftsman House 1995.

[188] Peterson S. The craft and art of clay. London: L. King Pub. 1999.

[189] Bou E, Moreno A, Escardino A, Gozalbo A. Microstructural study of opaque glazes obtained from frits of the system: SiO_2-Al_2O_3-B_2O_3-(P_2O_5)-CaO-K_2O-TiO_2. J Eur Ceram Soc. 2007; 27(2-3):1791-96.

[190] Herrera KK. From sample to signal in laser-induced breakdown spectroscopy an experimental assessment of existing algorithms and theoretical modeling approaches. Gainesville, Fla.: University of Florida; 2008.

[191] Hans Netten, Young IT, Vliet LJv, Tanke HJ, Willem HV, Sloos CR. Fish and chips: automation of fluorescent dot counting in interphase cell nuclei. Cytometry. 1997; 28(1):1-10.

[192] Zhimin Z, Pain B, Fossum ER. Frame-transfer CMOS active pixel sensor with pixel binning. Electron Devices, IEEE Transactions on. 1997; 44(10):1764-68.

[193] Sabsabi M, Cielo P. Quantitative analysis of aluminum alloys by laser-induced breakdown spectroscopy and plasma characterization. Appl Spectrosc. 1995; 49(4):499-507.

[194] Mohamed WTY. Improved LIBS limit of detection of Be, Mg, Si, Mn, Fe and Cu in aluminum alloy samples using a portable echelle spectrometer with ICCD camera. Optics & Laser Technology. 2008; 40(1):30-38.

[195] Ralchenko Y, Kramida AE, Reader J. NIST atomic spectra database (version 3.1.5). 2008 [cited 2009 February 27]; Available from: http://physics.nist.gov/asd3

[196] Álvarez-Trujillo LA, Ferrero A, Laserna JJ, Hahn DW. Alternative statistical methods for spectral data processing: applications to laser-induced breakdown spectroscopy of gaseous and aerosol systems. Appl Spectrosc. 2008; 62(10):1144-52.

[197] Gondal MA, Hussain T. Determination of poisonous metals in wastewater collected from paint manufacturing plant using laser-induced breakdown spectroscopy. Talanta. 2007; 71(1):73-80.

[198] Koskelo A, Cremers DA. RCRA materials analysis by laser-induced breakdown spectroscopy: Detection limits in soils. 1994:1-64.

[199] Yamamoto KY, Cremers DA, Ferris MJ, Foster LE. Detection of metals in the environment using a portable laser-induced breakdown spectroscopy instrument. Appl Spectrosc. 1996; 50:222-33.

[200] Cho H-H, Kim Y-J, Jo Y-S, Kitagawa K, Arai N, Lee Y-I. Application of laser-induced breakdown spectrometry for direct determination of trace elements in starch-based flours. J Anal At Spectrom. 2001; 16(6):622-27.

[201] Kurniawan H, Nakajima S, Batubara JE, Marpaung M, Okamoto M, Kagawa K. Laser-induced shock wave plasma in glass and its application to elemental analysis. Appl Spectrosc. 1995; 49(8):1067-72.

[202] Gautier C, Fichet P, Menut D, Lacour J-L, L'Hermite D, Dubessy J. Study of the double-pulse setup with an orthogonal beam geometry for laser-induced breakdown spectroscopy. Spectrochim Acta, Part B. 2004; 59(7):975-86.

[203] Gornushkin SI, Gornushkin IB, Anzano JM, Smith BW, Winefordner JD. Effective normalization technique for correction of matrix effects in laser-induced breakdown spectroscopy detection of magnesium in powdered samples. Appl Spectrosc. 2002; 56:433-36.

[204] Eppler AS, Cremers DA, Hickmott DD, Ferris MJ, Koskelo AC. Matrix effects in the detection of Pb and Ba in soils using laser-induced breakdown spectroscopy. Appl Spectrosc. 1996; 50(9):1175-81.

[205] Chaleard C, Mauchien P, Andre N, Uebbing J, Lacour JL, Geertsen C. Correction of matrix effects in quantitative elemental analysis with laser ablation optical emission spectrometry. J Anal At Spectrom. 1997; 12(2):183-88.

[206] Ko JB, Sdorra W, Niemax K. On the internal standardization in optical-emission spectrometry of microplasmas produced by laser ablation of solid samples. Fresenius Zeitschrift Fur Analytische Chemie. 1989; 335(7):648-51.

[207] Ciucci A, Corsi M, Palleschi V, Rastelli S, Salvetti A, Tognoni E. New procedure for quantitative elemental analysis by laser-induced plasma spectroscopy. Appl Spectrosc. 1999; 53(8):960-64.

[208] Mohamed WTY. Calibration free laser-induced breakdown spectroscopy (LIBS) identification of seawater salinity. Optica Applicata. 2007; 37(1-2):5-19.

[209] Herrera KK, Tognoni E, Omenetto N, Smith BW, Winefordner JD. Semi-quantitative analysis of metal alloys, brass and soil samples by calibration-free laser-induced breakdown spectroscopy: recent results and considerations. J Anal At Spectrom. 2009:-.

[210] Bulajic D, Corsi M, Cristoforetti G, Legnaioli S, Palleschi V, Salvetti A, Tognoni E. A procedure for correcting self-absorption in calibration free-laser induced breakdown spectroscopy. Spectrochim Acta, Part B. 2002; 57(2):339-53.

[211] Ciucci A, Palleschi V, Rastelli S, Salvetti A, Singh DP, Tognoni E. CF-LIPS: A new approach to LIPS spectra analysis. Laser and Particle Beams. 1999; 17(4):793-97.

[212] Corsi M, Cristoforetti G, Hidalgo M, Legnaioli S, Palleschi V, Salvetti A, Tognoni E, Vallebona C. Double pulse, calibration-free laser-induced breakdown spectroscopy: A new technique for in situ standard-less analysis of polluted soils. Appl Geochem. 2006; 21(5):748-55.

[213] Pandhija S, Rai AK. In situ multielemental monitoring in coral skeleton by CF-LIBS. Appl Phys B: Lasers Opt. 2009; 94(3):545-52.

[214] Tognoni E, Cristoforetti G, Legnaloli S, Palleschi V, Salvetti A, Mueller M, Panne U, Gomushkin I. A numerical study of expected accuracy and precision in Calibration-Free Laser-Induced Breakdown Spectroscopy in the assumption of ideal analytical plasma. Spectrochim Acta, Part B. 2007; 62(12):1287-302.

[215] Yaroshchyk P, Body D, Morrison RJS, Chadwick BL. A semi-quantitative standard-less analysis method for laser-induced breakdown spectroscopy. Spectrochim Acta, Part B. 2006; 61(2):200-09.

[216] Wang L, Zhang C, Feng Y. Controlled calibration method for laser induced breakdown spectroscopy. Chin Opt Lett. 2008; 6(1):5-8.

[217] Pandhija S, Rai AK. In situ multielemental monitoring in coral skeleton by CF-LIBS. Appl Phys B: Lasers Opt. 2009; 94(3):545-52.

[218] Singh VK, Singh V, Rai AK, Thakur SN, Rai PK, Singh JP. Quantitative analysis of gallstones using laser-induced breakdown spectroscopy. Appl Opt. 2008; 47(31):G38-G47.

[219] Burakov VS, Raikov SN. Quantitative analysis of alloys and glasses by a calibration-free method using laser-induced breakdown spectroscopy. Spectrochim Acta, Part B. 2007; 62(3):217-23.

[220] Xu L, Bulatov V, Gridin VV, Schechter I. Absolute analysis of particulate materials by laser-induced breakdown spectroscopy. Anal Chem. 1997; 69(11):2103-08.

[221] Gornushkin IB, Smith BW, Potts GE, Omenetto N, Winefordner JD. Some considerations on the correlation between signal and background in laser-induced breakdown spectroscopy using single-shot analysis. Anal Chem. 1999; 71(23):5447-49.

[222] Carranza JE, Hahn DW. Sampling statistics and considerations for single-shot analysis using laser-induced breakdown spectroscopy. Spectrochim Acta, Part B. 2002; 57(4):779-90.

[223] Gruber J, Heitz J, Arnold N, uerle D, Ramaseder N, Meyer W, Hochrtler J, Koch F. In situ analysis of metal melts in metallurgic vacuum devices by laser-induced breakdown spectroscopy. Appl Spectrosc. 2004; 58:457-62.

BIOGRAPHICAL SKETCH

Esperanza Mariela Rodriguez Celis, better known as Mariela Rodriguez, was born in Peru in 1979 and is the oldest of three siblings. In 2002, she graduated from Pontifical Catholic University with a bachelor of science in chemistry. In August 2004 she moved to Gainesville, Florida to attend graduate school at University of Florida. She joined the research group of Dr. Nicolo Omenetto in the analytical chemistry program and conducted research while simultaneously taking classes in forensic drug chemistry and forensic toxicology. In December 2007, she graduated with a Master of Science in Pharmacy and Pharmaceutical Sciences with concentration in Forensic Drug Chemistry. She completed her doctoral research in May 2009. Mariela has been married to Oscar Arroyo since 2006. They expected to move back to Canada, shortly after her graduation.